156

SATELLITE & MESOMETEOROLOGY
RESEARCH PROJECT

Department of the Geophysical Sciences
The University of Chicago

Manual of Downburst Identification For Project Nimrod

T. Theodore Fujita

MANUAL OF DOWNBURST IDENTIFICATION FOR PROJECT NIMROD

T. Theodore Fujita
The University of Chicago

SMRP Research Paper 156
May 1978

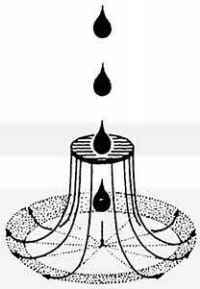

TABLE OF CONTENTS

INTRODUCTION

The purpose of this Manual is to present the evidence of downbursts available as of this date. It is expected that new data on this type of storm will be accumulated rapidly through Project NIMROD. Project NIMROD (National Intensive Meteorological Research On Downburst) is a two-year (1978-79) research project to collect meteorological data on a nationwide scale. NWS field offices will be advising the NIMROD Project office of significant downburst and/or tornadic events and will be assisting, when possible, in damage surveys. The Project starts with the operation of a triple-Doppler Network in Northern Illinois in May and June, 1978.

Straight-line winds, often preceded by an awesome-looking roll cloud, can induce widespread wind damage in and around thunderstorm areas. Damaging winds, usually lasting for a short period of time, are characterized by strong gusts which could seriously affect ground structures as well as low-flying aircraft.

Extensive aerial photography and mapping of the areas swept by straight-line winds has revealed the existence of diverging patterns of damage embedded inside of overall straight-line flows. A major breakthrough in this study was the analysis of the Independence Day, 1977 storms in Northern Wisconsin. At least 25 locations of divergent downburst flow were mapped from a low-flying aircraft.

Thereafter, microscale downbursts (microbursts), less than 3 miles in outflow diameter, were found in other parts of the country. Four aircraft accidents in 1975-77 and one more in 1956 have been related to microbursts whose sizes were comparable to the length of runways. Coupled with its small dimensions, damaging winds of a microburst last only for a few minutes, making its detection extremely difficult.

ACKNOWLEDGEMENTS

The author wishes to express his sincere appreciation to those who contributed in collecting downburst/tornado data, in offering valuable comments, and in assisting in the completion of this Manual. Without their dedicated assistance, this Manual could never have been completed. The following is only a partial list of individuals to whom I am endebted.

Robert F. Abbey, Jr.
Catherine Atkins
David Atlas
Babette M. Becker
Alfred J. Bedard
Donald W. Beran
Peter G. Black
Walter A. Bohan
Horace R. Byers
Fernando Caracena
James Carson
Stanley A. Changnon
William H. Cotton
Jennifer M. Cram
George P. Cressman
Raymond C. Crooks
James C. Dodge
Richard Dreiser
Antonio A. Dreumont
Edward Ferguson
Gregory S. Forbes
S. Susie Fujita
Rafael L. Gallegos
Joseph Golden
Mark R. Hjelmfelt
Ronald L. Holle
Karl R. Johannessen
Paul W. Kadlec
Frank Kornegay
Peter M. Kuhn
James Lebda
Michael W. Maier
Hubert McCaleb
Peter D. McGurk
H. Michael Mogil
L. Homer Mouden
Clifford J. Murino
Masao Nakamura
Vincent J. Oliver
Thomas C. O'Reilly
Fred Ostby
Edward W. Pearl
Allen D. Pearson
James F. W. Purdom
Marvin Russell
Robert J. Serafin
John A. Shanahan
William E. Shenk
Robert L. Somrek
Joseph Sowar
Ramesh C. Srivastava
Duane J. Stiegler
Verner E. Suomi
Jaime J. Tecson
Thomas A. Umenhofer
Thomas H. Vonder Haar
Roger M. Wakimoto
Raymond R. Waldman
Raymond Wexler
Linwood F. Whitney, Jr.

Research leading to the completion of the Manual was sponsored by:

NASA under Grant No. NGR 14-001-008
NOAA under Grant No. 04-4-158-1
NRC under Contract No. 04-74-239

Publication of the Manual sponsored by National Weather Service Headquarters.

Downburst damage is often highly localized, resembling that of tornadoes. Even an experienced investigator cannot always identify the nature of storms without mapping directions of damaging winds over a large area. There are significant interactions between tornadoes and nearby downbursts. The path of a tornado can be affected by downbursts, resulting in a right, left, or even a U turn. The vortex of a tornado could be wiped out by a strong downburst or it could intensify, being supplied vorticity by a twisting downburst.

Some insight into operational applications of these findings will be presented, too. However, development of operational guidelines must await further studies and operational evaluation. In the meantime, these assessments should be useful in ascertaining whether or not storm damage is tornado or downburst related.

May 1, 1978

T. Theodore Fujita
Professor
The University of Chicago

George P. Cressman
Director
National Weather Service

CHAPTER 1. SCALES OF THUNDERSTORM OUTFLOW

The leading edge of a thunderstorm outflow area is often characterized by strong straight-line winds, rapid temperature drops, and pressure surges. While typically associated with squall lines, such rapid changes can occur even in relatively "benign" isolated summer thundershowers.

Over 80 years ago, Durand-Gréville (1892) mapped pressure patterns of a squall line extending from near Berlin to southern Austria with amazing accuracy. Suckstorff (1938) investigated the surface-pressure disturbances in and around thunderstorms to find that the outflow is a result of the accumulation of cold air inside the subcloud layer due to precipitation cooling.

As air traffic increased in the 1930s, squall line-related accidents and difficulties occurred in various parts of the world, necessitating a better understanding of thunderstorm and squall-line circulations.

LINDENBERGER BÖENNETS (Squall Network) was established in 1939 near Berlin, leading to intensive data collection during the 1940 and 1941 seasons. In analyzing the data, special emphasis was made to determine the movement and intensity of the first gust across the network. An example of analysis is shown in Figure 1.1. For details refer to Koschmieder (1955).

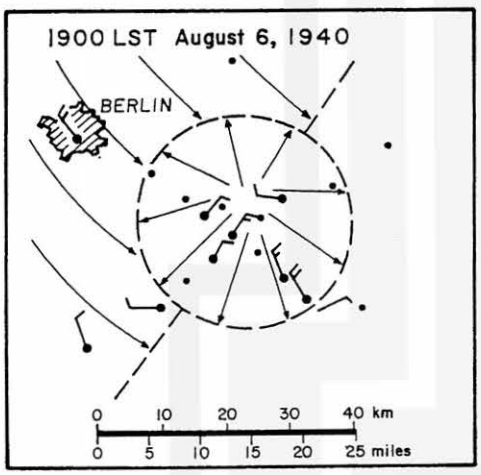

Figure 1.1 An outflow field over the Lindenberg Network. The outflow field formed to the southeast of Tempelhof, Berlin and moved away without affecting the station.

The leading edge of the outflow moved toward the southeast at 36 km/hr (22 mph) causing a 15 m/sec (34 mph) peak gust at Lindenberg near the network center.

MAEBASHI RAIU KANSOKUMO (Thunderstorm Network) in 1940 was operated by the Japan Meteorological Agency. The network with 21 recording stations was located near Maebashi, 60 miles northwest of Tokyo. Post-operation analyses revealed an increase of surface pressure inside the outflow areas (see Figure 1.2). For details refer to Fujiwara (1943).

Note: Because many different data sources were used in preparing this report, it was not practical to standardize units.

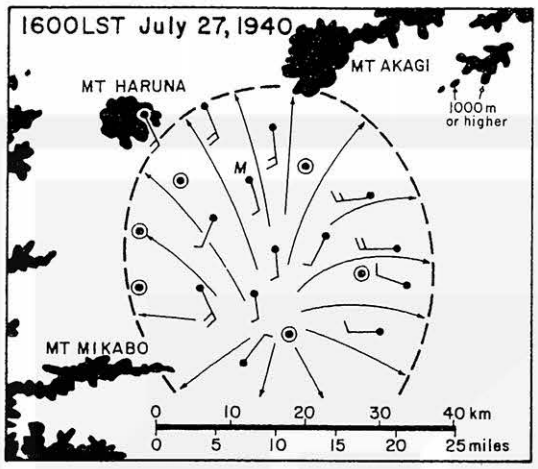

Figure 1.2 A pattern of cold-air outflow over Maebashi Network, northwest of Tokyo. The network consisted of 21 stations spaced at 5- to 7-mile intervals.

The outflow in this figure was in its early dissipating stage, characterized by weak, generally anticyclonic trajectories covering a large, elliptic area, 30-mile long and 25-mile wide.

THUNDERSTORM PROJECT NETWORK operated in 1946 (Florida) and 1947 (Ohio) generated basic data which led to a better understanding of the thunderstorm circulation associated with isolated and groups of thunderstorms. For details refer to Byers and Braham (1949).

Figure 1.3 shows the variation of gust speeds as the first gust line expanded from an isolated cell near the southwest corner of the Thunderstorm Project Network, Ohio.

Since the peak-gust speed increases toward the source region, it is likely that the highest gust speed is found just outside the downdraft center. In order to measure the maximum windspeed both in time and space, it would be necessary to have a very dense surface network.

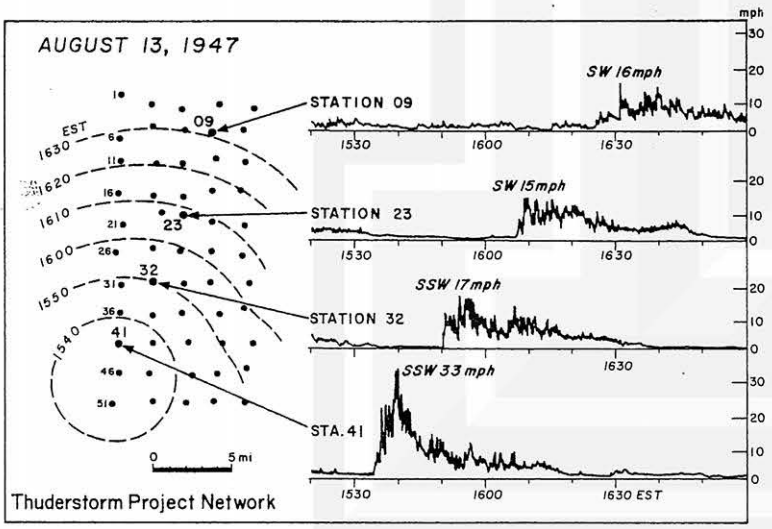

Figure 1.3 An example of first-gust line expanding from an isolated thunderstorm cell.

Note the general increase of the peak-gust speeds from 10 to 33 mph toward the source region. Higher peak speeds could have been recorded if there were denser network stations in and around the downdraft center.

Large-scale gust fronts, such as those analyzed by Newton (1950) were depicted by the Thunderstorm Project Network. Figure 1.4, for example, shows an advancing gust front (or shear line) across the network. The flow behind the front was distorted appreciably when showers developed about 20 minutes later.

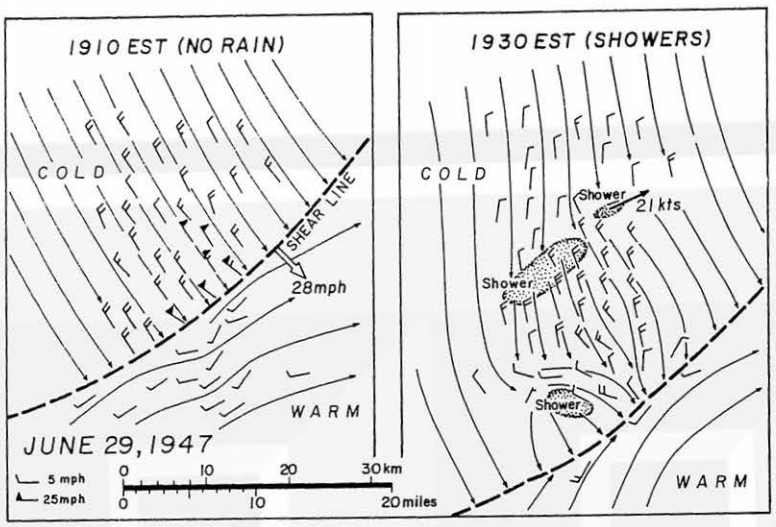

Figure 1.4 Fields of divergence developed behind a shear line moving across Thunderstorm Network, Ohio. In case a divergence field is significant, a shear line could be distorted into a bulge which advances faster than the overall shear line.

SINGLE-STATION DATA can be used to depict time variations of meteorological parameters effectively. Nevertheless, they are often misleading when presented on a time cross-section chart. For instance, data from an instrumented tower are frequently analyzed on z - t (height vs time) or z - x (height vs distance) coordinates. This type of presentation can give a false impression that the analyzed field remains unchanged in the y direction which is perpendicular to the system movement.

Flow patterns in three-dimensional space should be estimated by combining the time-sequence data with two-dimensional wind fields around the tower. An example of a combined analysis is shown in Figure 1.5. In this case, the acoustic-microwave radar was close to the downdraft center but it was several miles away from the area of the highest peak gust encircled by the 20-kt isotach.

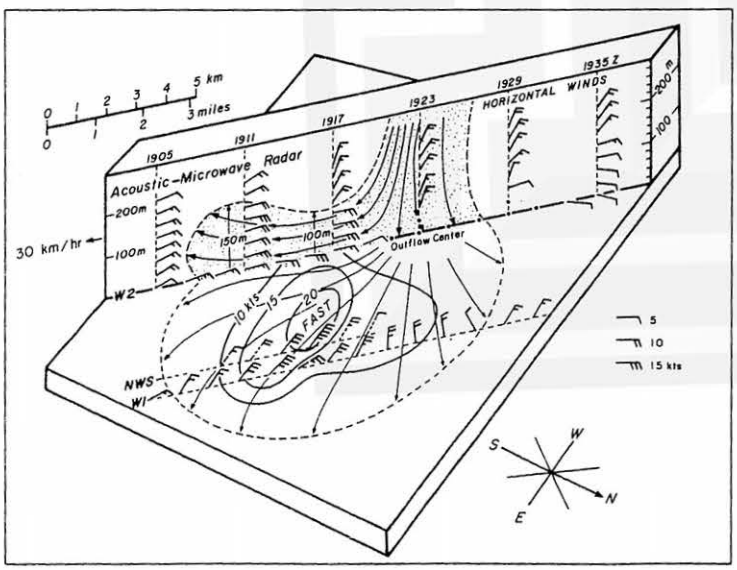

Figure 1.5 An analysis of a cellular outflow at Dulles Airport, Virginia. Analysis period: 1905 to 1935 GMT May 18, 1977.

Acoustic-microwave radar data introduced by Hardesty et al (1977) and Pressure Sensor data, by Bedard et al (1977) were supplied by WPL, NOAA, Boulder.

HORIZONTAL EXTENT OF DAMAGING WINDS cannot always be determined by the data from a mesonetwork. Some wind systems are so small in horizontal extent that they may form and dissipate without affecting network stations unless they are closely spaced.

Faust (1947) made an extensive survey of forests near Frankfurt, Germany, damaged by the July 13, 1941 squall line. The squall line was accompanied by a 7-mb pressure jump and a 33 m/sec (74 mph) peak gust at Frankfort airport. In mapping damage patterns Faust devised a 1 to 12 damage scale based on tree damage. Damage-scale contours in Figure 1.6 reveal the existence of swaths and pockets of high winds. Their dimensions are only 1/2- to 1-mile across, suggesting that the systems of damaging winds embedded inside the overall squall line were extremely small.

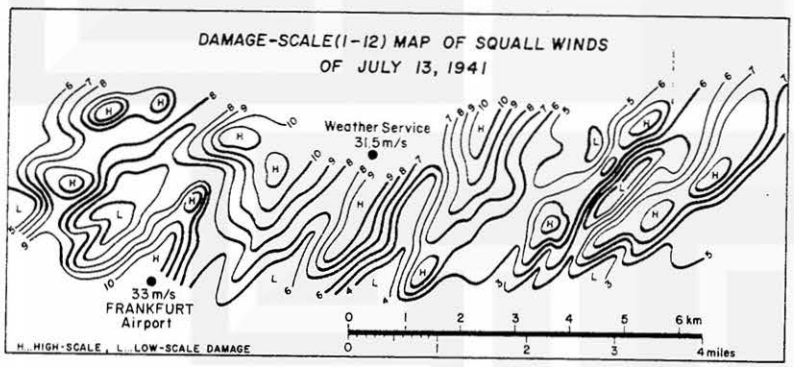

Figure 1.6 Patterns of damaging winds mapped by the 1 through 12 scale of damage degradation. Based on Faust (1947).

Müldner (1950) mapped directions of trees damaged by the July 22, 1948 squall line. As shown in Figure 1.7, he found two scales of damaging winds--one is characterized by large-scale straight-line winds and the other by small-scale diverging flows, only 2- to 3-miles across. These small-scale outflow systems are called microbursts. For a definition of microbursts see Chapter 3.

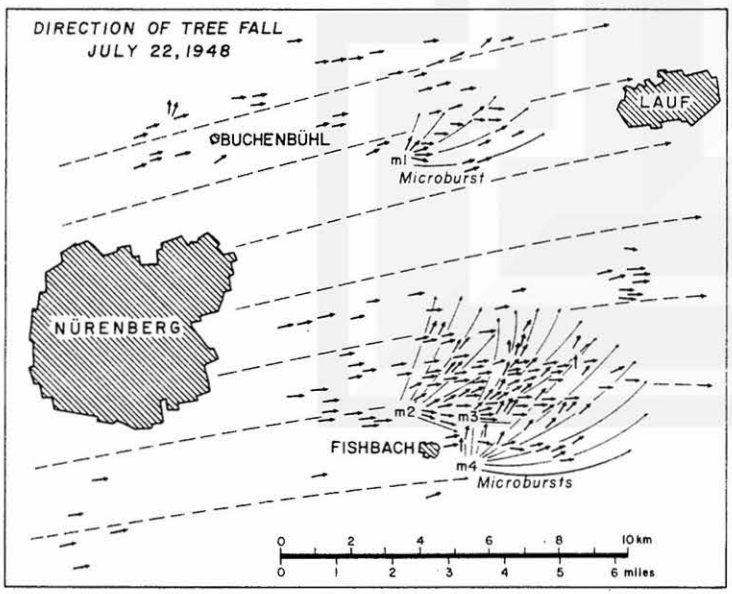

Figure 1.7 Two scales of outflow fields depicted by the direction of tree fall on July 22, 1948. Based on Müldner (1950).

Four diverging patterns identified by m1, m2, m3, and m4 were probably microbursts which are defined and discussed later in detail.

PROPER NETWORK RESOLUTIONS must be selected in order to perform mesoanalyses of various sized wind systems. A cyclone with 1,000-mile dimensions can be analyzed on synoptic charts with a 100-mile resolution of synoptic stations. But a synoptic network may not be able to depict small mesohighs, for example.

Fujita (1963) classified mesonetworks into Alpha, Beta, and Gamma categories, characterized by mean station spacings, 30, 5, and 1 mile, respectively. Figure 1.8 reveals, however, that even the gamma mesonet is not dense enough to map the flow of microbursts. A 1/8-mile (200 m) resolution or a delta network would be necessary to map the flow field of a microburst (see Figure 1.8).

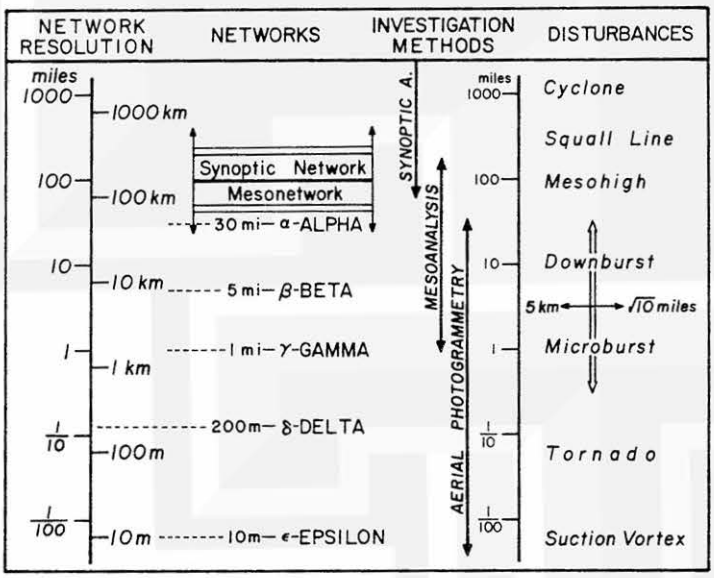

Figure 1.8 Comparison of disturbance size with network resolution. Delta and Epsilon networks were added to the initial 3-resolution, Alpha, Beta, and Gamma, networks introduced by Fujita (1963).

Several stations are necessary within a disturbance in order to depict the flow patterns. For example, the feature of a microburst cannot always be depicted unless the network resolution is finer than the Gamma spacing.

Ishizaki (1978) analyzed microscale fluctuations of winds recorded by 25 anemometers along a 720-m line on Tarama Island, Japan. The distance between anemometers is 30 m, which falls into a one-dimensional epsilon network category. But, a two-dimensional network with either delta- or epsilon-network spacing is not practical in view of its small aerial coverage and high cost. To overcome this difficulty, aerial photography and photogrammetric methods were developed by the author during the past years.

AERIAL PHOTOGRAMMETRIC MAPPING of the damage left behind by damaging winds permits reconstruction of the swaths (or trajectories) of the air motion. These swaths do not always represent instantaneous flows (or stream lines). But by virtue of the relatively short life of such winds it is often possible to infer stream lines from the photogrammetrically mapped swaths.

Figure 1.8 shows the dimension of disturbances which can be mapped by means of aerial photogrammetry. By virtue of high resolution of aerial photos, it is feasible to map flow patterns with better than 10-m resolution. Typical dimensions of microbursts are on the order of 1 km. This is why microbursts have not been depicted by data from alpha and beta networks alone.

It is highly desirable to combine mesonet data with aerial photographs, because the former clarify the time sequence of an event with coarse spacial resolution while the latter reveal a time-integrated pattern with high spacial resolution. Thus, a combined analysis of these data permits us to unscramble wind effects on ground objects into a time dependent solution of small-scale disturbances, which cannot be depicted otherwise.

CHAPTER 2. AERIAL PHOTOGRAPHS OF DOWNBURST DAMAGE

During the aerial survey, leading to the completion of Color Maps 1 - 9, numerous damage pictures were taken from the air and on the ground. Examination of these pictures revealed that damage caused by strong downbursts is often very similar to that by tornadoes. For example, roofs were sometimes lifted off walls, while most of the walls were left in upright positions, and weak structures or small silos were blown completely off their foundations. However, straight-line winds are naturally suspected when a large number of trees in a forest are pushed over in essentially one direction. But in some situations overlapping downbursts can produce a confusing debris pattern. It is, therefore, very difficult to determine the nature of damaging winds without mapping in detail the patterns of wind direction and speed inside the area of a questionable storm.

The flattened forest of pine trees in Figure 2.1 was taken in easternmost Sawyer County which was affected by the Northern Wisconsin Downbursts (see Color Map No. 4). The photo represents typical damage by straight-line winds.

Detailed mapping of the fallen trees revealed the existence of a fan-shaped, diverging flow from Downburst 13. Since the change in the overall flow direction was only about 5 degrees per mile, this type of wind could have been regarded as straight-line wind.

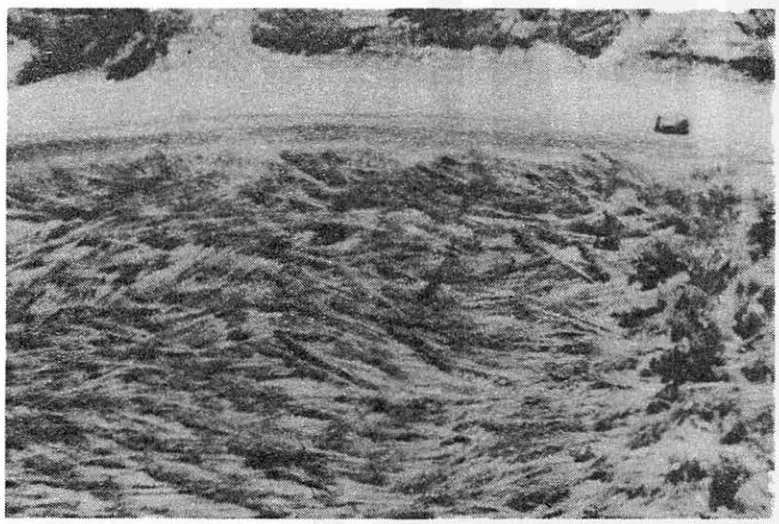

Figure 2.1 A pine forest flattened by the Northern Wisconsin Downburst 13 of July 4, 1977.

This aerial photo was taken just to the west of Flambeau River looking south toward Phillips-Winter Highway (see Color Map No. 4).

Figure 2.2 shows numerous birch trees blown down by strong winds from left (west-southwest) to right. This picture was taken near the west shore of Musser Lake, 7 miles NE of Phillips, located near the center of the downburst areas in Color Map No. 4. As a low-flying Cessna flew southward from the lake, the flow direction changed from WSW to W and finally to NW within about 10 miles. The source of the outflow was thus identified as Downburst 19, after flying along a zigzag course.

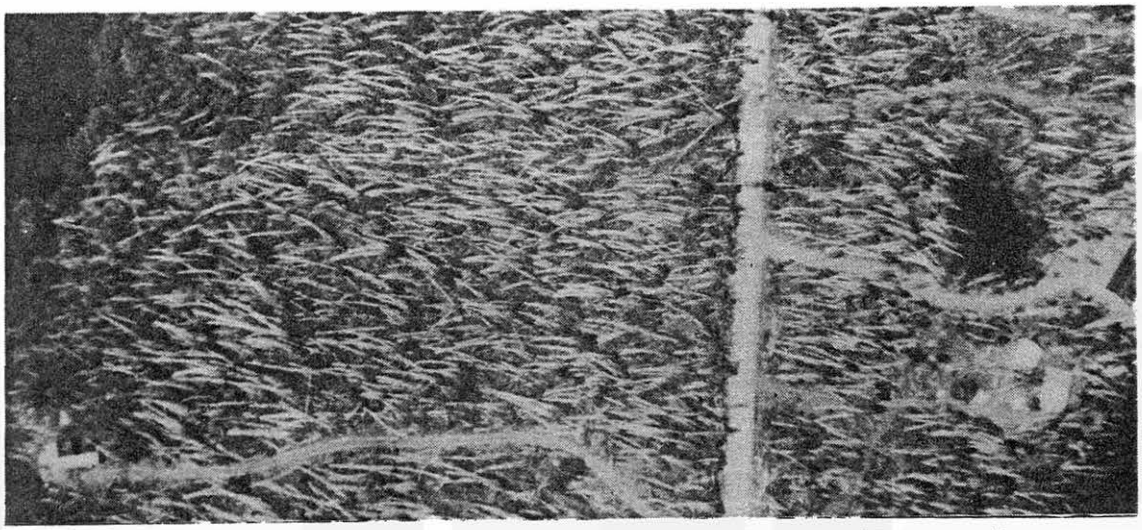

Figure 2.2 Birch trees near Musser Lake, 7 miles northeast of Phillips, blown down by Downburst 19 (see Color Map No. 4).

Downburst 6, northeast of Haver, Sawyer County (see Color Map No. 4), was characterized by a 90 degree change in fallen tree directions within two miles.

It may be concluded that "straight-line winds" have occurred as long as the area of concern is at least one order of magnitude smaller than the divergent parent wind system.

LIFTING OF ROOFS during a downburst is a result of the dynamic lift force. Lift is defined in the "Glossary of Meteorology (1959)" as being the component, perpendicular to the relative wind and in the plane of symmetry, of the total force of air on an aircraft or airfoil.

The large roof of the farm building in Figure 2.3 was lifted and carried by "straight-line winds" from Downburst 19 in Color Map 4. Numerous objects, large and small, were blown into the forest, resulting in the tornado-like damage.

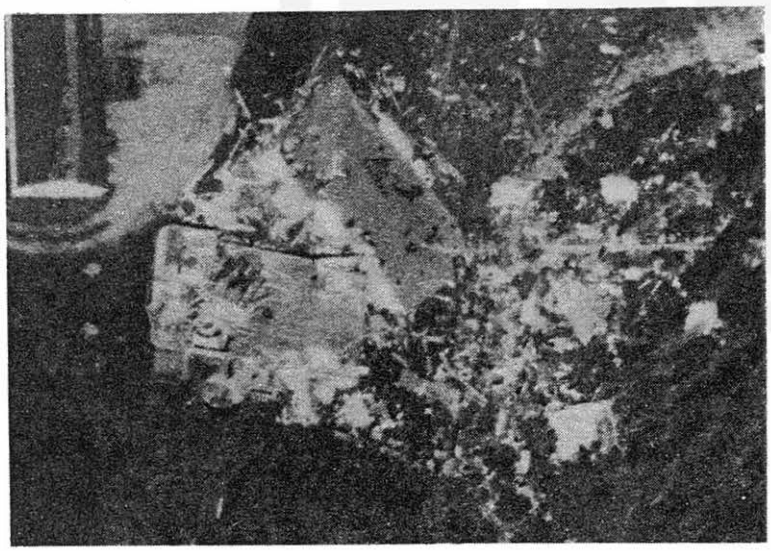

Figure 2.3 A large farm building west of Phillips pushed over and smashed by Downburst 19, northern Wisconsin storm. Estimated damage scale is F2 (see Table 2.1).

Pieces of tin roofing scattered in the plowed field in Figure 2.4 (see Color Map No. 6) came from a tool shed at A. Minor damage to roofs was spotted in other parts of the farm, but there was no other structural damage visible from the air.

Figure 2.4 Tool shed debris from Downburst 7 near Wallace, Fountain County, Indiana (see Color Map No. 6). Estimated damage scale is F1.

STORAGE BINS AND SMALL SILOS are vulnerable in a downburst. The bin in Figure 2.5, looking ESE, was uprooted at A. Thereafter, it travelled, half of the time in the air and half of the time on the ground, through a distance of 1/2 mile. The damage was caused by Microburst m7 (see Color Map No. 3) on June 13, 1976 in Central Iowa. The microburst was induced by a mesocyclone in its right quadrant as it travelled from west of Gilbert to Story City.

Damage similar to this case is often seen within several miles of a tornado. Detailed mapping of the area <u>almost always</u> reveals that damage was caused by nearby downbursts <u>not by a tornado several miles in diameter</u>.

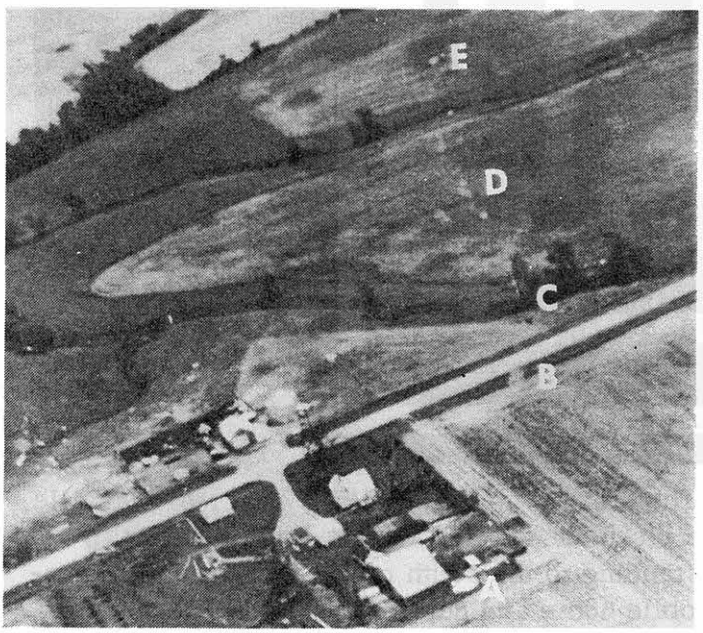

Figure 2.5 A storage bin uprooted and blown away by microburst m7 (northeast of Gilbert in Central Iowa (see Color Map No. 3).
The bin, after leaving A, hit roadside grass at B and clipped a few branches at C. The bin disintegrated between D and E.

DOWNBURSTS IN HURRICANES are now suspected in light of hurricane Celia damage in and around Corpus Christi, Texas (see Color Map No. 9). Under normal circumstances, we expect to experience the strongest winds on the right side of a travelling hurricane. Against expectation, the city received severe damage by the WSW winds while the hurricane center was travelling toward the WNW, some 10 miles to the north of the city.

Corpus Christi was inside the eye of the radar echo when damaging winds were in progress. Apparently, the damaging winds came from the direction of a thunderstorm which developed on the southwest side of an enlarged eye.

Typical damage in Corpus Christi is shown in Figure 2.6. A large motel on the north side of an east-west highway lost two major sections of the roof. Mobile homes in a trailer park were pushed over against each other. Some were overturned or rolled into the plowed field and smashed.

Figure 2.6 A motel and trailers west of Downtown Corpus Christi damaged by downburst winds in hurricane Celia (see Color Map No. 9). Damaging winds estimated to be upper F1 or lower F2 came from WSW. The hurricane center, to the north of the city, was moving WNW at 16 mph.

MOBILE HOMES WITHOUT TIE DOWNS are like tumbleweeds or match boxes in high winds (refer to Figure 2.15). The mobile home in Figure 2.7 (near Danville, Illinois) had been standing on foundation blocks at A. There was a propane tank, 2 to 3 ft high according to its shadow, standing to the south of the foundation. Downburst winds from the north lifted the mobile home and deposited it in the corn field. The propane tank was not disturbed by the mobile home.

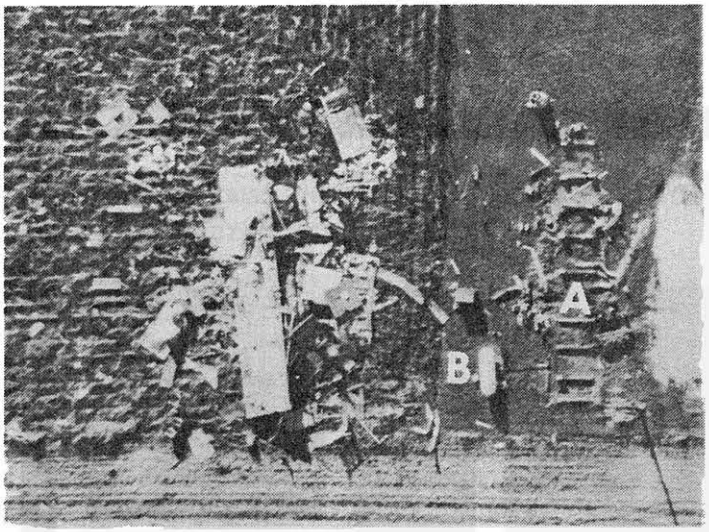

Figure 2.7 A mobile home destroyed by Microburst m6 southeast of Danville, Illinois (see Color Map No. 6). The mobile home left its foundation A, flew clear over a propane tank B, and disintegrated upon impact in the corn field.

Another Illinois mobile home, see Figure 2.8, was also lifted up from its foundation. It was smashed open as it landed in the backyard. An eyewitness in the house near the top center of the picture stated, "It was raining. Suddenly I heard a bang noise, and saw a smashed mobile home flying toward me. I took cover immediately because it was a tornado." Yet debris streaks, A and B, clearly show a diverging pattern <u>not found with tornadoes</u>.

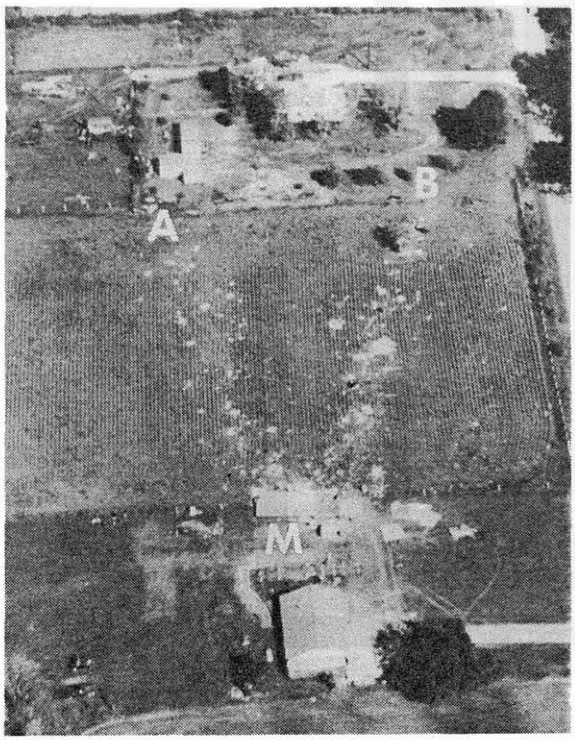

Figure 2.8 A mobile home destroyed by Microburst m2 northwest of Danville, Illinois (see Color Map No. 6). The mobile home was located about 1.5 miles south of Snider, Vermilion County, where damaging winds came from the south.

Picture was taken looking north. Foundation blocks are seen to the south of letter "M".

This microburst occurred in rain with <u>loud roar and a "bang" noise, like the sound of a tornado</u>.

DRESSED-UP TREES AND POLES are commonly seen after the passage of a tornado. A country club was blown down by Downburst 3 on May 11, 1973 (see Color Map No. 1). One after another, construction materials were blown against a power pole which was left standing during the downburst. Finally, the pole was dressed up by the captured debris (see Figure 2.9).

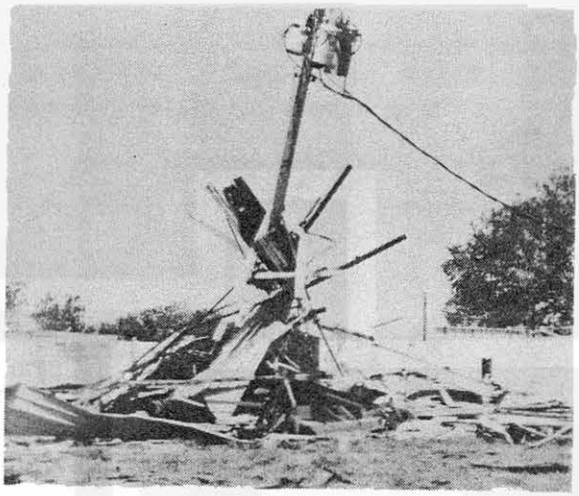

Figure 2.9 Debris of a country club building destroyed by Downburst 3, southeast of Chanute, Kansas (see Color Map No. 1.

A power pole was dressed up by the debris which somehow wrapped around the pole.

TOMBSTONES can be toppled by downburst winds. Since this stone was less than 2 ft high, the damage implies the existence of a strong wind very close to the ground (see Figure 2.10).

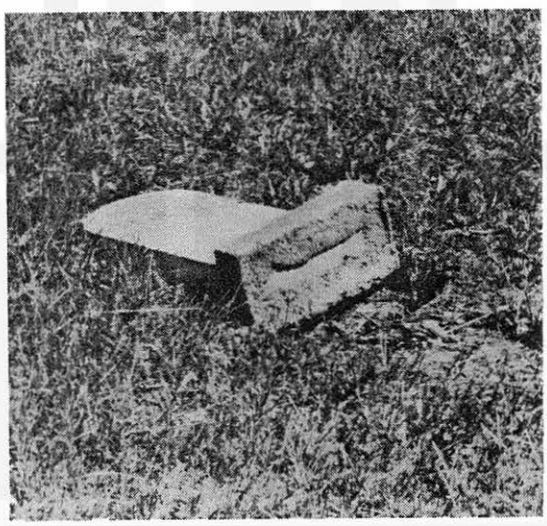

Figure 2.10 A tomb stone toppled by Downburst 4 in Neosho County, Kansas (see Color Map No. 1).

THE CENTER OF DOWNBURST is rather hard to identify, because it is a diffused spot rather than a geometric point.

Figure 2.11 shows corn stalks blown down near the center of a microburst. There were a large number of fan-shaped outflows, each up to about 100 ft in horizontal dimensions. More organized radial outflows are seen outside the central area of the microburst.

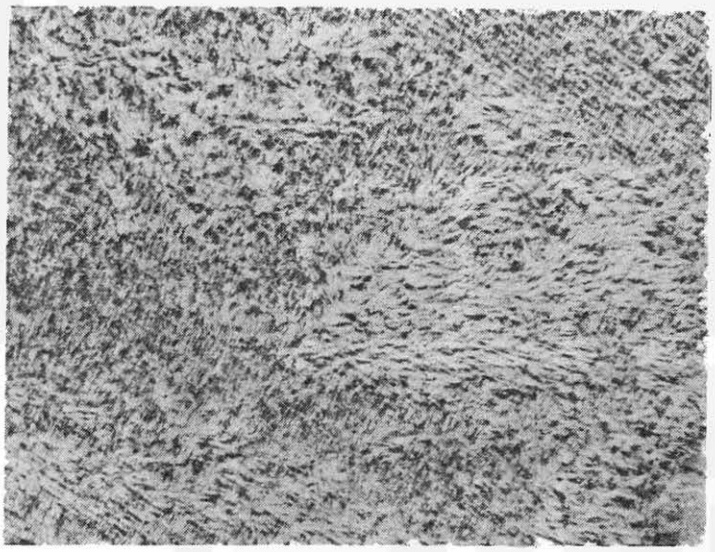

Figure 2.11 Corn field near the center of Microburst m8 on September 30, 1977 (see Color Map 6). Apparently, heavy rain and hailstones came down with the microburst. Seen in the vicinity of the downburst center are flattened cornstalks in diverging patterns. This picture was taken from 300 ft above the field.

DEFLECTED JETS are seen just outside the downburst center where slanted flows of downburst are expected.

A jet-like wind, indicated by numbers 2, 3, 4, was deflected by a small roof at 1. A portion of the roof was peeled off by the descending wind, which, in turn, shot out into the corn field. (see Figure 2.12).

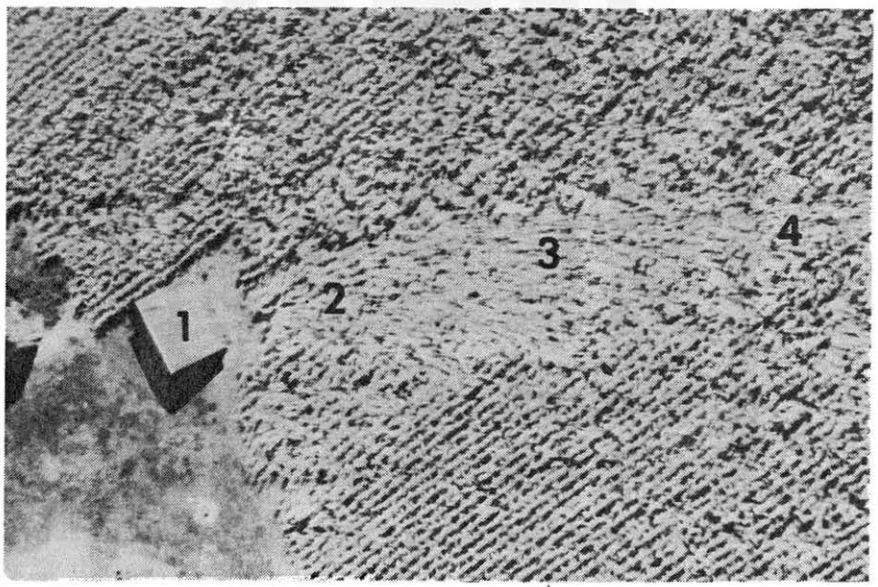

Figure 2.12 Trace of a localized jet caused by a slanted roof which deflected the descending wind of Microburst m8 (see Color Map No. 6) on September 30, 1977.

DOWNBURST FINGERS are the spreading ends of a downburst descending over a ragged terrain. Examination of the aerial photographs taken during the survey of the April 3-4, 1974 tornado outbreak revealed traces of downburst fingers.

The three fingers in Figure 2.13 descended deep into the Glade Creek Canyon, near Beckley, W. V. Most of the trees at high levels were flattened. As downburst winds descended toward the canyon bottom, trees in narrow bands were pushed down, resulting in the finger-like configurations of damage.

Initially, Fujita (1975) mapped these downburst fingers as being a part of the Meadow Bridge tornado, West Virginia. Remapping of the tornado, however, revealed that the early path of the tornado was characterized by a series of downbursts. Later, an organized pattern of a tornado vortex developed.

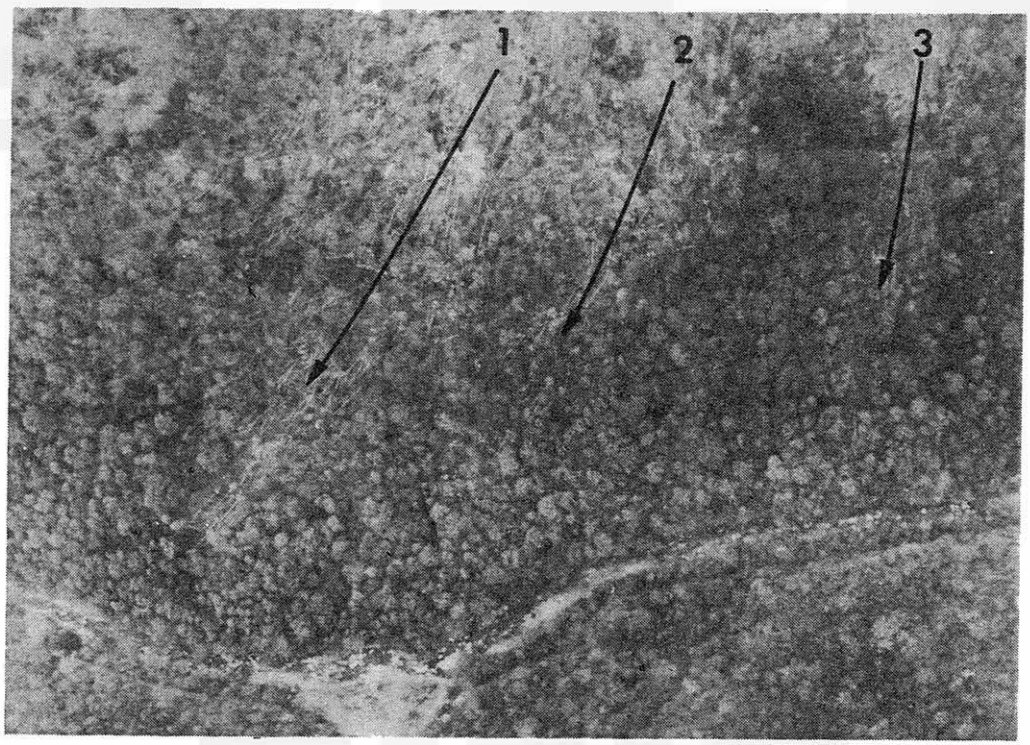

Figure 2.13 Three fingers of downburst winds descended into an 800-ft deep canyon of Glade Creek, 6 miles east of Beckley Airport, West Virginia. These fingers were located in the touchdown region of the Meadow Bridge tornado of April 3, 1974. Refer to Tornado 137 in Superoutbreak Tornado Map by Fujita (1975).

INTENSITY OF DOWNBURSTS is much less than that of violent tornadoes. Nonetheless, their top intensity may reach as high as F3.

According to the F-scale classification of 14,802 tornadoes by Wilson and Kelly (1977), 2.8% were F4 or stronger; 9% were F3; and 88% were F2 or weaker.

Of the 142 downbursts in Color Maps Nos. 1-9, 98.6% were F2 or weaker. None were F4 or stronger, but 1.4% were rated as F3 (see Figure 2.14).

These statistics imply that most (79%) downbursts are accompanied by F1 or weaker (112 mph or less) winds. Such winds could, however, cause serious damage to mobile homes if they were not tied down properly. Furthermore, the area of a downburst is much larger than that of a tornado, thus significantly increasing the probability of wind damage.

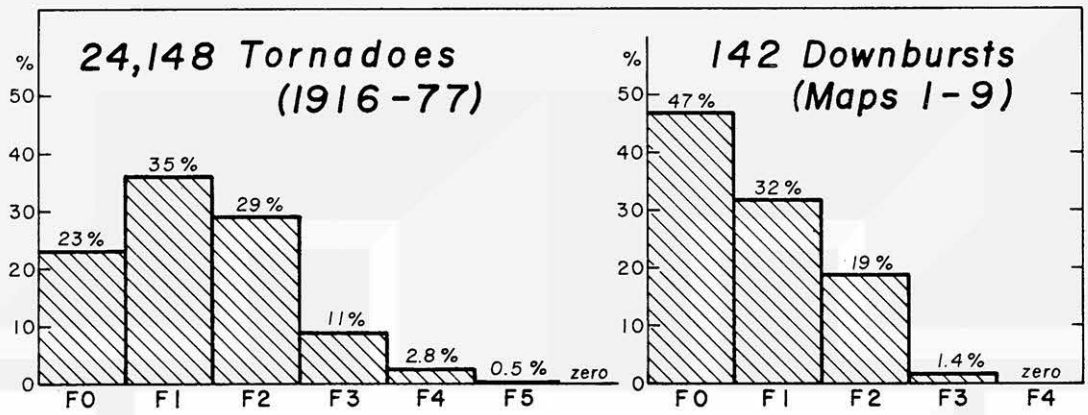

Figure 2.14 Intensity distribution of 24,148 tornadoes (left) during the 52-year period 1916-77, by Fujita, Tecson, and Abbey (1978). Intensities of the 142 downbursts in Color Maps 1 - 9 (right).

F PP TORNADO SCALE, devised initially in classifying tornadoes based on their intensity (F), path length (first P), and path width (second P), can also be used for downbursts. Because of the anticipated wider path width of downbursts, the path-width scale was extended up to scale 7 (see Table 2.1).

Table 2.1 The FPP (Fujita-Pearson) tornado scale is applicable to downbursts also. From Fujita (1971) and Fujita and Pearson (1973). For review of the FPP scale, refer to Abbey (1976).

Scale	- F - Max. Windspeeds	- P - Path lengths	- P - Path widths
-	less than 40 mph	less than 0.4 mile	less than 6 yds
0	40 – 72	0.4 – 0.9	6 – 17
1	73 – 112	1.0 – 3.1	18 – 55
2	113 – 157	3.2 – 9.9	56 – 175
3	158 – 206	10 – 31	0.1 – 0.3 mile
4	207 – 260	32 – 99	0.4 – 0.9
5	261 – 318	100 – 315	1.0 – 3.1
6	- - - - -	- - - - -	3.2 – 9.9
7	- - - - -	- - - - -	10.0 – 31.6

As has been pointed out by Minor et al (1977), windspeed estimates through F-scale assessments become inaccurate as the scale increases to 4 and 5. One reason for this is that "not all buildings are constructed uniformly". Hart (1976) computed the mean percent damage (in dollars) of various structures as a function of windspeed (see Figure 2.15). A similar diagram for trees was constructed by the author to show how trees withstand damaging winds differently (see Figure 2.16).

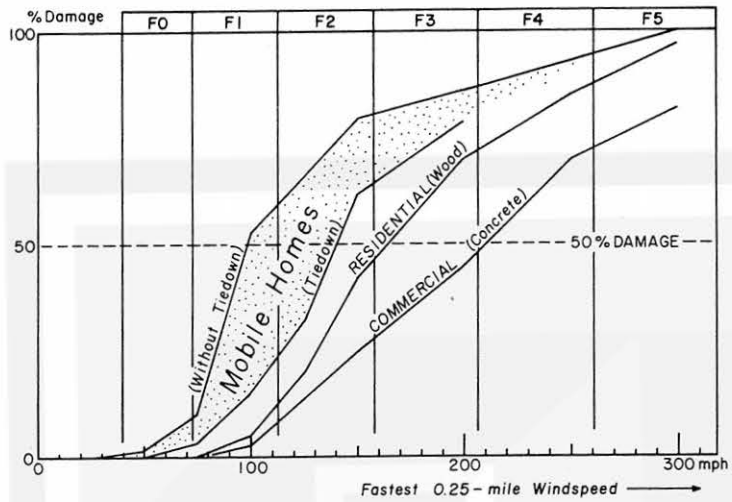

Figure 2.15 Percent damage of various structures as a function of windspeed. A 50% damage is caused by a 100 mph wind when mobile homes are not properly tied down. Tied-down mobile homes receive 50% damage by a 140 mph wind, instead. From Hart (1976).

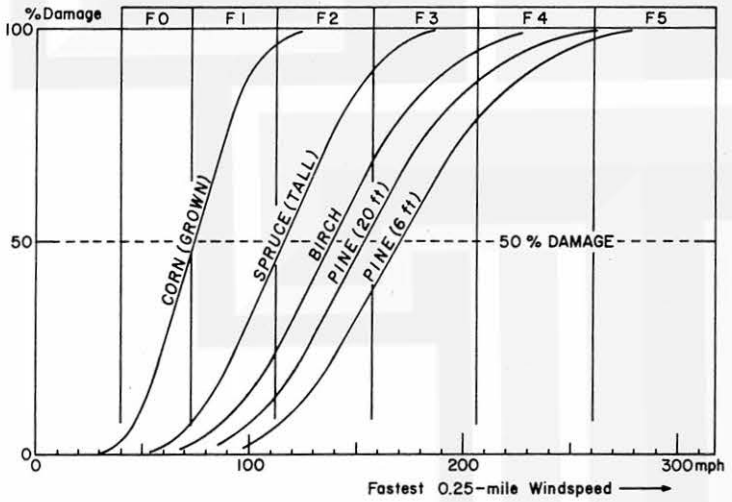

Figure 2.16 Percent damage of trees as a function of windspeed. This diagram was constructed based on the comparison of tree damages with nearby structural damages in large number of aerial photographs obtained by the author. Corn crops are excellent tracers of F0 and F1 winds.

These results lead to the conclusion that it is not feasible to estimate tornado or downburst windspeeds with extreme accuracy over the entire storm areas. First of all, the chance of finding any structure at the locations of the maximum windspeed is rather small. An existence of engineered structures at such locations are rare, if not nil.

Furthermore, a small unengineered structure, such as a mobile home, can be blown away by a sudden gust, lasting for a short period of time and affecting a small space. On the other hand, an engineered structure has a tendency to be affected by the mean wind averaged over a longer period and larger space than those applicable to a small structure such as a mobile home. By definition, the windspeed of the peak gust is always larger than that of the mean wind.

It should be noted that most engineering estimates of windspeeds are those of "the minimum windspeeds" required to cause the damage. "The maximum windspeeds" which had impinged upon a structure cannot always be estimated easily, especially when the object had been blown away. In such a case, the kinetic energy of the wind was used in both structural failure and missile generation.

Figure 2.17 shows damage patterns corresponding to F0 through F5 scale. This chart has been used in estimating the F scale of both tornadoes and downbursts with an anticipated accuracy of plus/minus one scale.

Figure 2.17 Reference pictures in determining F scale based on damage characteristics. Outbuildings or mobile homes could be flown away by F2 or F3 winds. Even well-constructed structures can be destroyed by F5 winds. For original pictures of F scale damage, refer to Fujita (1971).

CHAPTER 3. DEFINITION AND DIMENSIONS OF DOWNBURSTS AND MICROBURSTS

Since damaging winds, 40 mph or stronger, can be assessed by the F scale, individual downbursts are classified according to their maximum windspeeds (see Figure 2.14 for frequency distribution).

The concept of upgrading downdrafts into downbursts is similar to that of funnels aloft into tornadoes. A funnel cloud is not called a tornado, no matter how violent in mid-air it may be, unless the circulation reaches the ground (refer to Table 3.1 and the National Weather Service Operations Manual, Chapter C-40).

Based on these considerations, it is possible to define a downburst as

> A STRONG DOWNDRAFT INDUCING AN OUTWARD BURST OF DAMAGING WINDS ON OR NEAR THE GROUND

Table 3.1 Classification of local windstorms based on airflow characteristics on the ground and in mid-air.

CHARACTERISTICS OF WINDS mid-air	on the ground	HORIZONTAL WINDSPEEDS ON THE GROUND less than 40 mph	more than 40 mph
Upward	Convergent & Swirling	FUNNEL ALOFT	TORNADO
Downward	Divergent & Generally Straight	DOWNDRAFT	DOWNBURST

Frequency distributions of tornadoes and downbursts are presented in Figure 3.1 on PP (path length vs path width) coordinates.

It is seen that the maximum frequencies of tornadoes occur where $P_L = 0$ and $P_W = 1$. A total of 2848 tornadoes out of 14,802, or 19%, are classified as PP = 01 (see left figure).

The most frequent dimensions of downbursts, as determined by 142 downbursts in Color Map 1-9, are characterized by $P_L = 1$ or 2 and $P_W = 5$ (see right figure).

We see, quite often, damage patterns of small downbursts embedded inside an outflow field of a large downburst. To distinguish such a small downburst from a large one, it is important to define a microburst as

> A MICROSCALE DOWNBURST WITH ITS PATH LENGTH LESS THAN $\sqrt{10}$ = 3.16 miles (5.1 km).

A vertical dashed line in Figure 3.1 (right) represents the 3.16-mile path length.

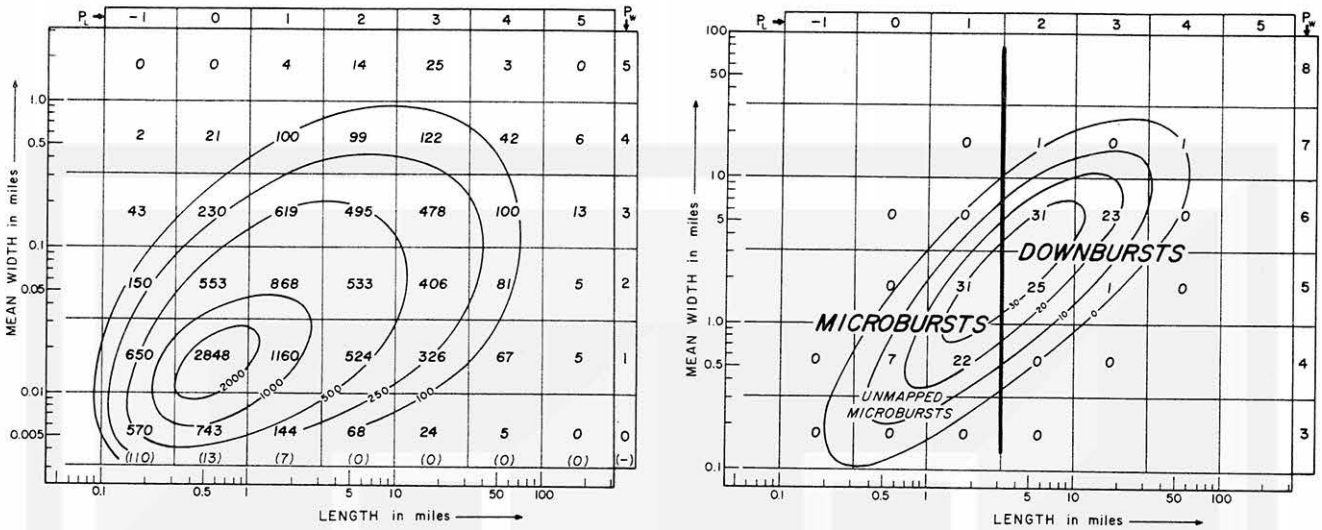

Figure 3.1 Path lengths and path widths of tornadoes and downbursts. The path statistics of 14,802 tornadoes (left) were from Wilson and Kelly (1977) and those of 142 downbursts (right) were from those in Color Maps 1 - 9. The vertical dashed line separates downbursts from microbursts.

DANVILLE MICROBURST, m 7 (see Color Map No. 6), classified as FPP = 004, covers an area of less than one mile square. Figure 3.2 shows a low-oblique view (left) and mapped trajectories of the outflow (right).

Characteristics of winds induced by this microburst can be estimated based on the damage of compacted and bundled haystacks. A 50 mph or stronger wind is required to blow apart such a haystack. Thus, the area bounded by a dashed line in Figure 3.2 was likely to be affected by such winds.

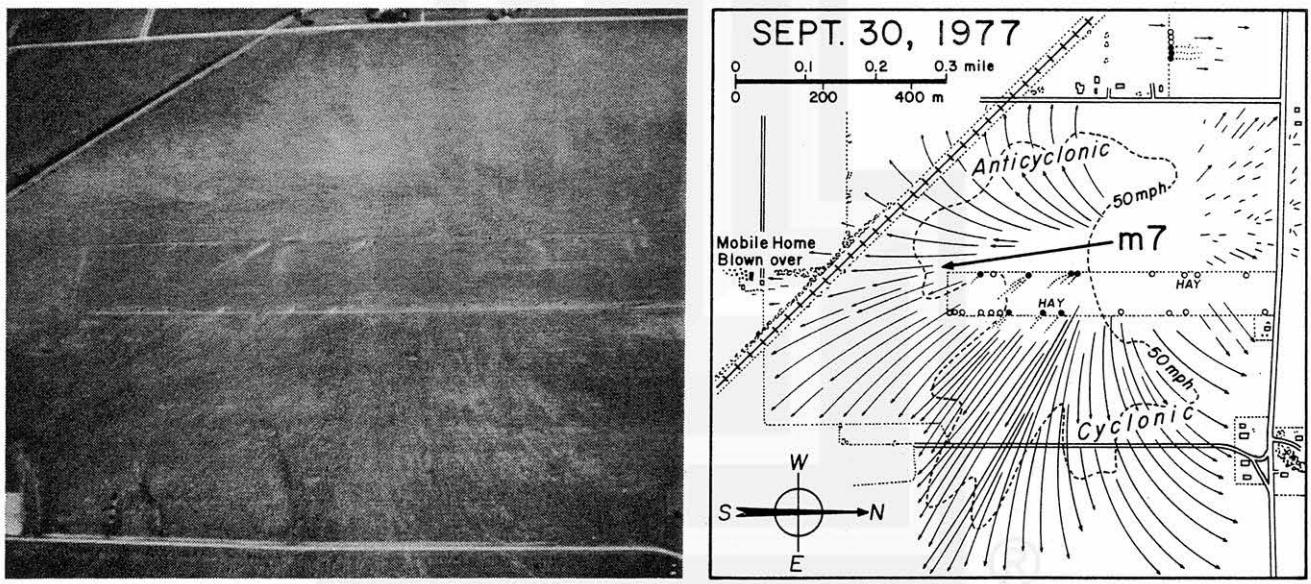

Figure 3.2 An aerial photograph taken from 6,000 ft AGL (left) and mapped trajectories of high winds (right) of Danville microburst, m7 in Color Map No. 6. Anticyclonic and cyclonic curvatures resulted from the movement of the microburst from right to left (north to south). The displacement vector of the downburst center during its lifetime (only 1 to 2 minutes) is shown by a heavy arrow.

DIVERGENCE near the center of this downburst can be computed from

$$\frac{2V_r}{R} = \frac{2 \times 20\ m\ sec^{-1}}{200\ m} = 0.2\ sec^{-1}$$

where V_r denotes the radial velocity averaged over the entire azimuths from the microburst nadir and R, the range from the nadir.

By assuming a constant divergence along the vertical, vertical velocities at various heights were computed (see Table 3.2).

Danville microburst, m 7 with 0.2 sec^{-1} divergence was characterized by a 5 m/sec (16 fps) downward current at 25 m, 10 m/sec (33 fps) at 50 m, and 20 m/sec (66 fps) at 100 m AGL if the divergence were constant.

Table 3.2 Vertical velocities at various heights above the ground computed as a function of divergence at the surface. Divergence is assumed constant along the vertical. Danville microburst m7 was characterized by 0.2 sec^{-1} divergence. Up to 1.0 sec^{-1} divergence was estimated elsewhere.

DIVERGENCE	HEIGHTS ABOVE GROUND (in m and ft)				
on the ground (sec^{-1})	5 16	10 33	25 82	50 164	100 meters 328 feet
0.04	0.2 m/s	0.4 m/s	1.0 m/s	2 m/s	4 m/s
0.1	0.5	1.0	2.5	5	10
0.2	1.0	2.0	5.0	10	20
0.5	2.5	5.0	7.5	25	50
1.0	5.0	10.0	25.0	50	100

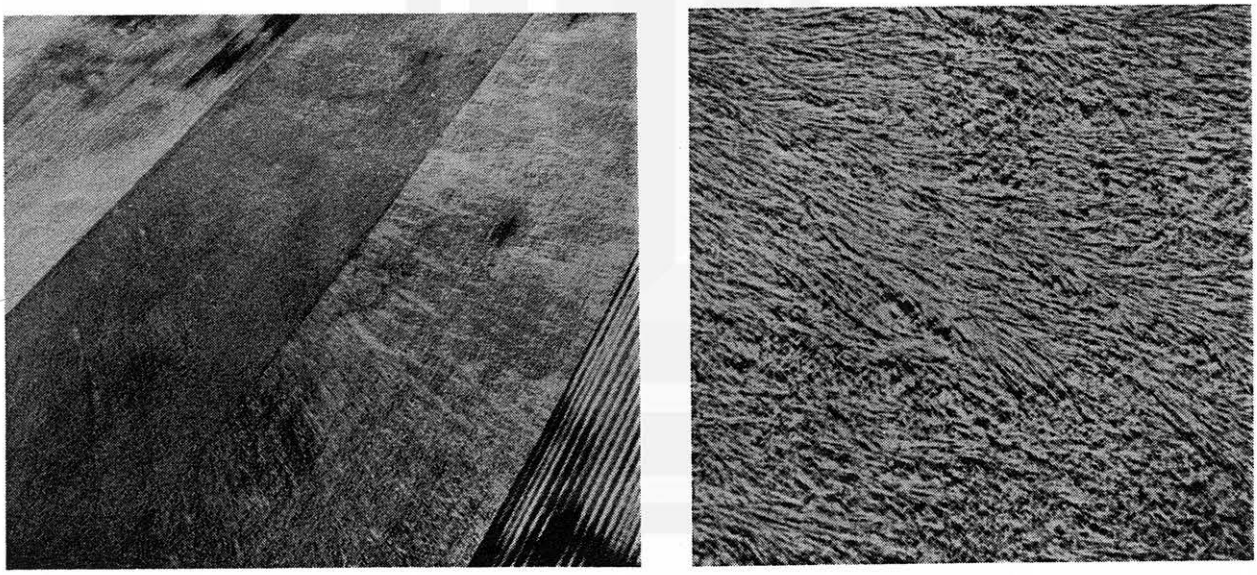

Figure 3.3 Aerial photographs of Danville microburst, m1 in Color Map No. 6. Diverging straight lines denote the directions of blown-down cornstalks as seen in a close-up picture taken from 500 ft AGL (right). This microburst traveled from upper left to lower right (NW to SE) of the overall picture (left).

MICROBURST, m 1 about 10 miles west of Danville (see Color Map No. 6) was similar in dimensions to those of m 7.

An overall (left) and a close-up (right) view of this microburst are shown in Figure 3.3. Corn stalks in light, straight-line bands were blown down flat to the ground with 100% loss. Divergence near the center is estimated to be 0.3 sec^{-1}.

NOAA's Florida Area Cumulus Experiment (FACE) mesonetwork south of Lake Okeechobee, Florida recorded a significant pressure nose associated with a microburst. As shown in Figure 3.4 a microburst descended to the west of the barograph, resulting in a 2.4-mb pressure nose.

Under the assumption that this pressure rise was induced when the vertical velocity decreased to zero at the surface, we equate

$$\tfrac{1}{2}\rho W^2 = 2.4 \text{ mb}$$

and obtain a downward vertical velocity, W, of 21 m/sec at some unknown height above the surface. This estimate is conservative, because the barograph was not located at the center of the microburst.

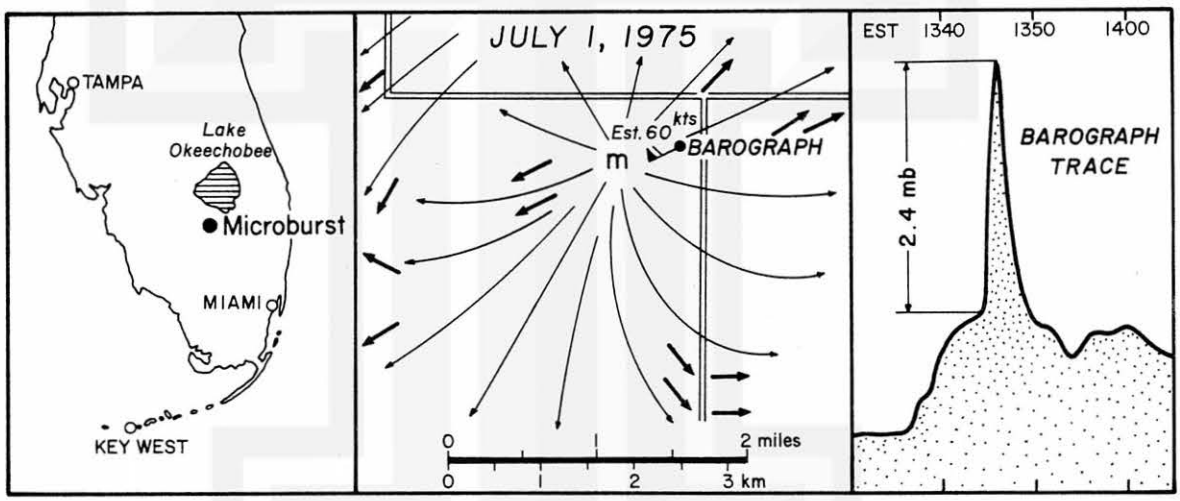

Figure 3.4 A microburst on July 1, 1975 over NOAA's FACE mesonetwork in Florida. Bold arrows indicate directions of sugarcane blown down by downburst winds. A barograph located about one-half mile to the east of the microburst center recorded a sharp pressure nose, lasting for about 4 minutes. From Caracena and Maier (1978).

Although the squall line outflow is deep, often reaching the base of convective clouds, the outflow depth of downbursts and microbursts appears to be very shallow (refer to Figure 1.5).

One of Ron Holle's pictures taken from the Panokee Site in the FACE Network clearly shows important features of such a shallow outflow from the region of a possible downburst or microburst to the right (northeast) of the picture looking southwest (see Figure 3.5). This picture also reveals a lifting effect of the outflow which was giving rise to the development of new convective activities along the arcus line.

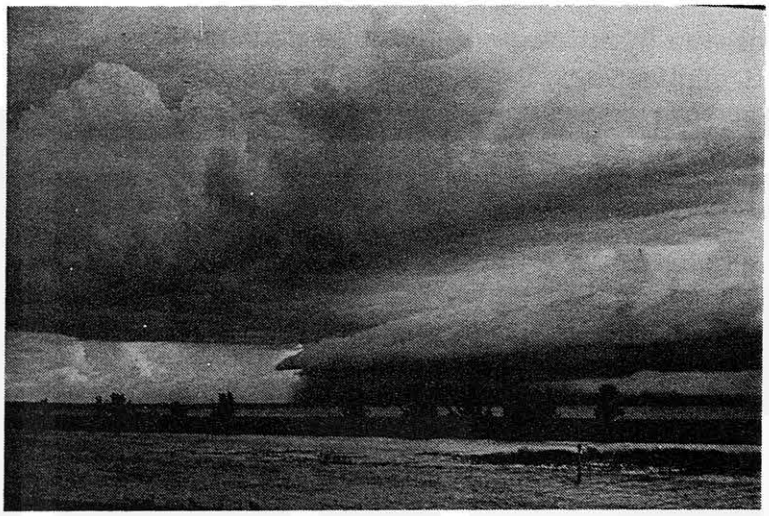

Figure 3.5 A view of an advancing front of the cold-air outflow accompanied by arcus (roll cloud) and dust cloud of August 12, 1975. The dust cloud extends up to about 200 m, revealing that the outflow depth is much shallower than the overall layer beneath the convective cloud base. Courtesy of Ron Holle.

THREE PERSONS WERE KILLED by a downburst at Ciudad Camargo, Mexico on May 31, 1976. A man was electrocuted when high-tension wires, snapped by high winds, fell onto his car. Two police officers were killed in their station when the walls caved in.

Antonio Dreumont, MIC of WSO, Brownsville, Texas, surveyed the entire area of the storm, and concluded that there was no evidence of a tornado. Instead, the storm was a group of six downbursts which had developed in Texas, just north of the Rio Grande. Five downbursts then moved into Mexico, crossing the river at about 8 p.m., CST (see Figure 3.6).

A large number of houses were unroofed (see Figure 3.7), leaving the typical F1 damage in both the U.S. and Mexico. At Rio Grande City the top of a cylindrical water tank was peeled off and a 100-ft long block fence at Rosita was knocked down by debris flying in high winds.

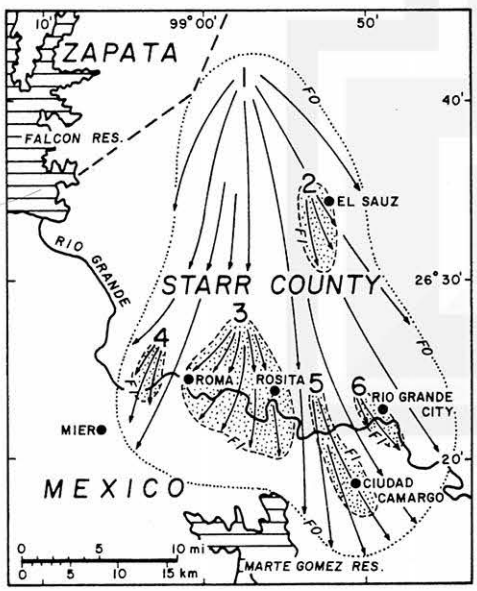

Figure 3.6 Patterns of high winds on May 31, 1976. Six downbursts occurred between 7:30 and 8:30 p.m. CST accompanied by hail larger than 3/4 inch. Winds estimated to be near 100 mph destroyed crops on 15,000 acres, damaged 150 farm dwellings, and destroyed 76 farm buildings. Downburst No. 5 moved into Mexico, killing 3 persons at Ciudad Camargo.

Figure 3.7 An unroofed house in Rosita, Texas. Courtesy of Mr. antonio A. Dreumont, WSO Brownsville, Texas.

DOWNBURST FAMILY or TORNADO FAMILY is defined as a series of local windstorms spawned by one parent cell. The total path length of a downburst family is the integrated length between the onset and the end points of downbursts in a family.

The Northern Wisconsin family was by far the longest of all families investigated by the author. Unlike tornado families, each consisting of less than 10 tornadoes, a downburst family may often include an aggregate of more than 10 downbursts/microbursts (see Table 3.3).

Table 3.3 Statistics of nine downburst families. Number of downbursts includes microbursts.

Locations	Total path length	Number of downbursts
Northern Wisconsin	166 miles	25
Chanute-Joplin, KS-MO	103	15
Danville, IL	75	23
Springfield, IL	43	27
Mattoon, IL	33	19
Earlville, IL	33	10
Rio Grande, TX-MEX	33	6
Canton, IL	26	10
Central Iowa	11	10

A LONG AND NARROW MICROBURST is often characterized by various features similar to those of tornadoes.

An example of this type of microburst is shown in Figure 3.8. The main microburst, across the picture from northwest (top) to southeast, was 1.2 miles (1.9 km) long and only 30 yds (27 m) wide (see Figure 3.9). The aspect ratio of the path is 70 to 1, very similar to that of a tornado. The estimated peak windspeed inside this path was 80 to 100 mph.

Downbursts and microbursts are often accompanied by a roar, like that of a tornado (see Figure 2.8, for example). These wind systems, when accompanied by peak winds in excess of 100 mph, will be capable of removing roofs off houses (see Figures 2.4 and 2.6), or lifting mobile homes off their foundations (see Figure 2.7).

Figure 3.8 An aerial photograph of a "long and narrow microburst" near Northwood Beach, northern Wisconsin. Refer to Color Map No.4. Eight small microbursts are seen in this picture.

Figure 3.9 A close-up view of long and narrow microburst "A".

Tornado researchers at Texas Tech University, Lubbock, Texas--Mehta et al (1971), Minor (1976), McDonald (1976)--and others have been using the straight-line wind approximation to explain successfully the nature of damages caused by tornadoes. They demonstrated that a typical, so-called "explosive" or "blow-out" damage can be caused by the dynamic pressure induced by strong, straight-line winds.

Needless to say, the pressure field of a moving tornado results in an additional rate of pressure change. Nevertheless, the rate of pressure change induced by gusty, damaging winds is so large that structures in strong downbursts and microbursts often sustain damages expected to occur only in tornadoes.

STATISTICS OF DOWNBURSTS presented in this chapter must be regarded as preliminary. Actually, about 50% of the detailed mapping was performed in Illinois because real-time damage reports were received, permitting us to perform aerial surveys without delay. However, downbursts, microbursts, and their families have been observed throughout the United States.

These results imply that the nationwide frequencies of downbursts are at least one order of magnitude larger than those included in this paper. This is true especially in case of microbursts which are not likely to be reported or confirmed unless (a) a community receives a non-tornadic, severe damage or (b) an aircraft experiences serious difficulties in a thunderstorm at low level.

CHAPTER 4. MICROBURSTS--AN AVIATION HAZARD

Microbursts, by virtue of their small horizontal dimensions, often induce strong shear of both horizontal and vertical winds. An aircraft attempting to fly through a microburst near the ground could encounter serious difficulties.

Based on investigations of four accident cases in 1975-77, we concluded that the loss of airspeed within less than 30 seconds, coupled with downward air currents, resulted in the unexpected loss of flight altitude. Most of these cases were associated with "weak-looking" afternoon summertime convection.

Characteristics of these accidents are presented in Table 4.1 along with the Kano, Nigeria accident in 1956. For details refer to Fujita (1976), Fujita and Byers (1977) for JFK, New York City; Fujita and Caracena (1977) for JFK, Denver, and Philadelphia; Caracena (1978a) for Philadelphia; and Burgess (1977) and Caracena (1978b) for Tucson accident. The Kano accident was reported by Her Majesty's Stationery Office, London (1957).

Table 4.1 List of five accident cases attributed to strong wind shear inside microbursts, 2.8 to 5.2 km (1.8 to 3.2 miles) in horizontal dimensions. The 1956 accident occurred at Kano, Nigeria. He, Ta, and Do in wind shear denote headwind, tailwind, and downward wind, respectively.

Years	1975	1975	1976	1977	1956
Dates	June 24	August 7	June 23	June 3	June 24
Local time	3:05 pm	4:11 pm	4:12 pm	12:59 pm	5:23 pm
Airport	JFK	Denver	Philadelphia	Tucson	Kano
Airlines	EA 66	CO 426	AL 121	CO 63	BOAC 252/773
Fl Phase	Landing	Takeoff	Landing	Takeoff	Takeoff
Fatalities	112	zero	zero	zero	32
Injuries	12	15	106	zero	7
Downburst dimensions	4.1 km 2.5 mi	5.0 km 3.1 mi	2.8 km 1.8 mi	3.1 km 1.9 mi	3.5 km 2.2 mi
Wind shear	16 kts He to 13 Do	10 kts He to 50 Ta	65 kts He to zero	30 kts He to 30 Ta	20 kts He to strong Ta

JFK AIRPORT, New York City on June 24, 1975.

While aircraft were landing at 1- to 2-minute intervals, three downburst cells moved across the glideslope of the active runway 22-L. The first cell, approximately 4 km across, passed over the approach end of the runway without affecting landing operations.

The second cell, 7 km across, induced a 50 kt crosswind from the west which was experienced by Flying Tiger on its final approach. One and one-half minutes later, Eastern 902 was pushed down while drifting toward the west. The wind shear was so strong that the aircraft abandoned the approach.

The third cell, 4 km across, caused a 20-kt drop of indicated airspeed and heavy sink at 1502 EST when an N-240 Beech landed. Three minutes later, Eastern 66 crashed 2,400 ft (730 m) short of the runway.

The tower winds, measured at the location 2 km south-southwest of the approach end of 22-L, were not affected by any of these micro-downbursts. The outflow of these microbursts were held back to the north of the runway area by a sustained sea-breeze front. The peak tower wind occurring at 1456 EST was SSW at 16 kts (see Figure 4.1).

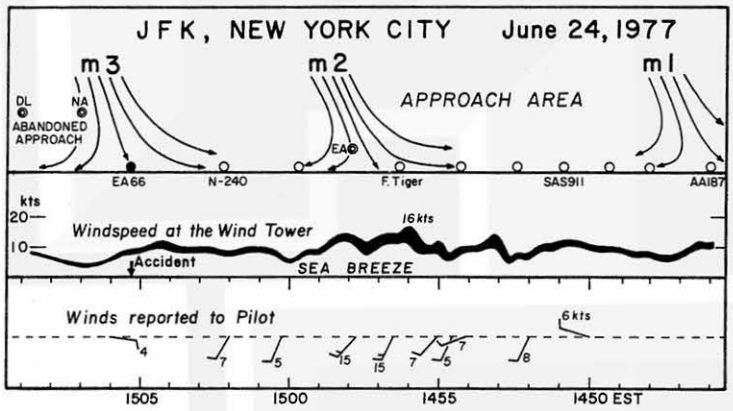

Figure 4.1 Time variations of winds at the wind tower, 2 km southwest of the approach end of 22-L. These winds were reported to the pilots during their final approach to 22-L.

Circles in the upper diagram denote the landing aircraft. The three abandoned approach.

The three aircraft that abandoned approach are identified as DL, NA, and EA.

DENVER AIRPORT on August 7, 1975.

The wind tower at Stapleton Airport, Denver was located 0.3 km to the east of the south end of runway 35-L. Prior to the Continental 426 takeoff, the tower reported a 12-kt crosswind from the southwest (see Figure 4.2).

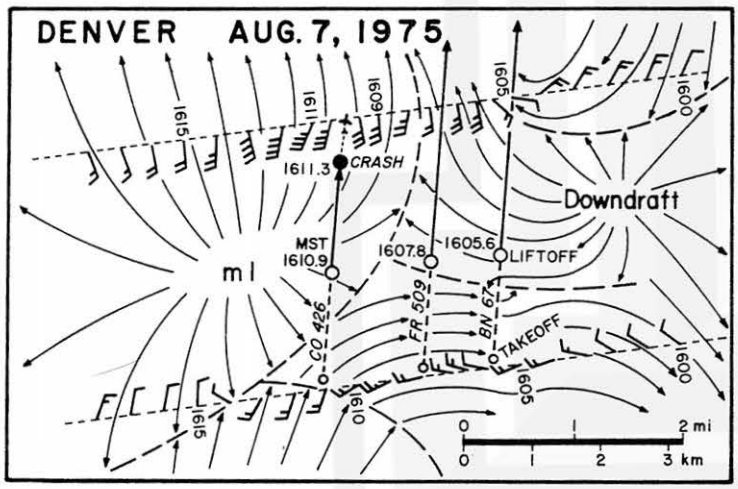

Figure 4.2 Paths of three aircraft that took off from runway 35-L of Stapleton Airport on August 7, 1975.

This diagram was constructed by converting time variation of winds from the wind tower at Stapleton and that of the Rocky Mountain Arsenal located 300 m east of the south end and 700 m northwest of the north end of 35-L, respectively.

Continental 426 took off at 1610.3 MST, heading north on runway 35-L, in 12-kt tailwind. Aircraft, then, crossed the outflow boundary of microburst, m1. After experiencing a brief headwind the aircraft lifted off at 1610.9 MST.

About 10 seconds later, while climbing 30 m (100 ft) above the runway, airspeed dropped from 158 to 116 kts in 5 seconds. The captain lowered the nose to 10° pitch, but the aircraft continued to descend onto the ground.

Apparently, the aircraft flew into the tailwind region of a microburst which developed rapidly in less than 10 minutes. At about 1615 MST the wind tower began detecting the outflow winds from the microburst. Since the accident aircraft took off at 1610 MST and crashed about one minute later, the wind shift at the tower was too late for assessing the outflow situations.

The horizontal dimension of the downburst involving this accident was 5.2 km or 3.1 miles. It was a microburst by definition. The wind shear induced by the microburst along the flight path was 10-kt headwind to 50-kt tailwind. This wind shear was experienced by the aircraft during the most critical period of the climbout.

PHILADELPHIA AIRPORT on June 23, 1976.

The wind tower was located 2.2 km to the west-southwest of the approach end of runway 27-R. Analyses of gust recorder and triple register traces (see Figure 4.3) revealed the passage of a gust front at 1606 EST.

There were two peaks of rainfall intensity. Apparently, the recording equipment was located near the edge of the Rain 2 area, because sunshine was also recorded during the rain.

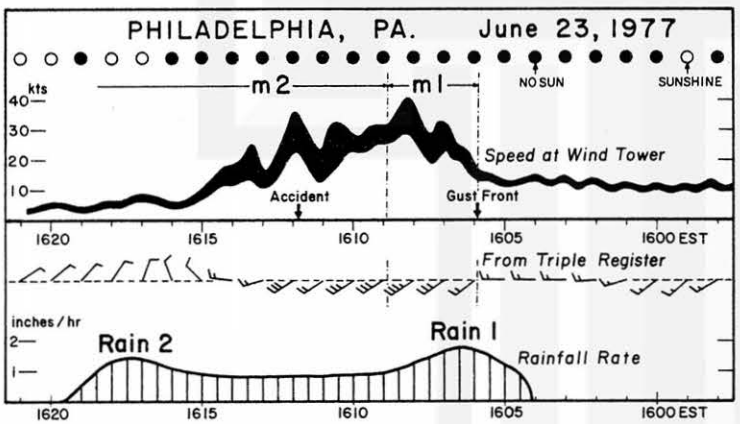

Figure 4.3 Variation of weather elements at the wind tower, 2 km south-southwest of the approach end of 27-R. 10 to 13 kt winds prevailed prior to the gust front at 1606 EST.

Allegheny 121 flew through Rain 1 from east to west encountering a 65-kt wind shear within one kilometer.

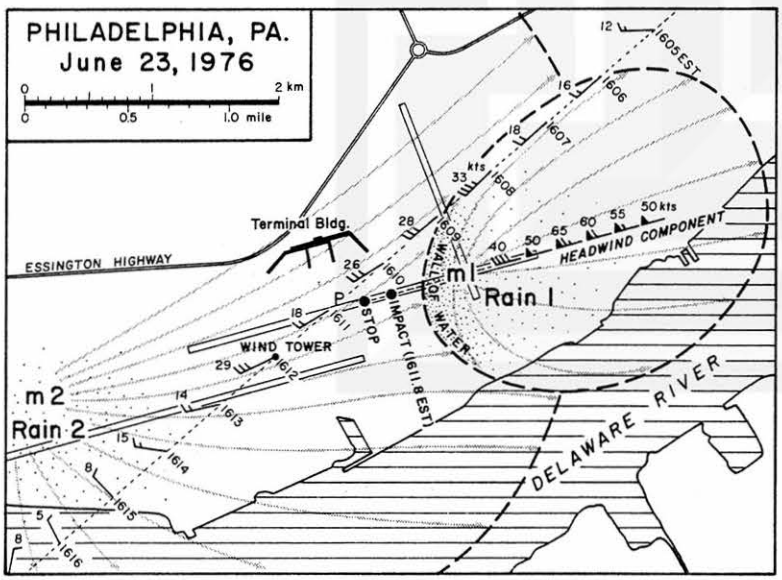

Figure 4.4 The path of Allegheny 121 in relation to two microbursts, m1 and m1, associated with two cores of heavy rain, 1 and 2.

Captain Bonn, waiting at P on taxiway "Charlie", saw the aircraft emerge from "a wall of water" between 75 and 125 ft above the surface. The aircraft sank onto the runway and skidded toward him, narrowly missing his aircraft. From Caracena (1978a).

As shown in Figure 4.4, Allegheny 121 was on final approach to 27-R when headwind increased to over 60 kts. The groundspeed dropped to 100 kts. In response to the pilot's decision to abandon approach, the aircraft started its climb from the height of approximately 18 m (60 ft) above the approach end of the runway. At 79 m (260 ft) above the runway, the headwind was gone, and the aircraft sank onto the runway.

The microburst as analyzed by Caracena (1978a) was only 2.8 km or 1.8 miles in horizontal dimensions. Nevertheless, the wind shear inside the microburst was as large as 65 kt within 1.0 km or about 3 kts/sec.

TUCSON AIRPORT on June 3, 1977.

Associated with a large build up of convective clouds to the south of Tucson Airport, a gust front moved across the wind tower at 1250 MST. The front was followed by a blinding dust storm with southwest winds gusting up to 49 kts (see Figure 4.5).

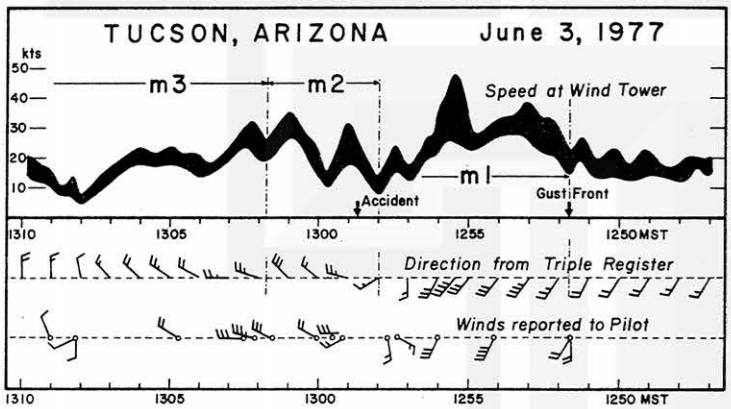

Figure 4.5 Time variation of winds at the wind tower, 500 m east of the terminal building. Continental 63 took off at 1258 MST when the outflow from microburst m2 was about to reach the wind tower. The peak gust at the tower, occurring at 1301 MST, was 36 kts. Wind direction at the wind tower shifted gradually because the microburst was 1.5 km away. (Each wind barb in the figure denotes 10 kts.)

According to an analysis by Burgess (1977) and Caracena (1978b), Continental 63 took off toward the southwest on runway 21 at 1258 MST. Although the tower wind, then, was south to southwest at only 11 kts, the aircraft took off in a 20- to 30-kt headwind. The tower was located 900 m south of the departure end of runway 21 (see Figure 4.6).

The dust storm behind the gust front was moving away from the aircraft at its takeoff position. While rolling down runway 21, crossing runway 29, the head wind changed into an 11- to 13-kt crosswind from the northwest. Upon liftoff, both crosswind and tailwind intensified. Eyewitnesses saw a second area of blowing dust in the direction of the aircraft as it was lifting off.

The aircraft did not gain altitude while flying through an estimated 50-kt wind from the north (34-kt crosswind and 37-kt tailwind). A few seconds after lifting off, the aircraft hit wires along Nogales Highway. Thereafter the aircraft gained altitude while making a gradual left turn for an emergency landing on runway 29.

The location of this wire impact was 5 km behind the gust front, and 3 km behind the peak gust accompanied by a blinding dust storm. This time, again, the aircraft flew through two microbursts, m 1 and m 2, which produced strong tailwind shear. The total variation of winds was 60 kts (30-kt headwind to 30-kt tailwind) within a 2.2-km distance.

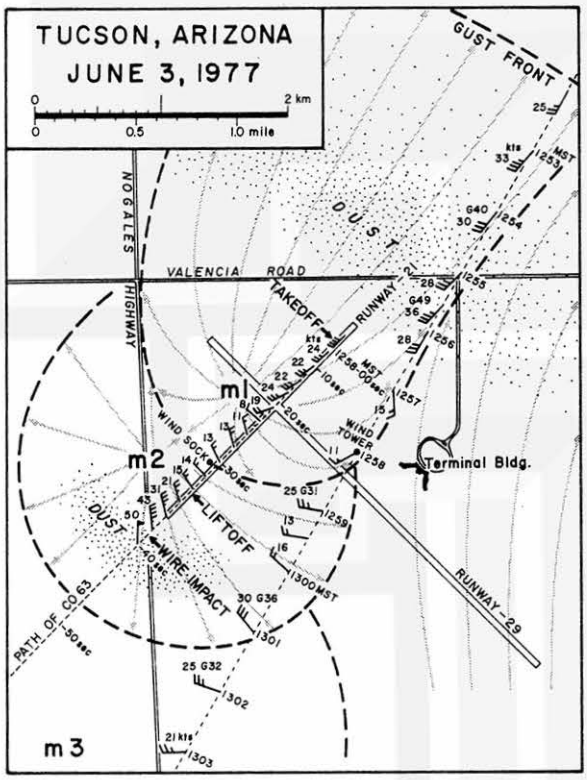

Figure 4.6 Two microburst cells, m1 and m2 analysed by Caracena (1978b). Continental 63 took off toward the southwest against a 30-kt headwind behind a zone of peak gust accompanied by blinding dust. The aircraft, then, encountered strong tail winds as it was flying through downburst m2.

FLIGHT PATHS of the four accident aircraft described herein were summarized in Figure 4.7 along with the path of BOAC 252/773 at Kano Airport in 1956.

In all 5 cases, the aircraft encountered serious difficulties during their flights below 100 m (300 ft). Apparently, the loss of airspeed near the downburst center was the most important cause of such difficulties. Furthermore, strong downward currents as experienced by Eastern 66 and 902 at JFK present an additional problem in gaining altitude inside strong downbursts.

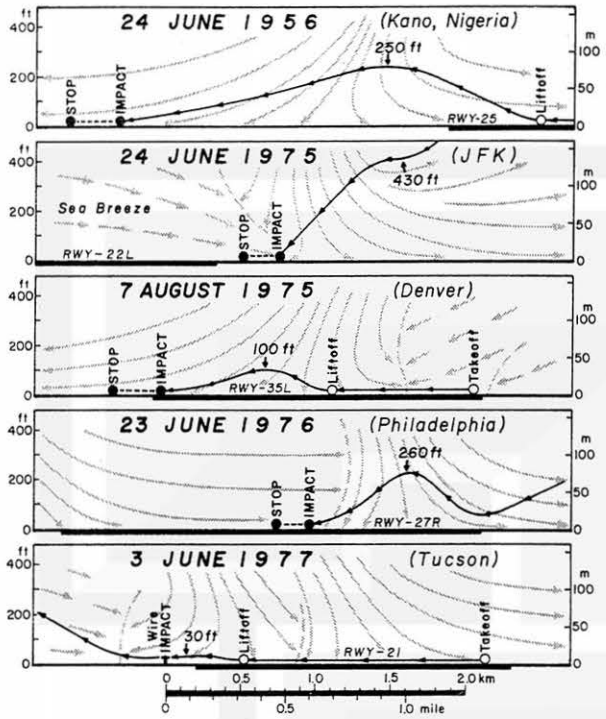

Figure 4.7 Summary of the five flight paths in a vertical plane. In all of these cases, strong horizontal shear and strong downward motion on scales of only a few kilometers were observed.

HORIZONTAL DIMENSIONS of microbursts in relation to simplified paths of 5 aircraft are shown in Figure 4.8. Each square box in the figure represents a 10-mile square area around the accident site.

It is seen that microbursts under discussion are extremely small compared to the average distance between meteorological observing stations.

Figure 4.8 also includes 2 microbursts which caused a $20,000,000 damage in Danville, Illinois on September 30, 1977 (refer also to Color Map No. 6). The dimensions of these microbursts were comparable to those involved in the aircraft accidents discussed in this chapter.

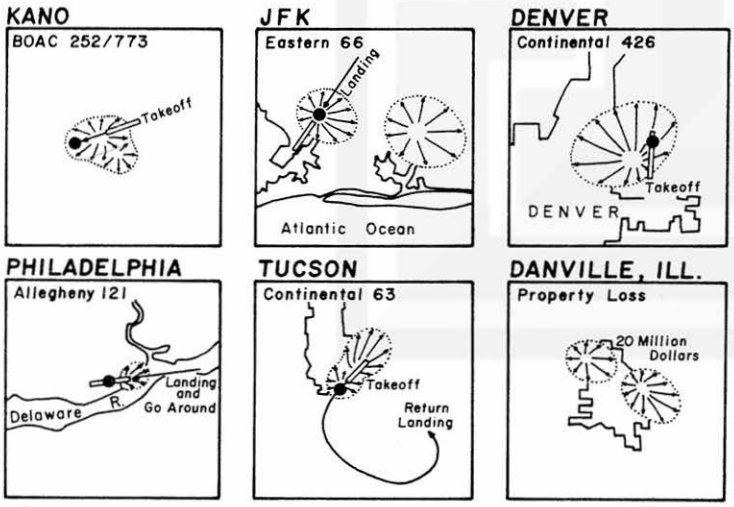

Figure 4.8 Summary charts of aircraft positions in relation to microbursts. Each box represents a 10-mile by 10-mile square.

Aircraft during either landing or takeoff phase could seriously be affected by a downburst with its horizontal dimensions comparable to the runway length.

CHAPTER 5. RADAR ECHO CHARACTERISTICS

Investigation of radar echoes for downburst situations in Color Maps 1 through 8 revealed that most downbursts were accompanied by two types of echoes which were identified as "hook" and "bow" (see Figure 5.1). The hook echo was first detected by Stout and Huff (1953) and has sometimes been associated with tornadoes. The bow echo has been named by the author because of its distinct shape, like that of a bow or crescent.

The preferable location of downbursts appears to be in and around the hook which is detectable with PPI scan at low levels, usually below 10,000 ft. As the elevation angle is increased, the reflectivity center shifts toward the center of the rotation which is topped by the dome of a tall echo as observed by Bigler (1958) with a CPS-9 radar at College Station, Texas.

Relative to the PPI echo at high level, downbursts are likely to occur on the right side of the reflectivity center.

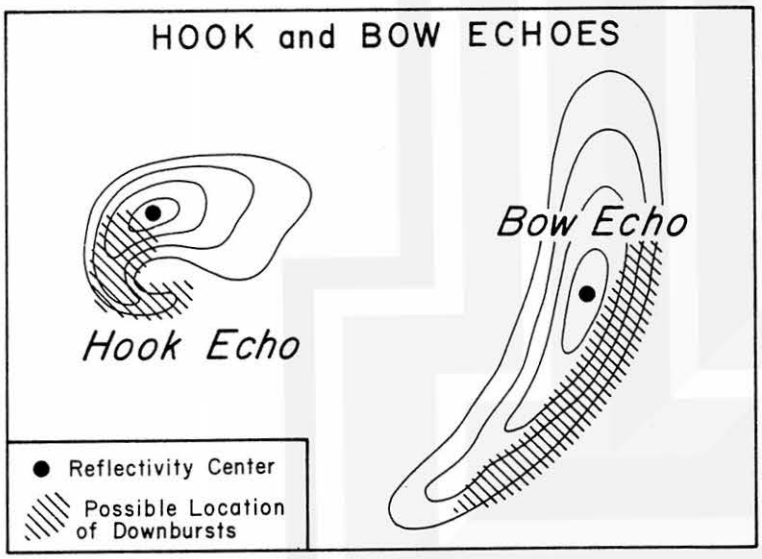

Figure 5.1 Hook and bow echoes commonly observed during downbursts. A Line Echo Wave Pattern (LEWP) often includes a fast moving bow echo. The maximum reflectivity within a bow echo is frequently seen on the left side of the bow center.

BOW ECHO is often embedded within the Line Echo Wave Pattern called by Nolen (1959). Hamilton (1970) pointed out that a bulge or concave-shaped echo within LEWP is closely related to damaging winds on the ground. He noted that the echoes on the bulge move faster than those near both edges, resulting in an arc-shaped configuration. The bow echo is Hamilton's bulge which can be identified and followed on a PPI scope a considerable distance from the radar site.

Combined analyses of surface damage and bow-echo configurations revealed that the possible location of downbursts is on the advancing side of the echo. As expected, the most intense downbursts are likely to occur near the forward center of the bow.

LIFE CYCLE of a bow echo can be described as a gradual transition from a large, strong, and tall echo to a bow which often turns into a "comma-shaped echo" (see Figure 5.2).

Although initial downbursts (DB) begin inside a large, strong, and tall echo (Figure 5.2. A), the downburst intensifies as a distinct bow echo develops. When the maximum downburst intensity is reached (Figure 5.2. C), the bulge of the bow becomes so eminent that the echo appears somewhat like a broken bow or spearhead.

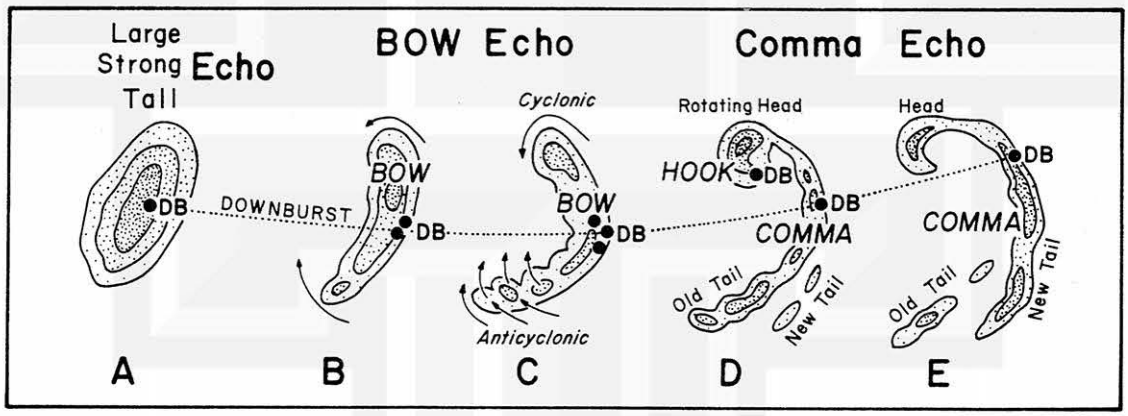

Figure 5.2 A typical morphology of radar echoes associated with strong and extensive downbursts. Some bow echoes disintegrate before turning into comma echoes. During the period of strongest downbursts, the echo often takes the shape of a spearhead or a kink pointing toward the direction of motion.

Both cyclonic and anticyclonic motions of small echoes are seen near the ends of the bow. Although the anticyclonic motion does not amplify with time, cyclonic rotation on the left side often turns into a rotating head.

A bow echo with a rotating head displays the impressive shape of a comma. The head, by virtue of its rotation, often induces a hook accompanied by weak downbursts.

Usually a comma echo appears during the weakening stage of downbursts (Figure 5.2. E). The tail of a comma extends over a long distance while swinging cyclonically like a hurricane rainband. The end of the comma tail cannot always catch up with the fast swing. Thus, a new tail forms on the advancing side of the old one. Eventually, the old tail is left behind, being overshadowed by the new tail.

BOW ECHO OF NORTHERN WISCONSIN DOWNBURSTS appeared on Minneapolis radar about one hour before the first downburst began in eastern Minnesota (see Figures 5.3 and 5.11). In fact, the Mille Lacs resort area in eastern Minnesota was hit hard before 11 CST, about two hours in advance of the Wisconsin downbursts.

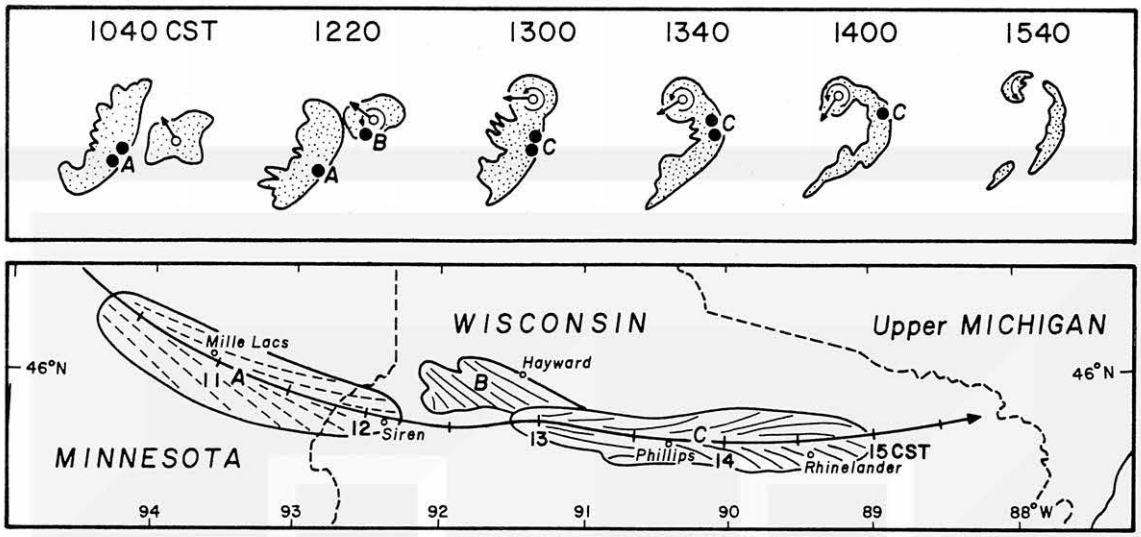

Figure 5.3 Evolution of a bow echo into a comma echo during the 4th of July, 1977 downbursts in Northern Wisconsin. Downbursts "A" and "C" were associated with a bow echo while "B" was associated with a hook echo. Motion of the hook echo is relative to the bow echo. No tornado was associated with this storm.

When the bow echo was advancing across eastern Minnesota, a small, irregular-shaped echo approached the north end of the bow echo. It, then, began rotating cyclonically while moving around the north end of the bow echo. Finally, the small echo turned into a rotating head while the bow echo was rapidly becoming a comma echo.

Three groups of downbursts identified as A, B, and C swept across eastern Minnesota and northern Wisconsin. Both A and C were induced by a bow echo, while B occurred to the southwest of the rotating head, where a hook is expected. An examination of Color Map No. 4 reveals the existence of a distinct flow boundary between B and C in central Sawyer County. It should be pointed out that the overall intensity of C was much stronger than that of B.

Shown in Figure 5.4 are radar pictures from Minneapolis and Neenah. At 1304 CST, downburst 5 in Color Map No. 4 has ended and downbursts 8 and 9 have descended to the east of Radisson in Sawyer County.

At 1338 CST the bow echo changed into a spearhead pointing eastward. Downbursts 18 and 19 were in progress to the west of Phillips in Price County. This was the peak intensity time during the Northern Wisconsin downbursts.

Weakening downbursts swept across Rhinelander, in Oneida County, at 1430 CST. The anemometer of North Central Airlines was blown away after registering 100-kt gust.

A comma echo at 1518 from the Neenah radar signaled the end of downburst activities.

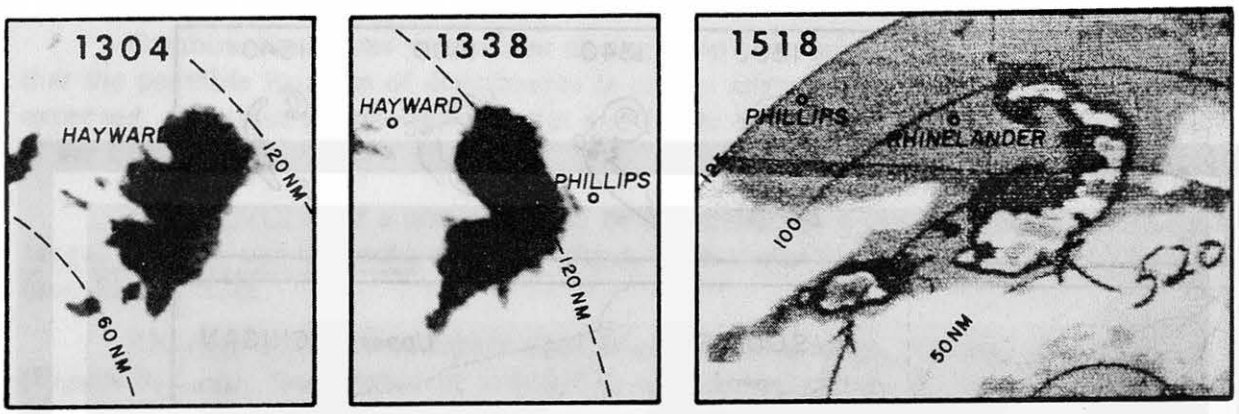

Figure 5.4 Three features of echoes during Northern Wisconsin downbursts. Downbursts No. 6 and 7 in Sawyer County (Color Map No. 4) were in progress at 1304 CST (left). Downbursts were most intense when the bow echo was spearheaded at 1338 CST (center). A comma echo at 1518 CST (right) was free from downburst. Range markers are 60 and 120 nm from Minneapolis and 25, 50, 75, 100, and 125 nm from Neenah (right).

EARLVILLE DOWNBURSTS AND TORNADOES were spawned by an early stage of a bow echo which began bulging out from an isolated line of echoes. Until 0802 CST, echoes were more or less on a straight line. During the next 20 minutes, when the line turned into a bow, the first tornado and downbursts near Earlville, Illinois occurred (see Figure 5.5 and Color Map No. 5).

The location of downbursts advanced eastward, then east-northeastward. Five tornadoes formed on the left side of downbursts 1, 2, 5, 8, 9, and 10 which apparently acted as the vorticity feeders to these tornadoes. This subject will be discussed in Chapter 7.

Downburst 4, to the southeast of Leland, was the strongest of all downbursts. No sign of a tornado was detected on the left side where strong winds simply diverged outward without curling into vortex motions.

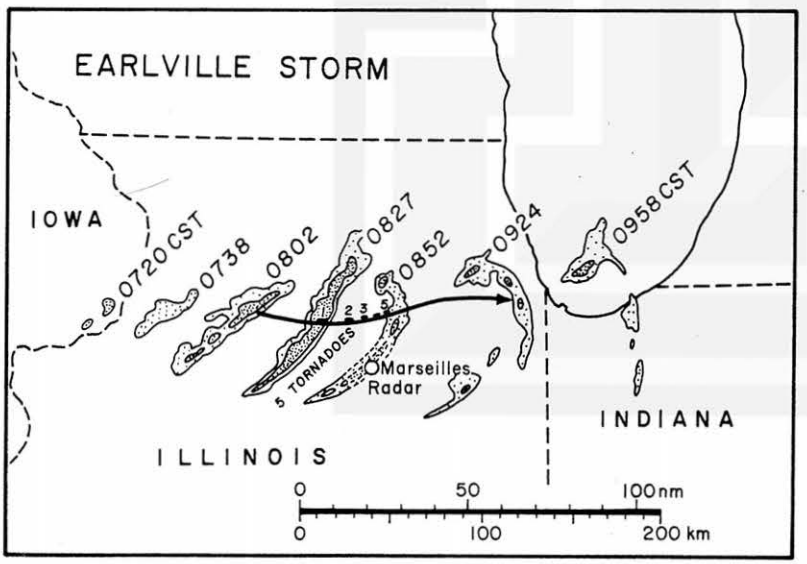

Figure 5.5 Evaluation of radar echoes associated with the Earlville downbursts and tornadoes of June 30, 1977. Refer to Color Map No. 5.

SPRINGFIELD DOWNBURSTS AND TORNADOES are rather spectacular. Forbes and Wakimoto (1977) confirmed that there were 18 tornadoes, one of which was anticyclonic (see Color Map No. 8).

Eight tornadoes formed on the left side of the downbursts while 10 others were not associated with a downburst.

Figure 5.6 reveals that the parent echo at 1341 CST was a large, strong, and tall echo. It turned into a distinct bow by 1511 CST. A rotating head on the PPI scope formed at about 1530 when the first tornado occurred.

The location of these tornadoes extended far to the south of the rotating head. Their southernmost points were more than 15 miles to the south of the rotating head, characterized by a hook-shaped echo.

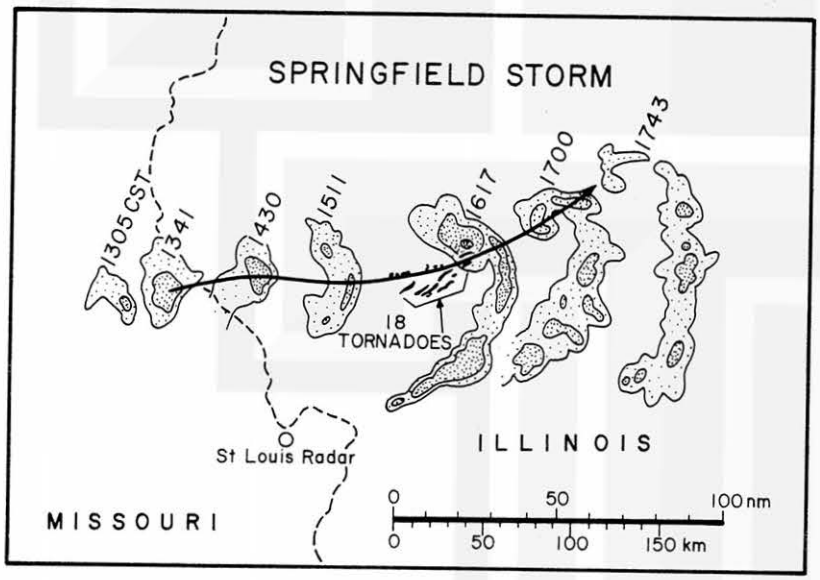

Figure 5.6 Evolution of radar echoes associated with Springfield downbursts and tornadoes of August 6, 1977. Refer to Color Map No. 8.

No severe storms were reported from the area of the tail section of the comma echo.

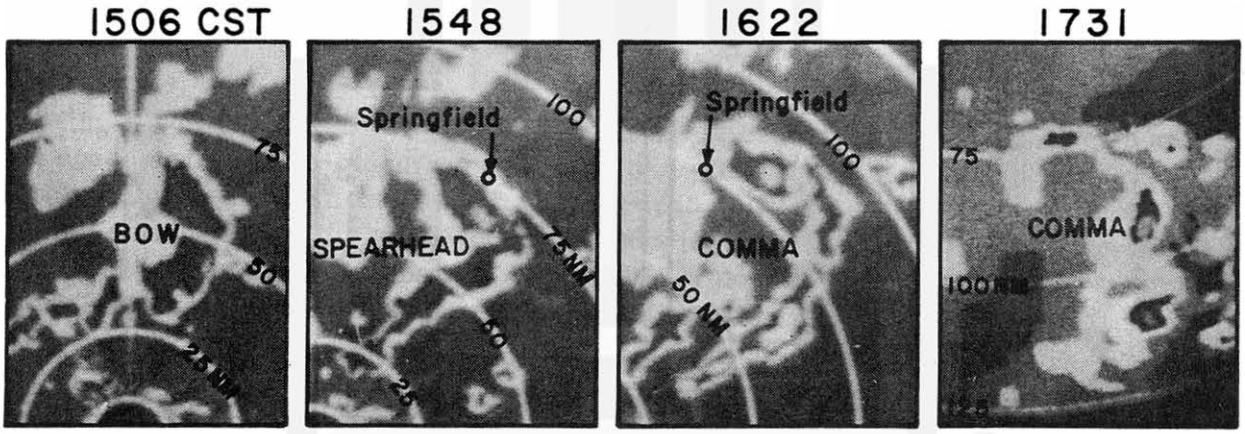

Figure 5.7 Radar pictures of Springfield storm. A bow echo is seen at 1506 CST. The bow echo was spearheaded at 1548 when downbursts were most intense. A comma echo with a rotating head is seen at 1622 when both downburst and tornado ended. Left 3 pictures were from St. Louis radar. The final stage of the comma echo was photographed by Marseilles radar at 1731 CST. Range markers are at 25 n.m. intervals.

The final stage of the Springfield storm was depicted as a comma echo, similar to that of the Northern Wisconsin and Earlville storms.

Reproduced in Figure 5.7 are radar pictures from St. Louis at 1506, 1548, and 1622 CST and from Marseilles at 1731 CST. A typical bow echo seen at 1506 turned into a spearhead shape at 1548 when downbursts reached their peak intensities.

Although there was a hook-shaped rotating head at 1622 CST, most downbursts and tornadoes ended prior to this time. The comma echo drifted toward the south of Marseilles radar. The final stage of the comma at 1731 CST is shown at the end of the sequence.

CHANUTE - JOPLIN DOWNBURSTS on May 11, 1973 began at 0430 CST to the west of Chanute, Kansas. Before ending at 0630 CST, 15 downbursts occurred, one after another, along the path of a bow echo which moved from northwest to southeast at 54 mph.

Although nobody was killed by this storm, 21 persons were injured. A trailer park several miles west of Joplin was smashed, causing injuries. Six thousand trees were uprooted in Joplin.

Shown in Figure 5.8 are near-simultaneous views of a bow echo as it was moving between Chanute and Joplin. F2 downbursts were in progress. Echoes near the south end of the bow echo were moving anticyclonically around the end. Barograph traces from Chanute and Joplin show a sign of mesoscale pressure drops, suggesting the existence of a rotation to the north of the bow-echo center.

The bow echo moved toward the southeast until it disappeared without turning into a comma echo.

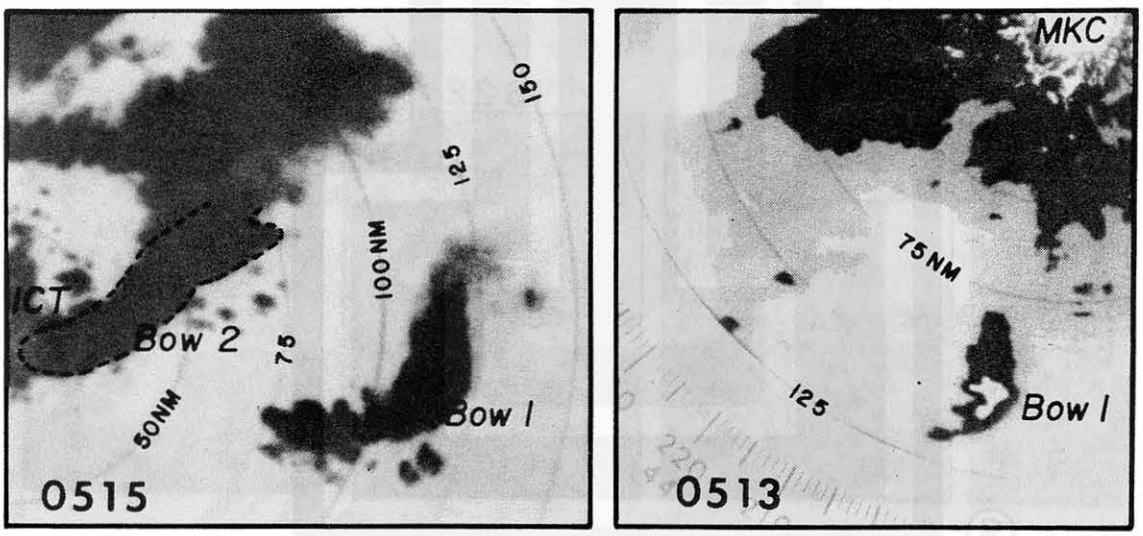

Figure 5.8 A bow echo of May 11, 1973 as photographed by Wichita radar at 0515 CST (left) and by Kansas City radar at 0513 (right) when strong downbursts were in progress northeast of Parsons, Kansas. Refer to Color Map No. 1. The second bow echo is seen in the left picture (see also Figure 5.21).

DANVILLE DOWNBURSTS of September 30, 1977 started to the northeast of Champaign, Illinois. A 20-mile long bow echo was the parent echo of these downbursts (see Figure 5.9 and Color Map No. 6).

The city of Danville received 20 million dollars damage by two strong microbursts which descended to the north and northeast of the city. Some damage was caused by hailstones which were driven by high winds against windows in shopping centers. Roof damage was seen from the air at various locations in the city.

The bow echo moved toward the southeast until it was lost outside the 125 mile range of the St. Louis radar.

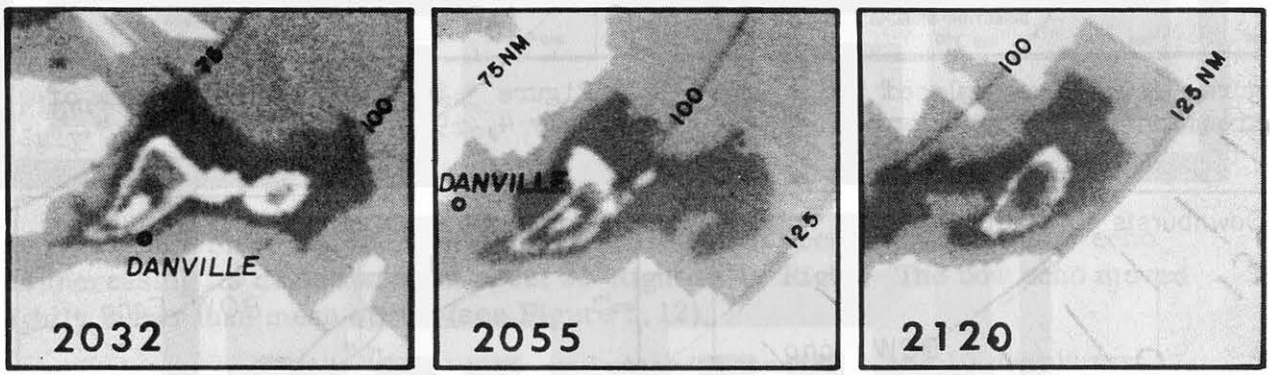

Figure 5.9 A small bow echo which induced strong downbursts in the Danville area on Sept. 30, 1977. Left picture shows the echo at 2032 CST when Danville was hit. The echo at 2055 (middle) and 2130 (right) indicates only a slight change in the shape while the direction of echo motion deviated significantly to the right. Refer to Color Map No. 6.

D - S DIAGRAM in Figure 5.10 is a key diagram with echo direction and speed as coordinates. Dots denote velocities of individual echoes during 20 to 60 minutes preceding the onset of a storm. The origin at the intersection of mean direction and mean speed of these pre-storm echoes permits us to determine the deviation (left or right) and the speed (fast or slow) of a storm echo relative to the mean velocity. Figure 5.10 also shows the time-dependent velocity of a storm echo which is called the "echo hodograph" in this paper. Intensities of downbursts and tornadoes are shown along the echo hodograph as a function of time.

The echo hodograph (see Figure 5.11) of the northern Wisconsin bow echo reveals the maximum deviation of 59° Right at 1020 CST when downbursts began in eastern Minnesota. Then the echo deviation decreased to about 22 right prior to the onset of the Northern Wisconsin downbursts. F 2-scale downbursts were in progress when the echo deviated again to a maximum of 31 right.

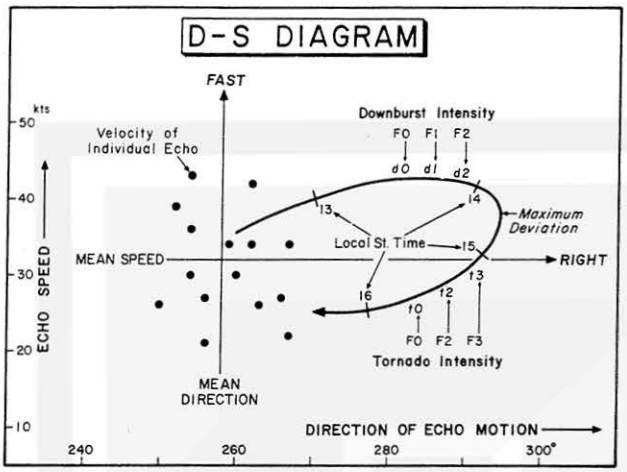

Figure 5.10 An example of D-S (Direction vs Speed) diagram.

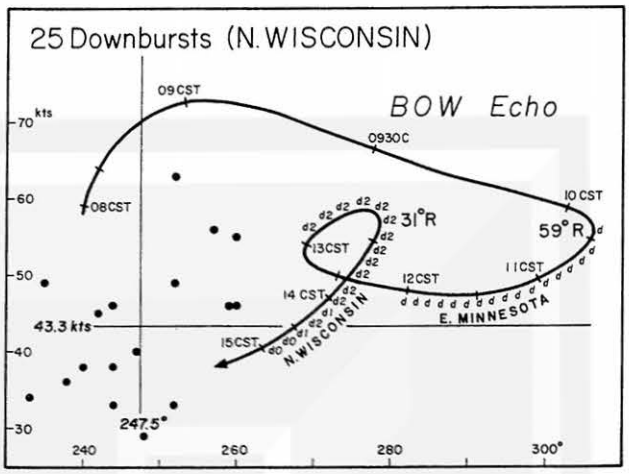

Figure 5.11 N. Wisconsin storm of July 4, 1977 in Color Map No. 4.

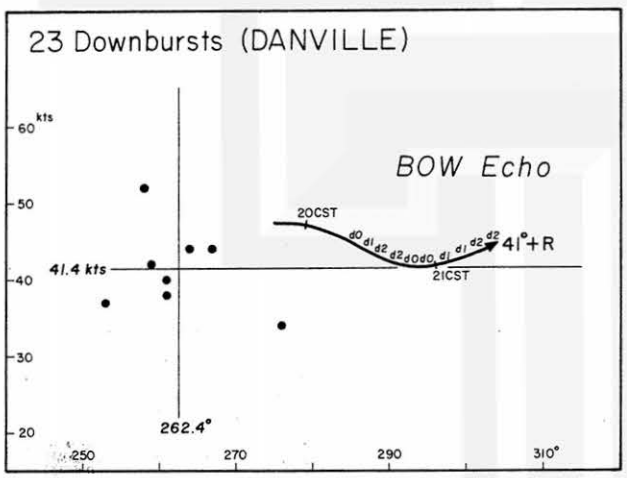

Figure 5.12 Danville storm of Sept. 30, 1977 in Color Map No. 6.

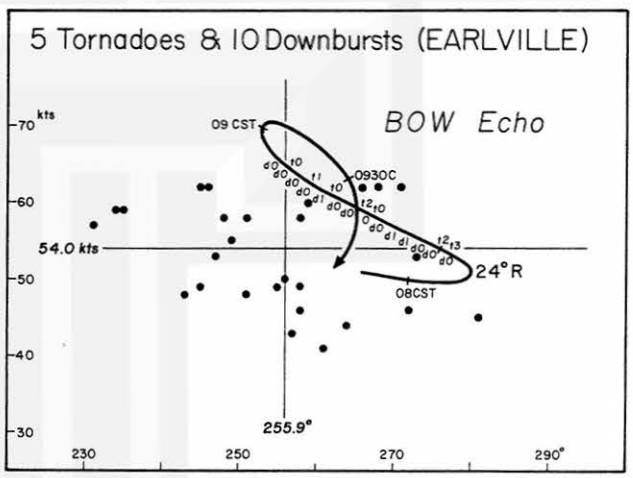

Figure 5.13 Earlville storm of June 30, 1977 in Color Map No. 5.

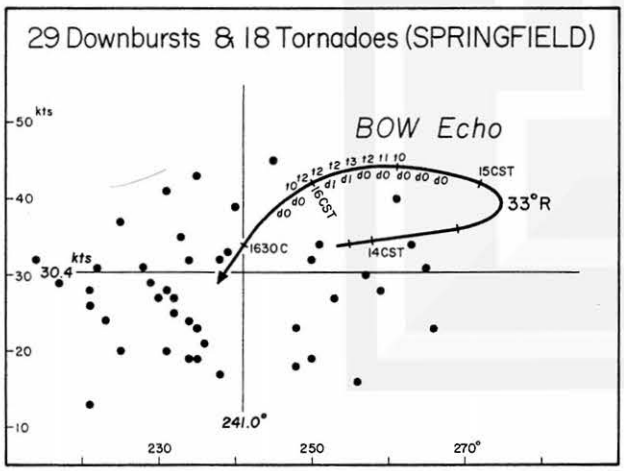

Figure 5.14 Springfield storm of August 6, 1977 in Color Map No. 8.

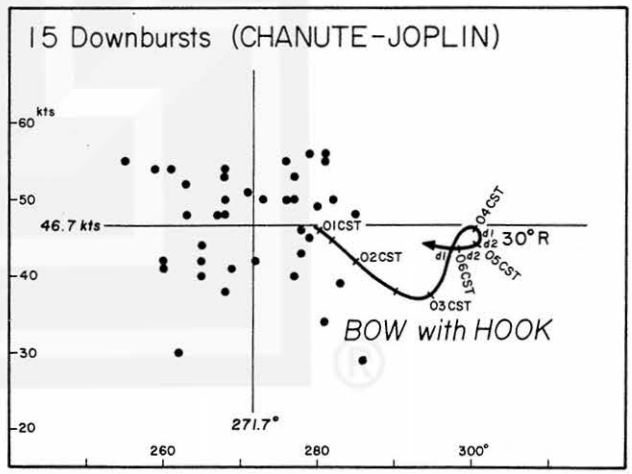

Figure 5.15 Chanute-Joplin storm of May 11, 1973 in Color Map No. 1.

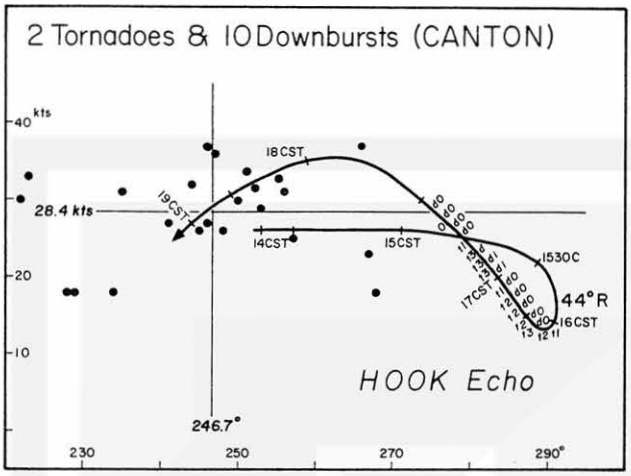

Figure 5.16 Canton storm of July 23, 1975 in Color Map No. 7.

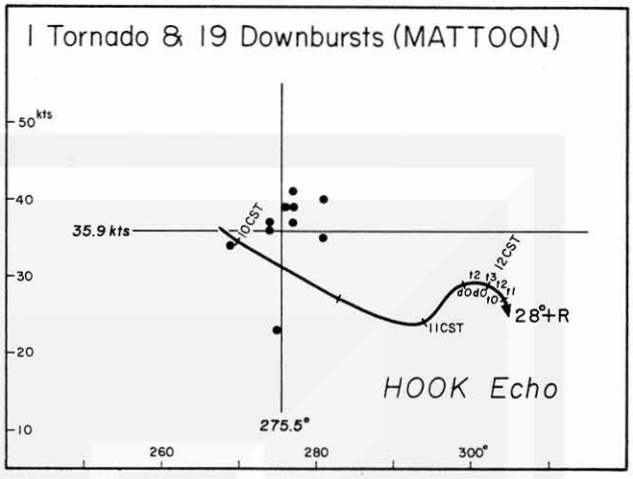

Figure 5.17 Mattoon storm of August 21, 1977 in Color Map No. 2.

Twenty-three downbursts of the Danville storm occurred when a bow echo was increasing its deviation from about 22° Right to 41° Right. The bow echo moved slightly faster than mean speed (see Figure 5.12).

A bow echo of the Earlville storm induced 5 tornadoes and 10 downbursts shortly after it reached a 24° Right deviation. The storm continued until the deviation became near zero while moving 10 kts faster than mean speed (see Figure 5.13).

Springfield downbursts started about 30 min after a bow echo reached the maximum deviation of 33° Right. The storm continued until the deviation decreased to only a few degrees (see Figure 5.14).

Chanute - Joplin echo deviated to the maximum of 30° Right. Downbursts started shortly before this maximum deviation was reached (see Figure 5.15).

The parent storm of the Canton storm (see Color Map No. 7) was a hook echo which deviated 44° Right shortly before the first tornado occurred at 1600 CST. The echo hodograph is characterized by an elongated loop. Tornadoes and downbursts occurred while the deviation angle was decreasing to about 25° Right (see Figure 5.16).

Mattoon tornado and downbursts were associated with a typical hook echo. It deviated 28° Right when the tornado ended. The first downburst occurred when the deviation was 24° Right. The tornado occurred some 10 minutes later (Figure 5.17).

HODOGRAPHS of 4 BOW ECHOES were located predominantly inside the upper right sector of the D - S diagram. This would suggest that bow echoes have a tendency to move fast while deviating to the right (see Figure 5.18).

HODOGRAPHS OF 3 HOOK ECHOES are seen in the lower right quadrant of the D - S diagram. It has been known during the past 25 years that hook echoes move slower than the mean echo speed while deviating to the right. Numerous documentations of the right deviation and slow movement of hook echoes are available.

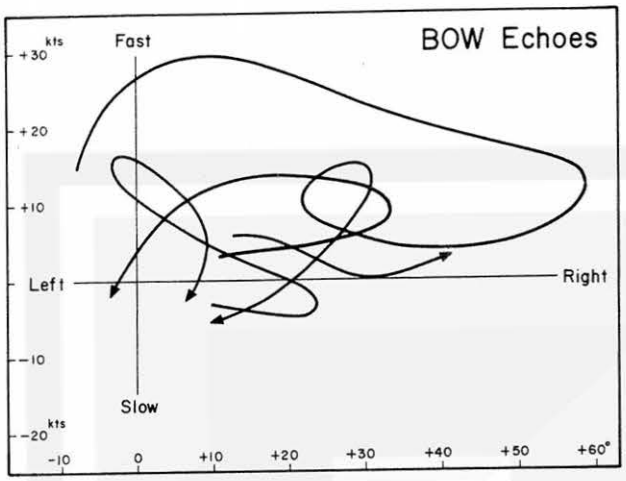

Figure 5.18 Evolution of bow echoes plotted on a D-S diagram. Their deviations are predominantly in the upper-right quadrant, indicating that bow echoes deviate to the right and move fast.

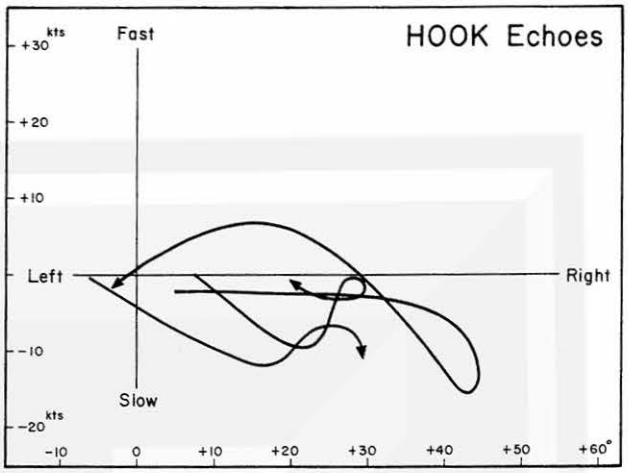

Figure 5.19 Evolution of hook echoes plotted on a D-S diagram. Their deviations are predominantly in the lower-right quadrant, indicating that hook echoes deviate to the right and move slow.

It is important to realize that both bow and hook echoes deviate equally to the right of the mean echo direction. The latter, however, moves slower than the mean speed while the former moves faster.

LEAD TIME BEFORE TORNADO AND DOWNBURST OCCURRENCES can be computed after the fact based on various deviation angles, because hook and bow echoes deviate to the right prior to the onset of these storms. But deviation does not always mean that tornado or downburst will occur, and some tornadoes and downbursts could occur without deviation.

An attempt was made to compute the lead time based on the 7 situations in color maps. Presented in Table 5.1 are the times of 15°, 20°, and 25° Right deviations along with those of the first and the last tornadoes and downbursts. This table can be used in computing the lead time of specific deviation angles before tornado and downburst.

Lead times of 15° Right deviation before tornado and downburst are presented in Table 5.2. The lead times before the first tornado and the first downburst are 71 min and 68 min, respectively. The lead times before the last tornado and downburst are naturally much longer than those before the first storms.

It should be pointed out that lead time increases when touch-down time is estimated to be later than it actually was. Detailed aerial surveys almost always extend the reported storm's path toward both directions, resulting in earlier touchdown and later liftoff times. This is why well-surveyed cases were used exclusively in computing the lead time.

Lead times of 20° Right and 25° Right deviations before the storms were also computed and presented in Tables 5.3 and 5.4. These tables reveal an appearance of negative lead times when the deviation angle was increased beyond about 20° Right.

Table 5.1 Times (CST) of the first 15°, 20°, and 25° Right deviations of echo velocities. Deviation angles were measured from the mean echo motion prior to storms. First T. and Last D. denote the first tornado and the last downburst during each storm situation.

	15°R	20°R	25°R	First T.	Last T.	First D.	Last D.
Chanute-Joplin	0210	0240	0315	none	none	0430	0625
Mattoon	1035	1110	1140	1140	1230	1130	1230
N. Wisconsin	0910	0915	0925	none	none	1020	1500
Earlville	0800	0810	0815	1820	0850	0820	0855
Danville	1950	2010	2030	none	none	2015	2145
Canton	1440	1450	1500	1610	1720	1555	1740
Springfield	1340	1410	1415	1530	1615	1510	1620

Table 5.2 Lead times in minutes of tornadoes and downbursts measured from the first 15° Right deviation of parent echoes.

Storms	First T.	Last T.	First D.	Last D.
Chanute-Joplin	not applicable		140	255
Mattoon	65	115	55	115
N. Wisconsin	not applicable		70	350
Earlville	20	50	20	55
Danville	not applicable		25	115
Canton	90	160	75	180
Springfield	110	155	90	160
Mean	(71 to 120 min)		(68 to 176 min)	

Table 5.3 Lead times in minutes of tornadoes and downbursts measured from the first 20° Right deviation of parent echoes.

Storms	First T.	Last T.	First D.	Last D.
Chanute-Joplin	not applicable		110	225
Mattoon	30	80	20	80
N. Wisconsin	not applicable		65	345
Earlville	10	40	10	45
Danville	not applicable		5	95
Canton	80	150	65	170
Springfield	80	125	60	130
Mean	(50 to 99 min)		(48 to 156 min)	

Table 5.4 Lead times in minutes of tornadoes and downbursts measured from the first 25° Right deviation of parent echoes.

Storms	First T.	Last T.	First D.	Last D.
Chanute-Joplin	not applicable		75	190
Mattoon	0	50	-10	50
N. Wisconsin	not applicable		55	335
Earlville	5	35	5	40
Danville	not applicable		-15	75
Canton	70	140	55	160
Springfield	75	120	55	125
Mean	(37 to 86 min)		(31 to 139 min)	

Finally, the range, mean, and worst lead times before tornadoes and downbursts are shown in Table 5.5. For 26 tornadoes, the mean lead time was 95 min from the first 15°Right, 75 min from 20°Right, and 61 min from 25°Right deviations. By limiting statistics only to the first tornadoes, lead times become much shorter; 71 min from the first 15°Right, 50 min from 20°Right, and 37 min from 25°Right deviations.

Based on Doppler measurements at NSSL, Lemon et al (1977) reported lead time of tornadic mesocyclones before tornadoes to be 36 min and before maxi-tornadoes to be 41 min.

Table 5.5 Range, mean, and worst lead times before tornadoes and downbursts from the first deviation angles of parent eches. All tornadoes and downbursts in 7 situations in Table 5.1 were used in compiling statistics.

Storms	15° Right	20° Right	25° Right
26 Tornadoes	71 to 120 min	50 to 99 min	37 to 86 min
	mean 95 min	mean 75 min	mean 61 min
	worst 20 min	worst 10 min	worst 0 min
157 Downbursts	68 to 176 min	48 to 156 min	31 to 139 min
	mean 122 min	mean 102 min	mean 85 min
	worst 20 min	worst 5 min	worst -15 min

Lead times are extremely important in assessing predictability of tornadoes and downbursts. Thus, it is necessary to obtain various lead times based on the specific aspects of storms. Such an attempt will, hopefully, increase the warning time while suppressing over warning. The following items should be useful in predicting tornadoes and downbursts:

1. Reflectivity level of echo
2. Characteristic shape at different levels
3. Echo size and height
4. Rotational velocity by Doppler radar
5. Translational velocity by echo tracking
6. Satellite tracked cloud velocity
7. IR temperature of cloud top
8. Characteristics of anvil cloud

Items 1 through 5 can be achieved primarily by radar, while items 6 through 8, by geostationary satellite. Ultimately, we will have to combine above items, because individual items are likely to cause uncertainties, no matter how promising they may appear to be. Operational evaluations will be needed to determine lead times better and to ascertain warning criteria.

MOTIONS OF SMALL ECHOES relative to bow echo were computed for the purpose of estimating the flow around the bow echo. In reality, however, no echoes move with environmental winds.

Small echoes of convective origin move approximately with the mean wind between the cloud base and the top. Rain showers from stratified clouds travel with their sources at higher levels. Therefore, the tracer echoes must be limited as much as possible to small convective echoes characterized by well-defined, circular or elliptic boundaries.

The relative motion of small echoes in Figure 5.20 shows that the bow echo of the Northern Wisconsin downbursts acted as an obstacle moving at 54 kts from the 305 direction. An irregular-shaped echo was approaching at 21 kts from the southwest, toward the north end of the bow echo. While approaching the bow echo, the echo began rotating cyclonically.

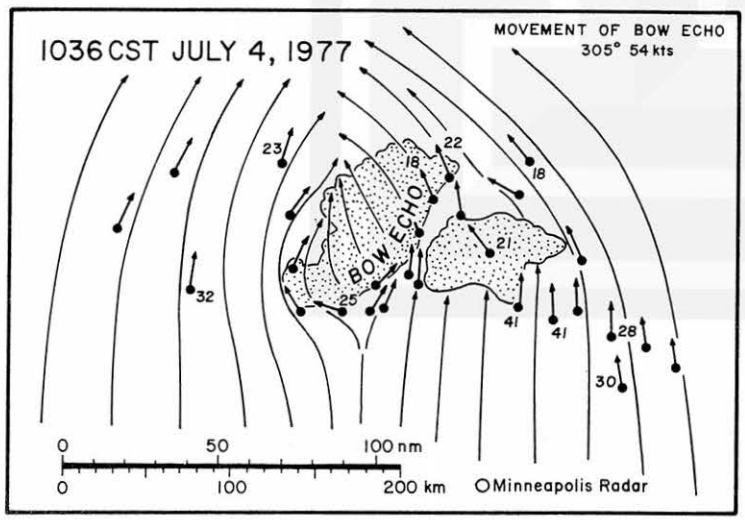

Figure 5.20 Relative motion of echoes with respect to the Northern Wisconsin bow echo at 1036 CST July 4, 1977.

RELATIVE FLOWS around three bow echoes of the Chanute - Joplin storm were very similar to those of the Northern Wisconsin case. It was bow echo 1 which induced the downbursts in Color Map 1. Bow 2 was rather weak, but it caused heavy damage later in northwest Arkansas. Bow 3 remained weak, lasting only for a short time.

These examples reveal that the wake flow behind bow echoes are caused by the relative motion between drifting small echoes and fast-moving bow echoes. The direction of a bow-echo often coincides with the wind direction at the tropopause, suggesting that the high-level momentum is transported downward inside an active bow echo.

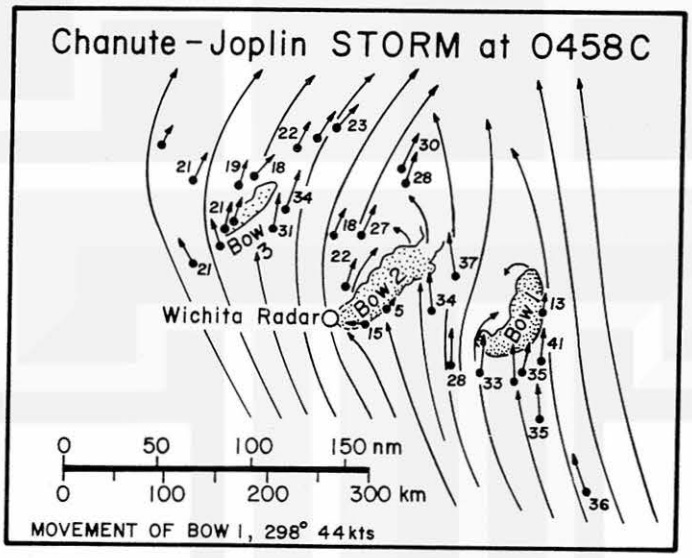

Figure 5.21 Relative motion of echoes with respect to the Chanute-Joplin bow echoes at 0458 CST May 11, 1973.

This is probably why bow echoes tend to move faster than other echoes, while deviating to the right of the mean wind. Another important evidence is the warming of cloud-top temperature during downburst. This subject will be discussed further in Chapter 6.

CHAPTER 6. INFRARED IMAGERY FROM GOES/SMS

The Geostationary Operational Environmental Satellite (GOES) System, which includes the Synchronous Meteorological Satellite (SMS), provides meteorologists with both visible and infrared data.

Visible pictures with 1-km resolution and infrared pictures with 8-km resolution were examined in an attempt to detect cloud-top characteristics of downburst thunderstorms. Despite their high resolution imagery, visible pictures were not found to be useful for this purpose.

The reasons for this fact are that (1) Reflectance variations of thunderstorm tops are relatively small, except when sun angles are low; (2) Anvil-top brightness does not always represent the anvil height, and (3) Pictures are not available during the hours of darkness. However, infrared data though low in resolution, can be used in detecting (1) Patterns of cloud-top temperature related to both cloud height and emissivity, and (2) Cloud-top radiance day and night.

This chapter discusses the characteristics of anvil tops, based mainly on the pattern of equivalent blackbody temperature depicted in pictorial forms.

ENHANCED IMAGERY has been produced by converting the input digital count into output digital count, thus generating a set of new digital count. The total digital count values for both input and output are $2^8 = 256$, increasing from 0 to 255. Refer to Corbell et al (1976).

As shown in Figure 6.1, the input count (at the bottom) corresponds to the satellite-measured effective radiance which varies with the equivalent blackbody temperature (at the top).

An enhancement curve generates an output count which will result in a gray-scale presentation of specific nephsystems. Curves M_B and 30 have been used in mapping anvil-top temperatures at one-degree intervals. 17 shades of gray scale of Curve M cover -63 to -80 °C temperature range and those of Curve 30, -59 to -76 °C (see Figure 6.1).

These enhancement curves generate pictures with dark (or black) cloud edges with -60, -54, and -33 °C temperature for Curve M_B and -59 and -45 °C for Curve 30 (see Figure 6.2).

The 17 gray-scale shades inside -60 °C (M_B) and -59 °C (30) anvil boundaries show clearly the existence of warm and cold spots. For example, in Figure 6.2, the temperature difference between these spots is 9 °C.

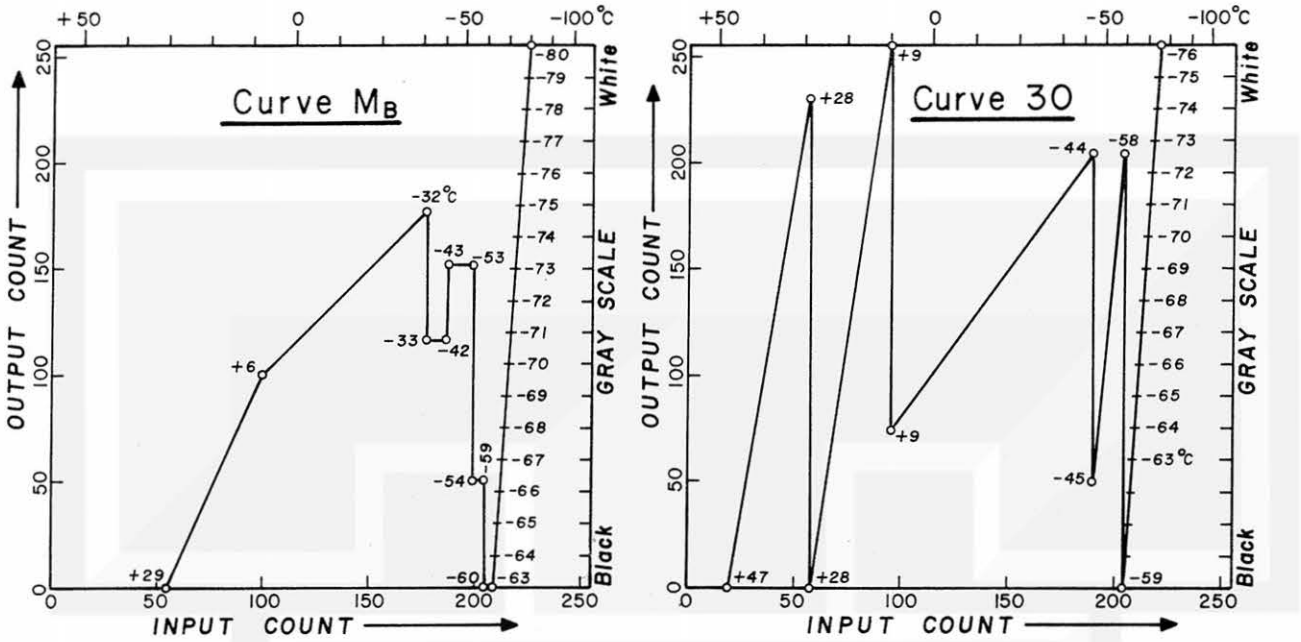

Figure 6.1 Enhancement curves M_B and 30 suitable for depicting anvil-top temperatures. 17 gray-scale shades correspond to every digital count value between 208 and 225 (Curve M_B) and 204 and 221 (Curve 30).

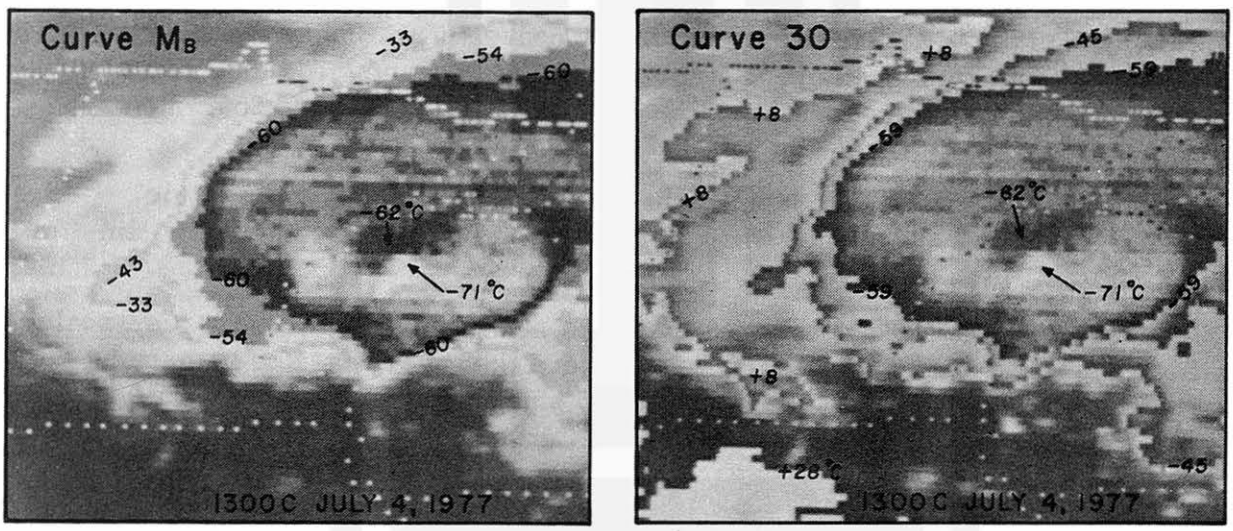

Figure 6.2 Examples of Curve M_B (left) and Curve 30 (right) enhancement applied to 1300 CST picture of the northern Wisconsin thunderstorm of the 4th of July, 1977. Black or gray boundaries correspond to the lowest points of enhancement curves in Figure 6.1.

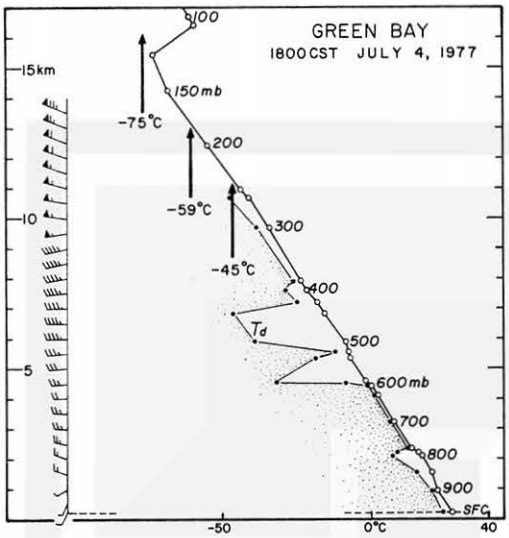

Figure 6.3 Green Bay sounding taken beneath the anvil cloud of Northern Wisconsin thunderstorm. There were relatively dry layers between 600 and 400 mb topped by a thick moist layer.

Southerly flows are seen below 850 mb. Westeries above the inflow layer extended to 10 km at which winds shifted toward west-northwest with 50 kts or stronger windspeed.

NORTHERN WISCONSIN THUNDERSTORM OF JULY 4, 1977 was investigated using a series of infrared pictures produced with enhancement Curve 30. This curve results in anvil boundaries with -45 and -59 °C equivalent blackbody temperatures.

Green Bay at 1800 CST was the only station located inside the vast anvil cloud. The sounding in Figure 6.3 reveals that -45 and -59 °C temperature corresponds to the heights of 240 and 180 mb surfaces, respectively. We should realize that the cloud-top emissivity could often be smaller than 1.0, resulting in a significant difference between equivalent blackbody and true cloud-top temperatures.

The west-northwest winds above 10-km MSL at Green Bay represent the anticyclonic flow around a high-level anticyclone centered near St. Louis, Missouri. Figures 6.4 (150 mb) and 6.5 (200 mb) reveal the location of the -59 °C anvil with respect to the flow characterized by both anticyclonic shear and curvature. Downburst activities terminated by 1530 CST, 2.5 hours before this map time.

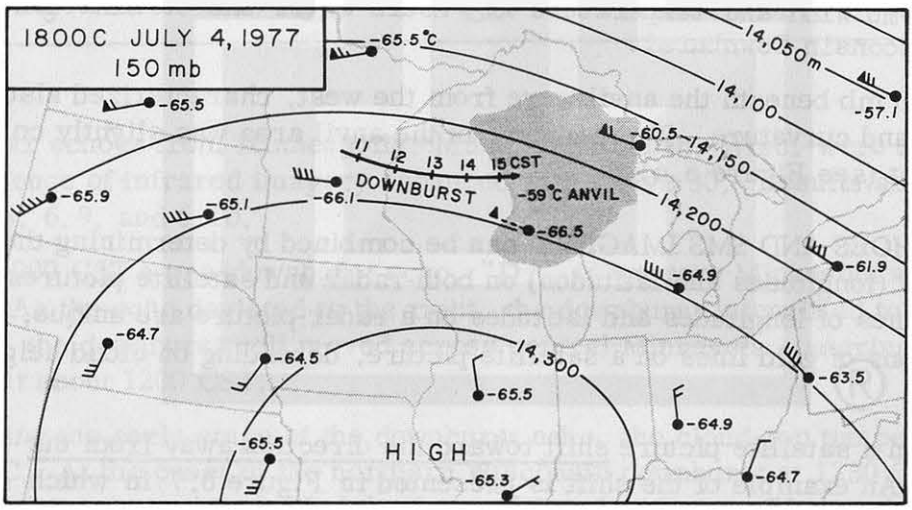

Figure 6.4 150-mb wind and temperature at 1800 CST about 2.5 hours after the end of downburst.

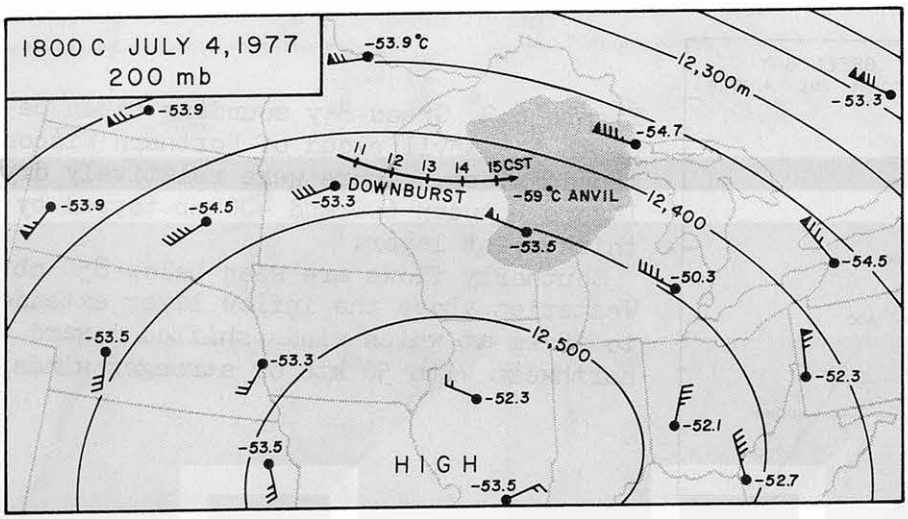

Figure 6.5 200-mb wind and temperature. Flow characteristics were anticyclonic in both shear and curvature.

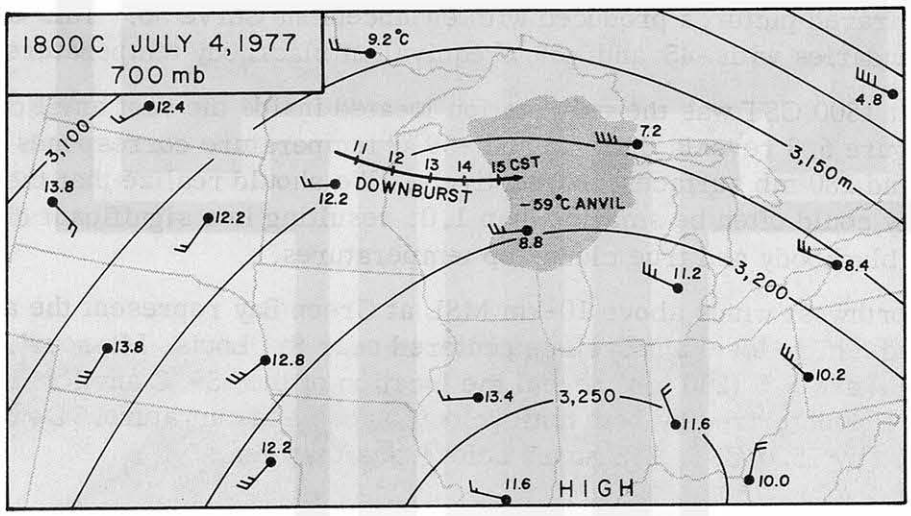

Figure 6.6 700-mb wind and temperature 2.5 hours after the termination of the Northern Wisconsin Downburst.

Winds at 700 mb beneath the anvil were from the west, characterized also by anticyclonic shear and curvature. Temperature in the anvil area was slightly colder than its environment (see Figure 6.6).

RADAR ECHOES AND SMS IMAGERY can be combined by determining the geographic coordinates (longitudes and latitudes) on both radar and satellite pictures. Although the grid lines of longitudes and latitudes on a radar picture are unique, there are multiple solutions of grid lines on a satellite picture, depending on cloud height and viewing angle.

Grid lines on a satellite picture shift toward the direction away from the subsatellite point. An example of the shift is presented in Figure 6.7 in which grid lines inside the cloud were computed at 14-km level while those outside the cloud were at sea level. About a 21 km (13 mile) shift is apparent.

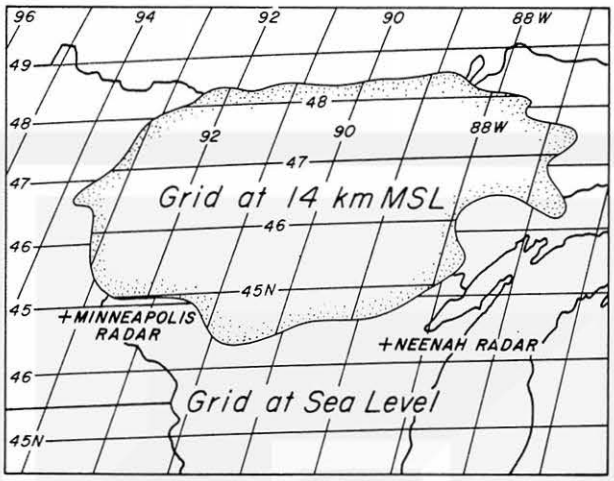

Figure 6.7 Shift of grid points away from subsatellite point due to the viewing angle from SMS located above the equator. The average shift inside the cloud area was 21 km (13 miles).

The shift of a grid point is proportional to the height of gridding surface (cloud-top height). It also varies significantly with the latitude as well as the azimuth of the grid point viewed from the SMS subpoint (see Table 6.1).

Table 6.1 Shift of grid points in km when the gridding surface is lifted from sea level to 10 km MSL. Azimuth denotes the angle of a grid point viewed from the SMS subpoint.

LATITUDES OF Grid points	AZIMUTHS OF GRID POINTS (in degrees) 0°	20°	30°	45°	60°
60°	24.9	38.7	--	--	--
50°	15.6	19.5	27.9	--	--
40°	10.5	11.8	14.3	34.2	--
30°	7.0	7.6	8.7	12.8	--
20°	4.3	4.6	5.2	6.7	11.3
10°	2.1	2.2	2.4	3.0	4.4
0°	0.0	0.0	0.0	0.0	0.0

Radar echoes from Minneapolis, Minn. and Neenah, Wisc. were superimposed upon a sequence of infrared imagery enhanced with Curve 30. Results are shown in Figures 6.8, 6.9, and 6.10.

At 0900 CST a pre-downburst echo, "D," in western Minnesota was moving eastward. As the echo deviated to the right, the downburst intensified to about F1. Thereafter, the downburst cell moved across central Minnesota, entering northern Wisconsin at about 1200 CST.

During the early stage of the downburst echo, the cloud-top temperature was about -70 °C. At the onset of the northern Wisconsin downburst at 1230 CST, an area of 8 °C warming is seen just behind the intensifying downburst. If the cloud-top emissivity remained unchanged, the warming implies a 1.5 km sinking of the anvil top.

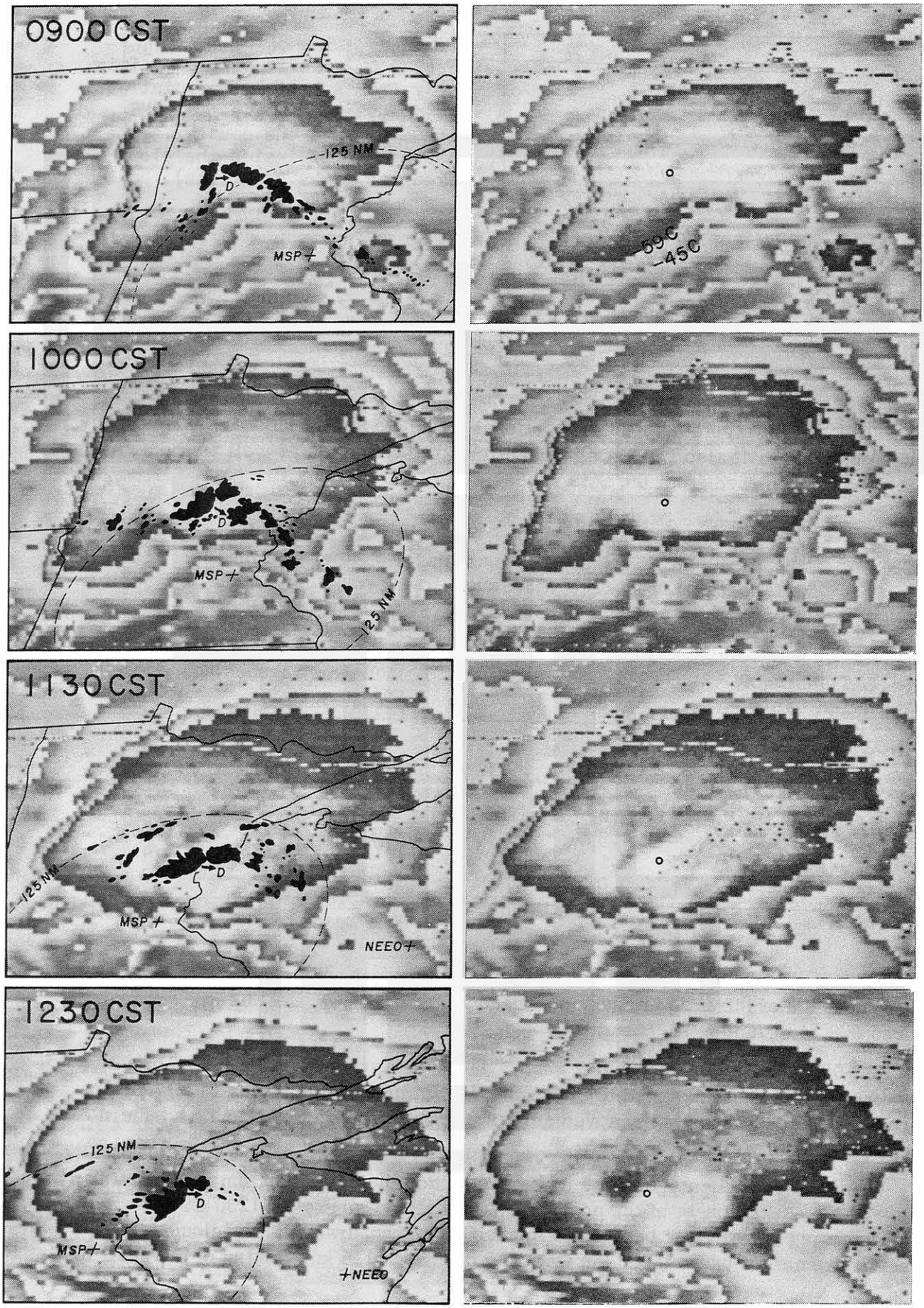

Figure 6.8 Curve 30 enhancement with radar echoes on July 4, 1977. Open circles are downburst locations.

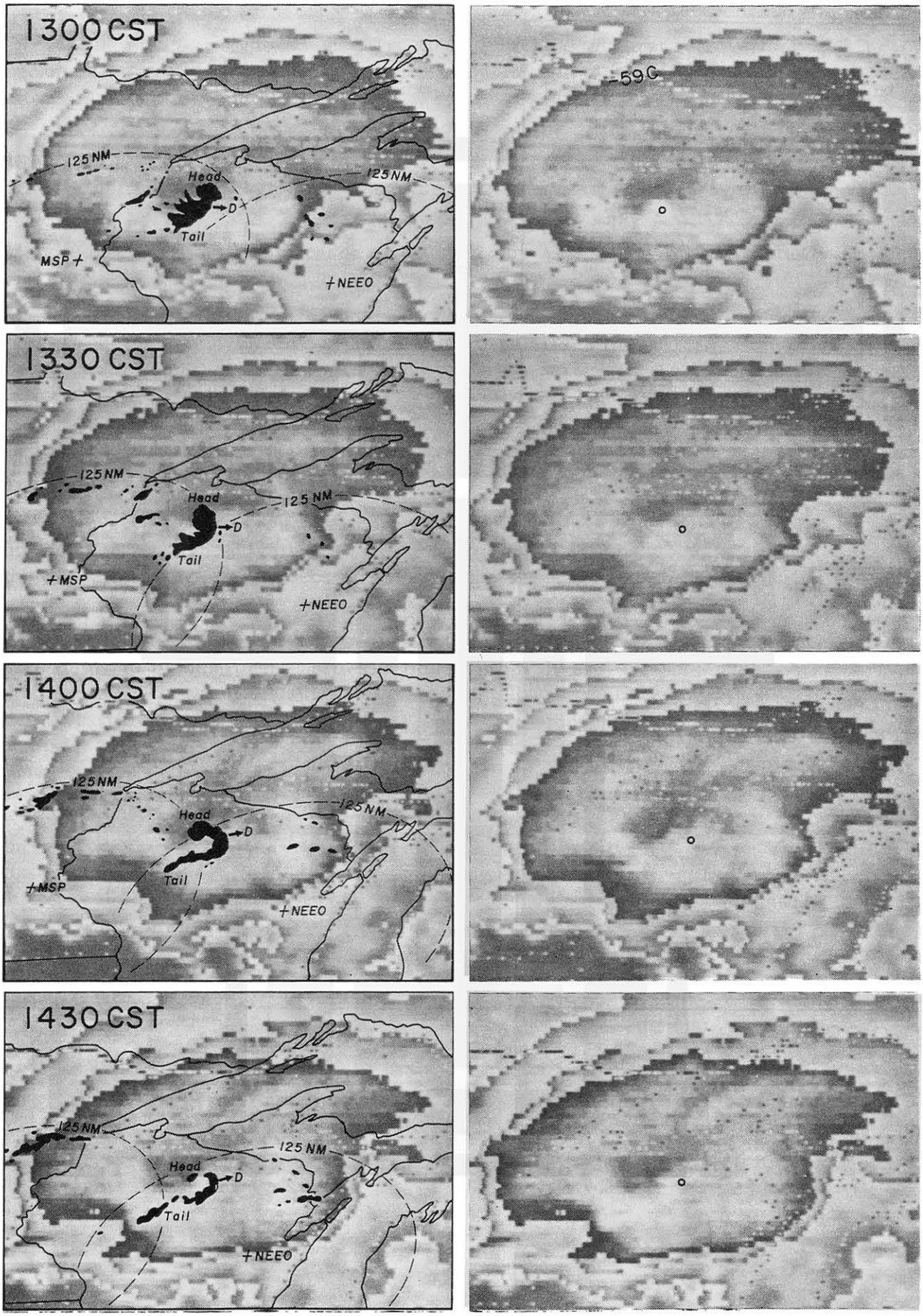

Figure 6.9 Curve 30 enhancement with radar echoes on July 4, 1977. Open circles are downburst locations.

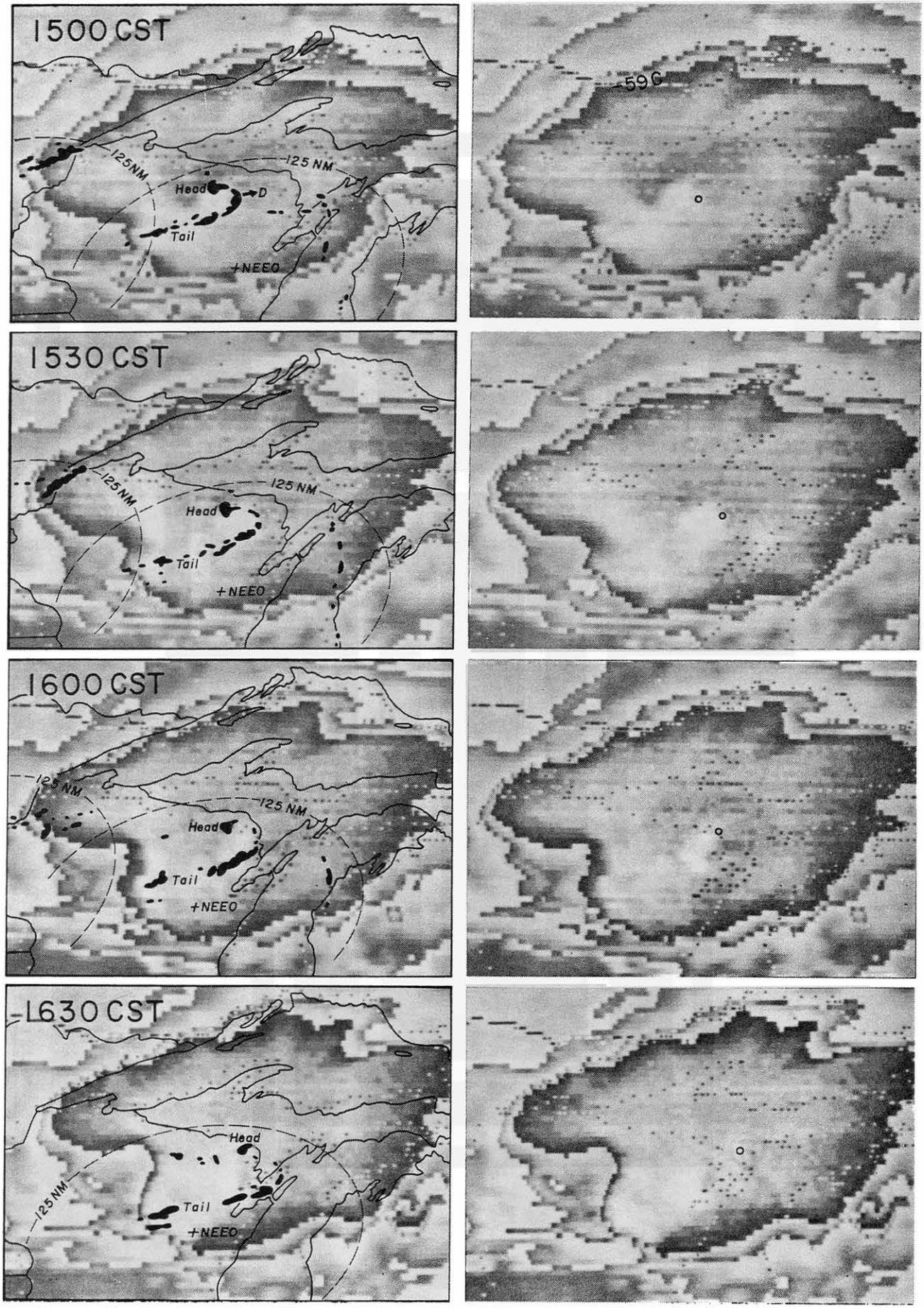

Figure 6.10 Curve 30 enhancement with radar echoes on July 4, 1977. Open circles are downburst locations.

The warm area moved eastward along with the downburst radar echo which became a typical bow echo with a rotating head attached to its north end. The head moved into the region of the warm pocket without modifying the temperature field.

In effect, the cloud-top temperature of the rotating head kept increasing from 1300 to 1430 CST. During this time the bow echo changed into a well-defined comma echo while the downburst top kept warming, slowly but steadily.

At 1400 CST, the time of peak intensity, the cloud-top temperature in the vicinity of the downburst increased as evidenced by the white areas which shrank or disappeared.

Strange-looking bands of cold cloud tops extended outward from the warm pocket, showing anticyclonic curvature of the band axis. The feature of the bands became most significant during the peak-intensity period around 1400 CST.

Beginning about 1500 CST, an extensive area of cold cloud top appeared just to the west of the comma echo. No radar echoes were seen to the west edge of the comma when the cold cloud top fully developed at 1530 CST. Note that the arc line of echoes are located along the advancing edge of the cold area.

At 1600 CST the cold area began shrinking rapidly while the comma echo broke up into pieces. Some 30 minutes later the large area of the anvil top, as depicted by the Curve 30 enhancement, became rather monotonous without showing specific patterns.

A comparison of the enhanced pictures at 1230 CST (onset), 1400 CST (peak), 1530 CST (break up), and 1630 (end) reveals an amazing response of cloud-top temperature fields to downburst intensities. This is probably because the northern Wisconsin downburst family was the largest in area and the longest in time of all downburst families investigated so far. The chance of depicting a temperature field with an 8-km (subpoint) resolution is rather slim if the storm system is much smaller than this case.

WARMING OF DOWNBURST WAKE has been evidenced by a series of enhanced infrared pictures. A time sequence of the events is described in Figure 6.11, showing the variation of equivalent blackbody temperatures at the downburst top and 20 to 30 miles west of the top.

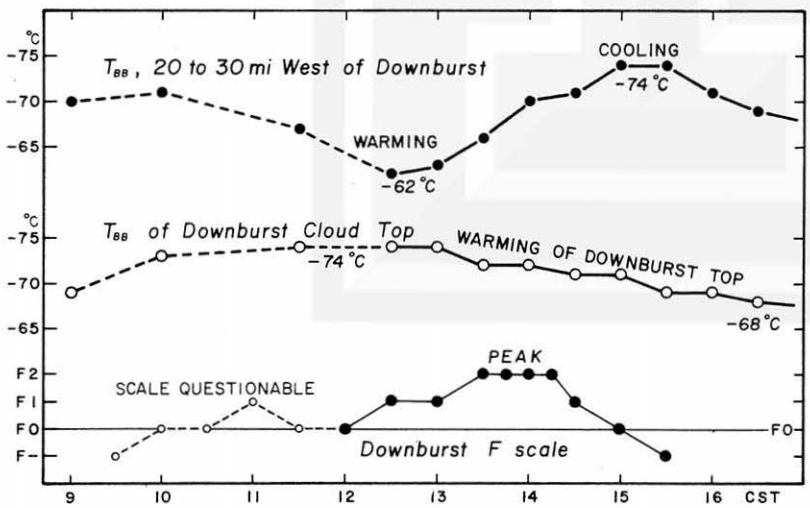

Figure 6.11 Variations of equivalent blackbody temperature, T_{BB} at the top of the downburst cell and that over the area 20 to 30 miles west of the cell.

Temperature at the top of the downburst cell increased from about -74 to -68 C during the downburst. On the contrary, the cloud-top temperature above the wake region (20 to 30 miles west) decreased while the downburst was intensifying. After the end of the peak intensity, cloud-top temperature behind the comma echo decreased further (see enhanced picture at 1530 CST).

A CONCEPTUAL MODEL OF WAKE FLOW behind a downburst cell is presented in Figure 6.12.

The top diagram shows the "speed-up" stage in which a bow echo began moving fast accompanied by wake flows in both horizontal and vertical planes. During this stage the anvil-top sinks behind the bow echo while cyclonic and anticyclonic flows develop on both sides of an accelerating bow echo (see enhanced picture at 1230 CST).

When the "peak speed" is reached, the echo turns into a pointed bow (spearhead) with a rotating head on the left-hand side. The sinking motion of the anvil top gradually disappears (see enhanced picture at 1400 CST).

During the "slow-down" stage of the comma echo the wake flow must also decelerate. The high-speed wake flow trapped behind the comma echo tries to expand outward horizontally and also vertically, resulting in a bulge of the anvil top behind the comma. The bulge (cold top) suddenly sinks to its original level along with the break up of comma echo (see enhanced picture at 1600 CST).

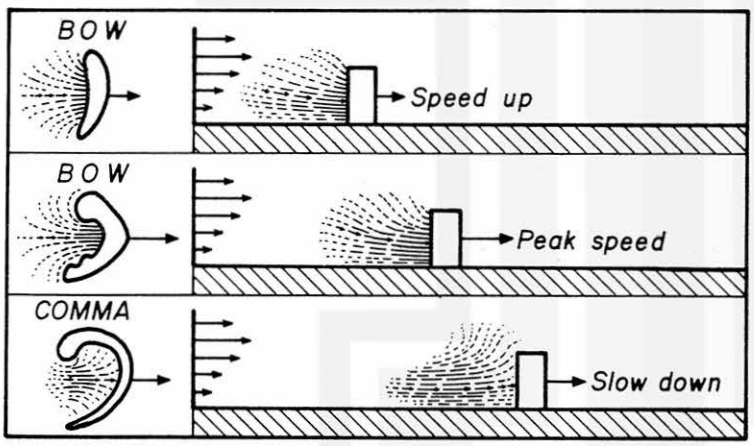

Figure 6.12 A conceptual model of wake flow behind a bow echo which turns into a comma echo.

HYPOTHETICAL CROSS SECTIONS in Figure 6.13 show patterns of downburst currents and wake flows at 1230 and 1530 CST on July 4, 1977.

The bow echo at 1230 CST was moving at 54 kts. Wake flows must catch up with the fast-moving bow echo to fill up the space behind the downburst. The anvil top could be pulled down during the acceleration stage. The pulled-down anvil will probably propagate from left to right just behind the downburst.

The comma echo at 1530 CST was accompanied by a fast-moving wake flow trapped to the west of the comma echo. As the leading edge of the comma slowed down, the wake flow undergoing deceleration resulted in a bulge of the anvil top behind the comma.

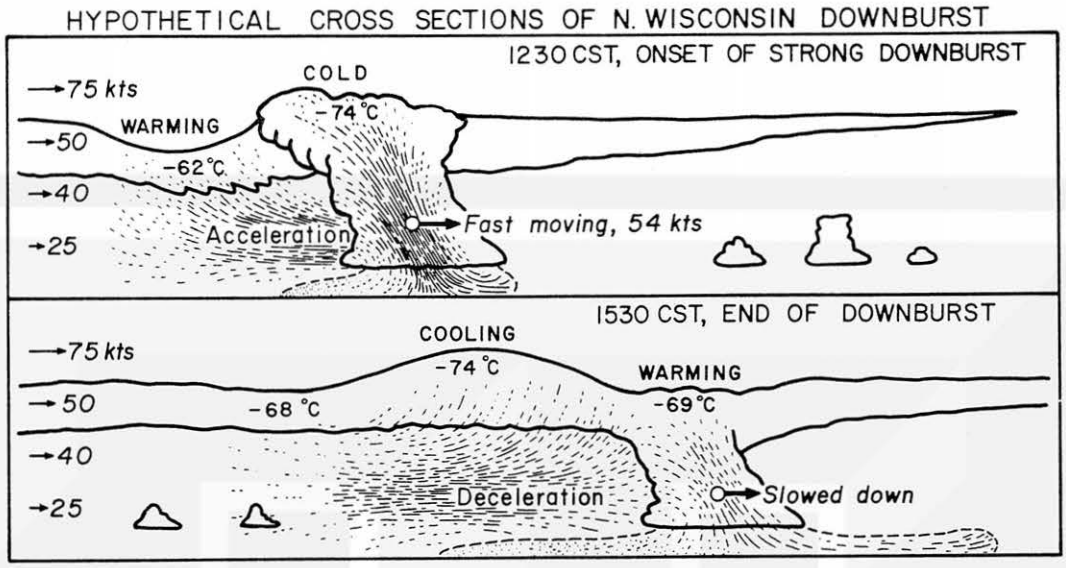

Figure 6.13 Hypothetical cross sections of northern Wisconsin downburst at 1230 and 1530 CST July 4, 1977.

Hypothetical cross sections and a conceptual model in Figures 6.12 and 6.13 are introduced in an attempt to explain characteristics of both satellite and radar imagery. No attempt has been made to offer alternative explanations of the analytical results. More case studies of extensive downburst families are necessary in order to understand this phenomenon better.

EXPANSION RATE OF GIANT ANVIL of the northern Wisconsin storm sheds light on the effect of a downburst upon the growth rate of the anvil area.

The area of an extensive anvil cannot be measured by simple planimetric means because the SMS imagery used in this analysis is not converted into a equal-area projection.

To overcome this difficulty, a dual planimetric method was developed. In this method the anvil area is measured twice by using a standard planimeter to obtain the ratio

$$\text{Area ratio} = \frac{\text{Area inside true boundary} \quad \text{(true area)}}{\text{Area inside grid boundary} \quad \text{(grid area)}}$$

where grid boundary denotes the boundary of an anvil cloud approximated by longitude and latitude segments (see Figure 6.14).

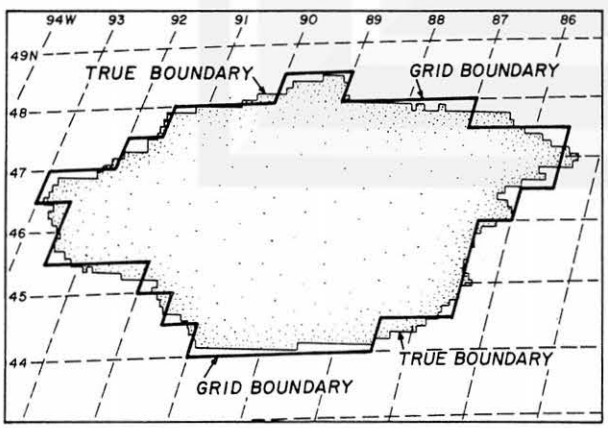

Figure 6.14 Computation of an anvil area by dual planimetric method. The grid boundary consists of a number of longitude and latitude segments, which follow approximately the true boundary of the anvil.

Since we know the true area within each one-degree square, the total area inside the grid boundary can be computed regardless of the map projection.

Since the area inside the grid boundary can be computed, we obtain the true area of an anvil from

True area = Area ratio x grid area on the earth

By keeping the area ratio as close as possible to 1.0, the true area can be computed with an accuracy better than 1%.

Results of the computations presented in Table 6.2 and in Figure 6.15 reveal a rapid expansion of the anvil when the downbursts began in Minnesota. As the northern Wisconsin downburst intensified the anvil area shrank significantly, reaching a minimum shortly after the peak intensity at 1400 CST. Likewise, the area of -70 °C or colder cloud tops near the downburst shrank to almost zero during the peak-intensity period.

Table 6.2 True areas within the outer boundaries of the anvil cloud defined by isotherms of -45 and -50°C temperatures. Areas of -70°C are those in the vicinity of the downburst and their extrapolated locations. 0900-1730 CST July 4, 1977.

Time	F scale	AREAS INSIDE ANVIL BOUNDARIES (in 1000 km²) -45°C	-50°C	-70°C
0900 CST	---	160	109	0.0
1000	F 0	198	148	1.1
1130	F 0	268	170	2.3
1230	F 1	276	186	0.8
1300	F 1	274	189	0.9
1330	F 2	266	179	0.3
1400	F 2	258	174	0.1
1430	F 1	259	171	0.5
1500	F 0	260	180	1.7
1530	F -	273	191	2.8
1600	---	278	197	0.2
1630	---	274	190	0.0
1700	---	270	174	0.0
1730	---	249	155	0.0

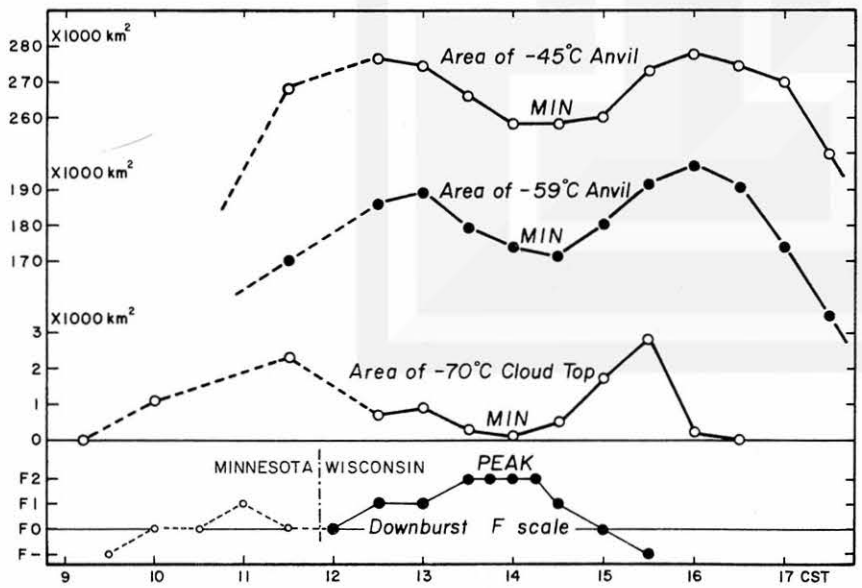

Figure 6.15 Variations of anvil area in relation to F-scale intensities of northern Wisconsin downburst. The anvil area shrunk to a minimum shortly after the downburst had reached the peak intensity.

A BREATHING THUNDERSTORM--TRUE OR FALSE? The occurrence of the minimum anvil area corresponding to the peak intensity of a downburst could be accidental or it could as well be governed by a cause and effect relationship.

This subject can be discussed further by comparing the three enhanced pictures which correspond to either maximum or minimum anvil areas. Characteristics of these pictures are shown in Table 6.3.

Outflow streaks are often visible inside the hurricane cirrus shield during its stage of rapid expansion. These streaks originate near the central region of the shield characterized by the cold cloud-top temperature.

Table 6.3 Characteristics of temperature patterns of the giant anvil cloud over Minnesota, Wisconsin, and upper Michigan on July 4, 1977.

Time	Anvil area	Characteristics
1230 CST	Maximum	A circular, warm area formed in the anvil cloud to the west of the downburst.
1400-30	Minimum	Significant streaks extended either outward from or inward to the warm area.
1600-30	Maximum	No specific pattern of the cloud-top temperature visible.

On the contrary, the streaks at 1400-30 CST point toward the warm area near the center of the giant anvil. At this time the anvil areas of both -45 and -59 °C shrink to their minimum values.

The above evidence leads to a speculation that the outward expansion of anvil materials near the warm area was suspended when the downbursts intensified. During the peak intensity period, a reverse flow toward the warm area could have taken place at the anvil-top level. Such a reverse flow could induce the inflow streaks pointing toward the warm area while the outer portion of the anvil kept expanding outward.

If this was the case, the huge downburst thunderstorm was characterized by three stages in its life cycle, somewhat like a giant morning glory which breathes outward during the developing stage, inward during the peak downburst stage, and outward again during the dissipating stage after the termination of downbursts.

The speculation presented in the foregoing discussion is based solely on the super-downburst thunderstorm of northern Wisconsin on July 4, 1977. When more data on such super-storms become available in the future, we will be able to determine if this speculation is true or false.

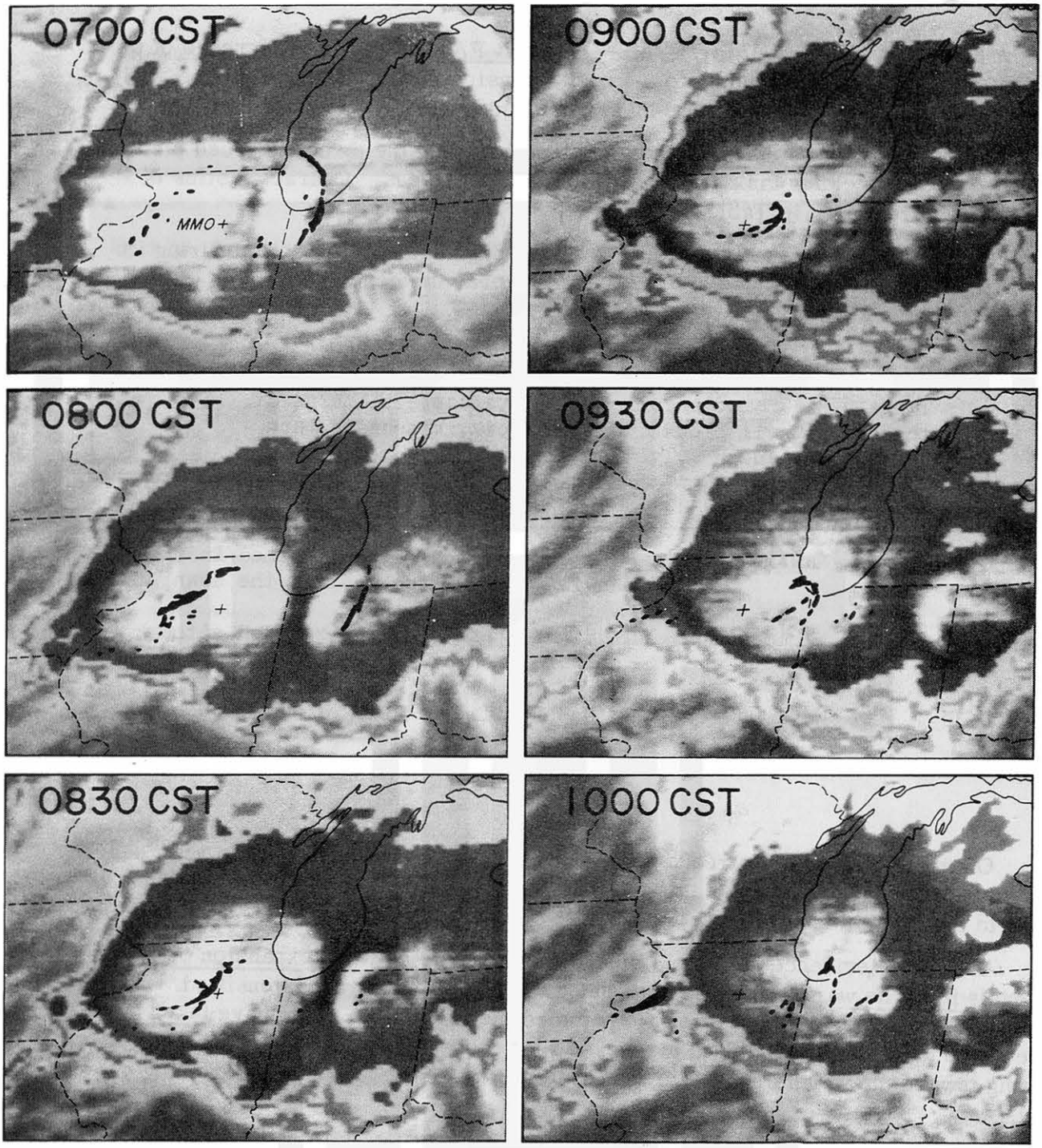

Figure 6.16 Combination of radar echoes from Marseilles, Illinois and Curve M_B infrared pictures. The Earlville tornado occurred at 0825 CST followed by four tornadoes ending 0850 CST. The location of tornado is shown by an arrow in the 0830 CST picture (Refer to Color Map No. 5 and Figure 5.5).

EARLVILLE STORMS of June 30, 1977 were characterized by 10 downbursts and 5 tornadoes. These downbursts and tornadoes lasted for 35 minutes between 0820 and 0855 CST, traveling through a distance of 33 miles at 57 mph.

Shown in Figure 16 are Curve M_B infrared pictures between 0700 and 1000 CST at 30-minute intervals. Radar echoes within 125 n.m. were superimposed upon the satellite imagery.

At 0700 CST a weakening squall line across the south shore of Lake Michigan. A large area of cold cloud tops is seen to the west of the line. This situation is similar to that of the comma echo at 1530 CST in Figure 6.10.

Large, strong echoes developed in the central region of an extensive cold cloud at 0800 CST. Both squall line and cold cloud to the east were weakening rapidly.

A bow echo at 0830 CST was approaching the Marseilles radar. The Earlville tornado ended at this time and an F1 downburst was in progress to the southeast of Leland, Illinois (see Color Map No. 5).

Between 0900 and 0930 CST a comma echo moved over Chicago and weakened. At 1000 CST the comma echo broke up while moving across the southern shore of Lake Michigan.

NO SPECIFIC PATTERN of cloud-top temperature was recognized in connection with the Earlville storms. One reason for this being the size and duration of these storms which were much smaller and shorter than the northern Wisconsin storms on July 4, 1977. Another reason is the quality of enhanced pictures which was not as good as that of the super-storm case.

SPRINGFIELD TORNADO/DOWNBURST FAMILY was 43 miles long, spawning 27 downbursts and 18 tornadoes between 1510 and 1620 CST. The peak intensity of both storms occurred at about 1550 CST.

Two infrared pictures at 1500 and 1600 CST are available for the purpose of combining radar echoes and satellite pictures. Both pictures were enhanced with Curve M_B so that the black boundaries of the anvil clouds denote -60°C isotherms (see Figures 6.17 and 6.18).

At 1500 CST, shortly before the onset of the downburst, a large echo was turning into a bow echo moving eastward at 42 kts. There was an extensive cold area extending from the bow echo westward. The equivalent blackbody temperature of the cold top was about -70 °C.

One hour later, at 1600 CST, the downburst had passed its peak intensity of F1, spawning tornado No. 17 in Color Map No. 8. The downburst top was characterized by a small area of -69 °C temperature, indicating that the extensive cold top had broken up.

At this time the head echo, somewhat like a hook echo (see Figure 5.7), moved toward the warm area which had developed near the center of the oval-shaped anvil. An outflow streak with an anticyclonic curvature extends from the warm area outward. These features are extremely similar to those of northern Wisconsin cloud at 1400 CST (see Figure 6.9).

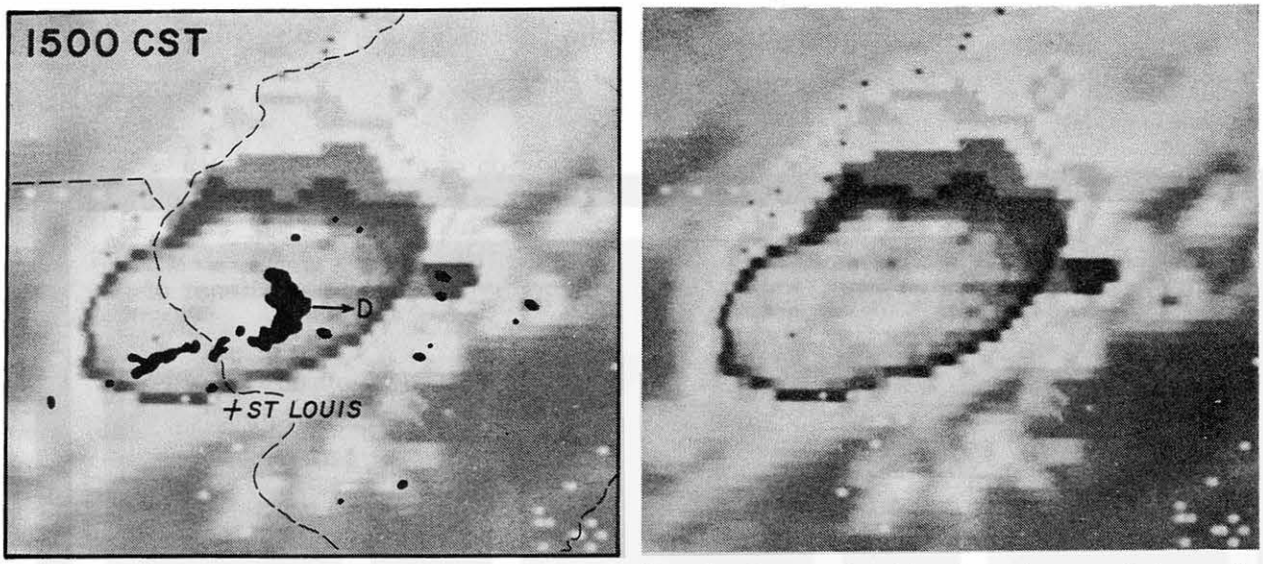

Figure 6.17 Cloud-top temperature of the Springfield thunderstorm of August 6, 1977. A bow echo was forming beneath the cold cloud top. (Curve M_B) From Forbes and Wakimoto (1978)

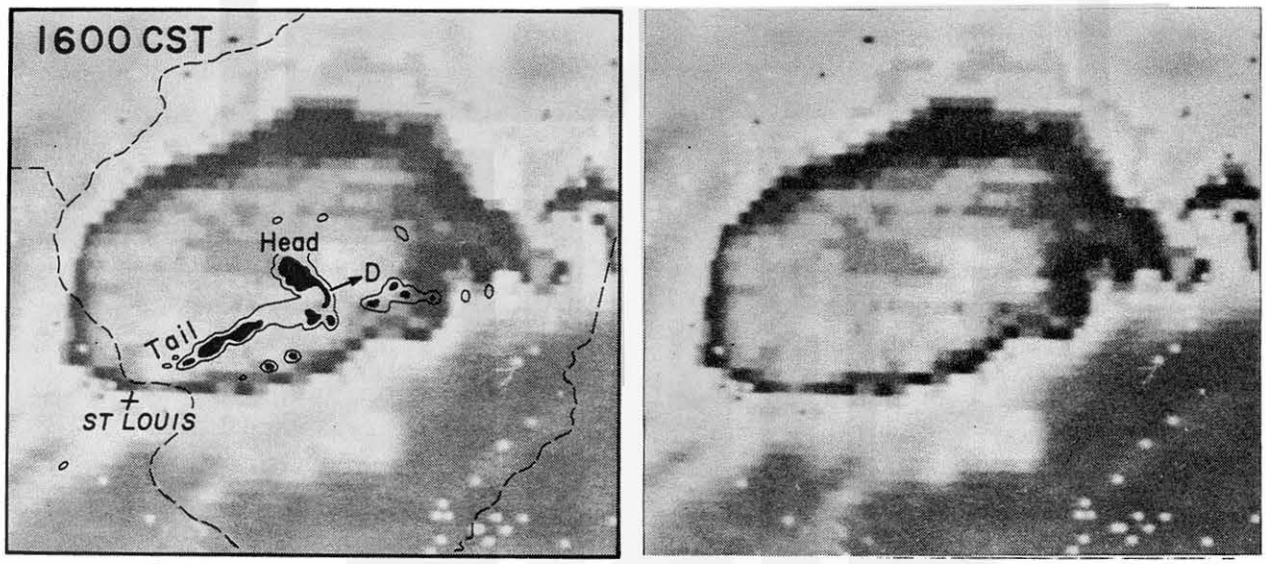

Figure 6.18 Temperature patterns (Curve M_B) at the peak intensity stage of the Springfield downburst. A warm hole is seen to the northwest of the downburst echo.

DANVILLE STORM AFFECTED BY 100 KTS WINDS at the anvil level displayed a feature of blow-off anvil accompanied by a wake flow downstream from the downburst cell. This wake pattern is different from the previous cases because the high level winds are strong.

The translational speed of the downburst cell was 42 kts, about 60 kts slower than the anvil level winds. As a result, anvil materials were blown off downwind so that the downburst echo was seen always near the upwind edge of the anvil cloud. This feature is in contrast to the Springfield and northern Wisconsin situations where anvil-level winds were about 70 kts while downburst echoes traveled at 45 to 55 kts with relative velocities less than 25 kts.

At 2000 CST, about 20 minutes prior to the onset of downbursts, there were two large echoes. During the next 30 minutes or so, the eastern echo weakened while the western echo induced a series of downbursts.

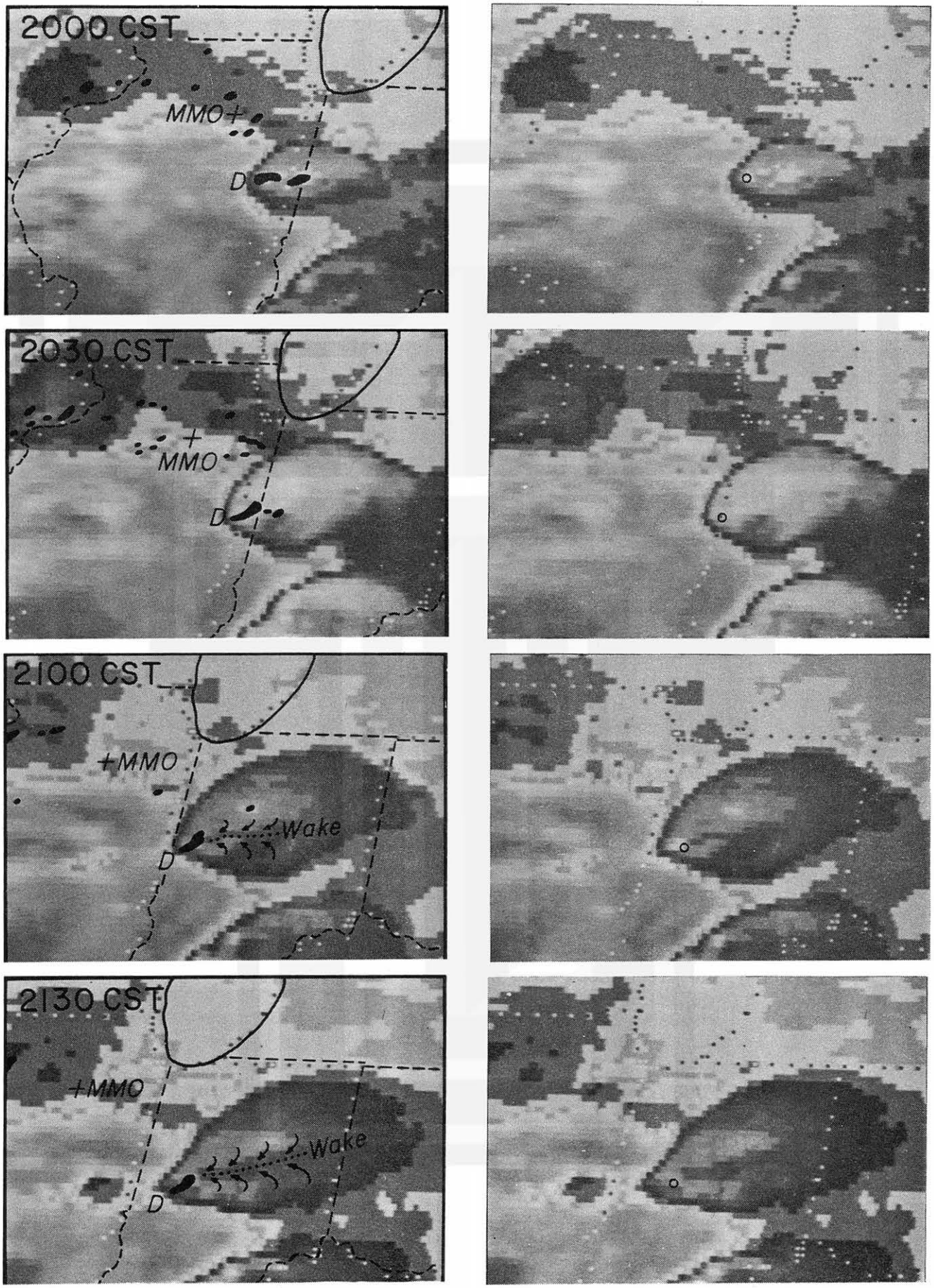

Figure 6.19 Enhanced (Curve M_B) infrared pictures of the Danville thunderstorm, Sept. 30, 1977. Downburst locations are indicated by circles.

A band of wake formed downstream from the downburst echo at 2100 CST. The band was about 70 miles long, characterized by 2 to 3 °C warmer temperature.

By 2130 CST the wake band extended over 100 miles, almost across the state of Indiana. The wake center was 4 to 5 °C warmer than its environment (see Figure 6.19).

It is likely that the band of warm wake represents a zone of depression on the anvil surface behind a convective region which travels much slower than anvil-level winds.

A WAKE TRENCH was photographed during the Lear Jet mission on April 4, 1977 over Alabama. A picture taken from 45,000 ft reveals a trench-like wake extending relative downwind from a convective region (see Figure 6.20).

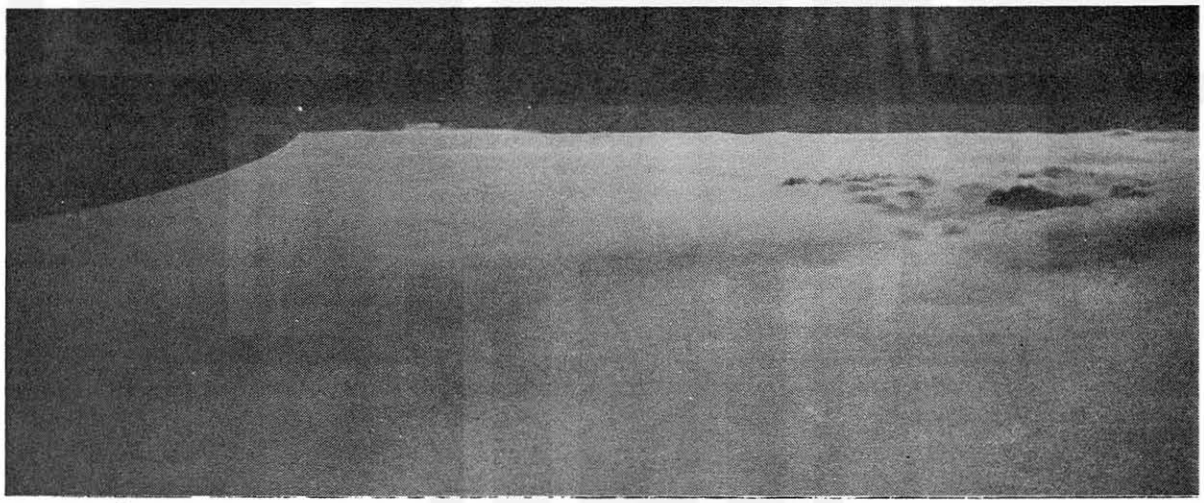

Figure 6.20 A trench-like wake extending downwind from a region of convective tower over westernmost Alabama. Photo by Duane Stiegler from Lear Jet at 45,000 ft. University of Chicago Research Flight: Date--April 4, 1977; Time--1630.5 CST; Direction--southwest; and Tropopause wind--240° at 121 kts.

MATTOON STORM was also under the influence of 100-kt winds at 12 km blowing from 285 degrees. The parent hook echo moved from 302 degrees at 29 kts. The relative velocity between anvil-level wind and echo motion was, therefore, over 70 kts. As expected, the parent hook echo was located near the upwind edge of a large, blow-off anvil cloud (see Figure 6.21).

At 0900 CST scattered echoes with cloudtop temperature -43 to 53 °C are located over central Illinois. A small echo formed to the south of these scattered echoes at 1000 CST. The small echo began deviating to the right while the cloud-top temperature decreased to below -54 °C by 1100 CST.

At 1200 CST the area of -54 °C or colder temperature decreased significantly leaving a small area of cold cloud top.

The Mattoon tornado was on the ground between 1140 and 1228 CST. No radar pictures are available at 1300 and 1400 CST. However, the area of -54 °C or colder cloud top over the extrapolated location of the tornado-induced echo increased significantly.

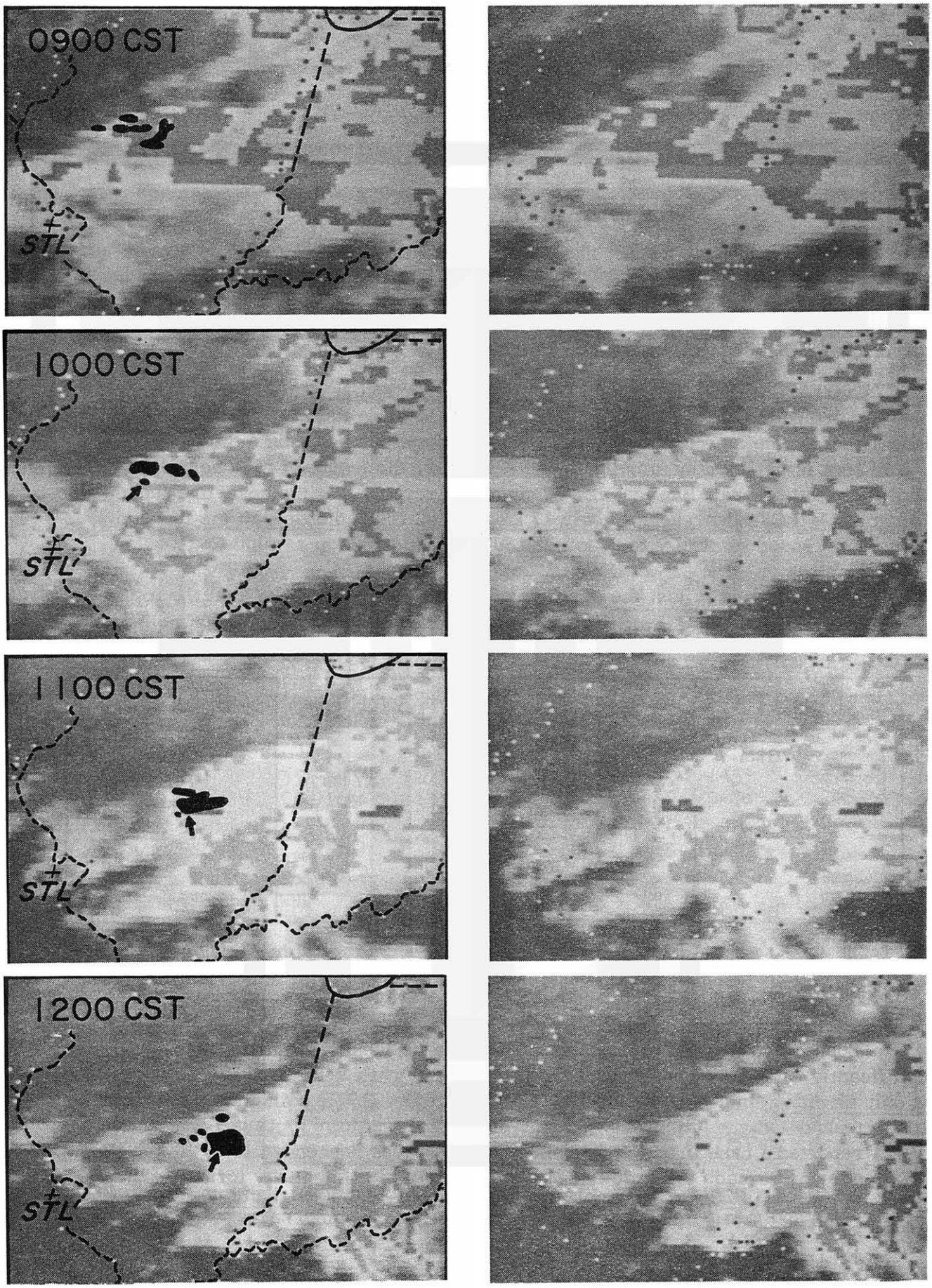

Figure 6.21 Mattoon tornado/downburst cloud enhanced with Curve M_B. Locations of the storm are shown with arrows or circles.

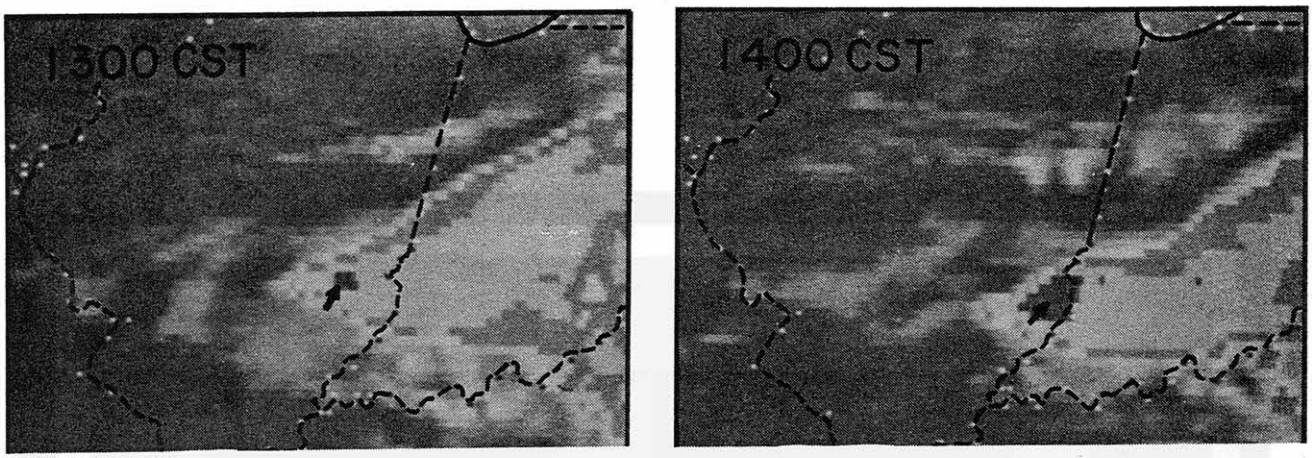

Figure 6.21--continued. Mattoon tornado/downburst cloud enhanced with Curve M_B. Locations of the storm are shown with arrows.

TOTAL SCAN-LINE LENGTHS of -54 °C or colder temperature were computed to determine the variation of cold areas (see Figure 6.22). The scan-line length denotes the true length of a scan-line segment projected onto the earth. When a cold area is depicted by more than one scan line, the length of each segment is added into a total scan-line length. Figure 6.22 reveals that the scan-line length of 70 km at 1100 CST decreased to only 17 km at 1200 CST, the time of the tornado. Then it increased gradually to 37 km at 1300 CST and 182 km at 1400 CST.

This evidence is just the opposite of the popular expectation that the top of a tornado-producing thunderstorm is characterized by an extensive area of cold cloud tops.

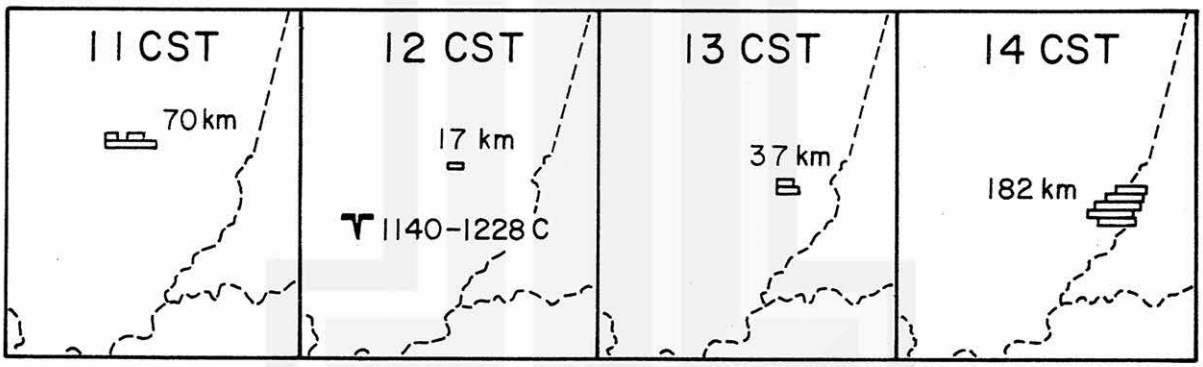

Figure 6.22 Total scan-line lengths of -54 °C or colder cloud-top temperature. The length reached a minimum during the time of the tornado, implying that the cloud-top was not characterized by an extensive cold area when the tornado was in progress.

Bonner and Kemper (1971) showed that the frequency of hail increases significantly with the echo height above tropopause, while tornado frequency does so only slightly. In his study of anvil growth, Purdom (1971) pointed out the formation of tornadoes when the expansion rate of anvil slows down or pauses. Fujita (1972) reported a case in which overshooting cloud tops descended 10 to 20 minutes in advance of a tornado touch down. A case study of the Union City tornado edited by Brown (1976) revealed a tornado formation when the top of the parent radar echo began collapsing.

Thus, there is additional evidence indicating that the cloud top may reduce in size, height, and vigor during tornado activities, contrary to popular expectation.

INFRARED SIGNATURES OF FIVE DOWNBURST THUNDERSTORMS presented in this chapter were summarized in Table 6.4. The mean winds in the table were computed for two separate layers; the higher layer being between 0 and 3 km below the height of the maximum wind and the lower layer, the next 3-km.

Table 6.4 A summary of cloud-top characteristics in relation to high-level winds and downburst movement. The range of heights in Item (9) indicates 3-km layers below the height of maximum winds, and Item (11), the next 3-km layers. Item (16) denotes the direction of the wake viewed from the downburst area.

Items	FIVE CASES OF DOWNBURSTS Wisconsin	Springfield	Earlville	Mattoon	Danville
(1) Dates	04 JUL 77	07 AUG 77	30 JUN 77	21 AUG 77	30 SEP 77
(2) DB movement (kts)	278-54	257-44	265-58	302-29	299-42
(3) Time of DB	1350 CST	1550 CST	0840 CST	1200 CST	2100 CST
RAWIN DATA					
(4) Release time	1800 CST	1800 CST	0600 CST	0600 CST	1800 CST
(5) Rawin station	Green Bay	Peoria	Peoria	Peoria	Salem
(6) Max. wind (kts)	300-76	230-60	-----	285-100	305-100
(7) Height (km)	13.1	12.5	-----	12.0	10.9
(8) Mean wind (kts)	292-58	227-56	-----	282-79	298-87
(9) Height (km)	10.1-13.1	09.5-12.5	-----	09.0-12.0	07.9-10.9
(10) Mean wind (kts)	261-48	247-40	242-57	261-52	279-61
(11) Height (km)	07.1-10.1	06.5-09.5	06.0-08.0	06.0-09.0	04.9-07.9
VECTOR DIFFERENCE					
(12) Diff. (8)-(2)	359-14	175-28	176-14	271-53	296-43
(13) Diff. (10)-(2)	158-16	135-08	162-23	229-36	246-26
ANVIL TOP					
(14) Anvil shape	Oval	Oval	Oval	Blow off	Blow off
(15) Wake shape	Hole	Hole	None	Band	Band
(16) Wake direction	WNW	NW	----	ENE ?	ENE

It is not feasible to generalize characteristics of downburst thunderstorms based solely on these five situations. Analytical results, nevertheless, revealed two interesting features of anvil clouds in relation to environmental airflow and downburst movement.

OVAL-SHAPE ANVIL forms when the vector difference between high-level (Item 8 in Table 6.4) wind and the downburst movement is relatively small, less than about 30 kts.

The anvil top is characterized by a hole of warm, cloud-top temperature located to the northwest or west-northwest of the downburst area. These directions are downwind side of the vector difference of Items (10)—(2) in Table 6.4.

BLOW-OFF ANVIL forms when the vector difference in Item (12) is relatively large, more than about 30 kts.

Anvil materials are blown downwind resulting in a band of wake characterized by warm cloud-top temperature extending toward the relative downwind in Item (12) or (13).

Schematical diagrams in Figure 6.23 show temperature patterns and cross sections of the oval-shape and blow-off anvil clouds with more than 100 miles in horizontal dimensions. The former develop usually under weak wind and the latter, under strong wind at anvil levels.

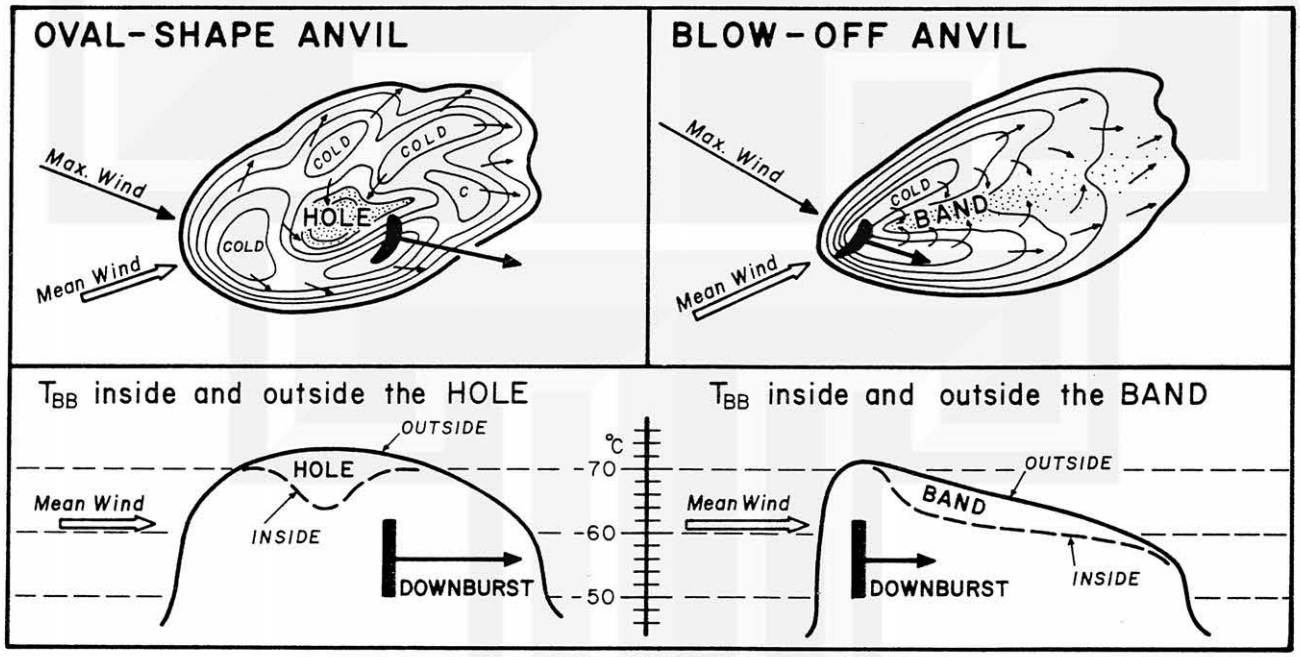

Figure 6.23 Schematic diagrams showing patterns and profiles of cloud-top temperature. Mean wind denotes the mean layer wind 0 to 3 km or 3 to 6 km below the height of the maximum wind near anvil level. Based on the analyses of four cases in Table 6.4.

FURTHER RESEARCH ON DOWNBURST THUNDERSTORMS is necessary because the number of cases investigated so far are not enough to generalize storm characteristics. The following are some efforts that may be required:

1. Perform SMS scans at frequent intervals (Rapid scan) to produce enhanced infrared pictures as well as digital radiation maps of cloud-top temperatures.
2. Obtain VIP radar pictures at frequent intervals (2 min or less) to identify and follow hook, bow, and comma echoes.
3. Take aerial photographs of downburst and tornado damage to determine their locations and interactions.
4. Interview persons in storm areas to obtain information on time, rain, hail, sound, and other accounts.

CHAPTER 7. DOWNBURST-TORNADO RELATIONSHIPS

An advancement in aerial mapping techniques in recent years now permits distinguishing between the damage paths of tornadoes and those of non-tornadic storms (i.e., downbursts and microburst). In some cases, however, the paths of tornadoes are also affected by downburst winds, thus necessitating mapping procedures in which the damage patterns caused by different storms may be identified properly.

A CLASSIFICATION OF DAMAGE PATHS of both tornadoes and downbursts was made (see Figure 7.1). As shown in the figure, the paths of tornadoes are divided into ten types while those of downbursts, into two. We expect, however, that a number of downbursts can be combined into aggregate paths with different sizes and shapes.

The ending portion of the path of an LT tornado turns gradually to the left and that of a RT, to the right. P1 tornadoes are characterized by the P1 scale path length while the path lengths of P0 tornadoes are less than 1.0 mile.

Statistics of the paths of 326 tornadoes mapped by Fujita and his collaborators are shown in Table 7.1. Straight or meandering (SM) tornadoes are apparently the most frequent (35%), followed by right-turn (RT) tornadoes (22%) and left-turn (LT) tornadoes (12%).

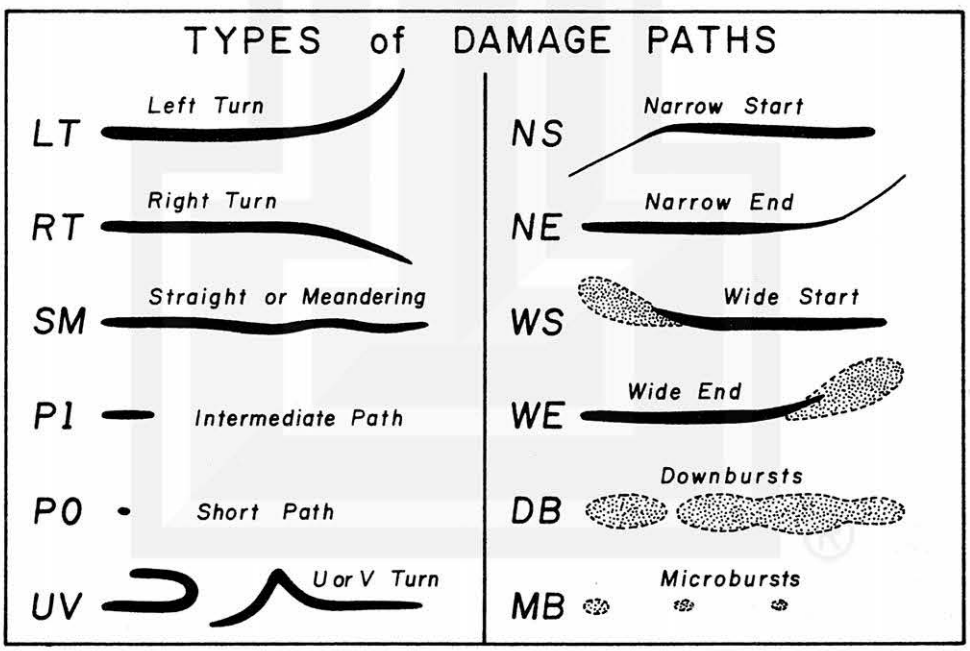

Figure 7.1 Ten types of damage paths left behind by tornadoes and two by downbursts. Downburst and microburst damages are often found in the vicinity of tornadoes.

Table 7.1 Frequencies of ten types of tornado paths and two types of downburst paths. The most significant path-type characteristic was used to categorize each storm. Statistics are based on aerial surveys performed by Fujita and his collaborators. Others include 61 storms surveyed by Forbes, 49 by Fujita, 11 by Tecson, and 7 by Stiegler.

Path Types	Superoutbreak (April 3-4, 1974)	Palm Sunday (April 11, 1965)	Color Maps (This Report)	Others (U of C)	Total
LT	34	1	3	28	66
RT	10	3	5	17	35
SM	55	16	8	52	131
PI	10	0	0	8	18
PO	14	0	2	3	19
UV	0	0	3	1	4
NS	6	1	7	2	16
NE	1	1	0	2	4
WS	8	0	2	6	16
WE	9	0	0	8	17
Total	147	22	30	127	326
Downburst	1	0	64	0	65
Microburst	0	0	56	1	57
Total	148	22	150	128	448

WIDE-END (WE) TORNADO had been regarded as the merger of a tornado into its parent mesocyclone, resulting in an unusually large swirl several miles in diameter.

Re-analysis of more than 10 WE tornadoes revealed that the trajectories inside the wide-end region are predominantly divergent. The damage patterns are very similar to those of the downbursts which were investigated intensively during the past several years (see Figure 7.2).

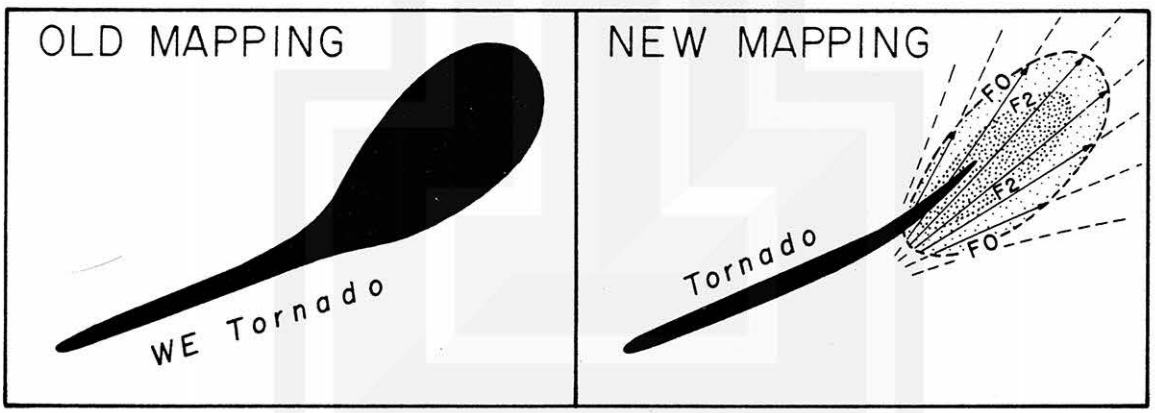

Figure 7.2 Spoon-shaped damage paths in old maps consist of both tornadoes and downbursts. However, it appears that a wide-end (WE) tornado can be represented more realistically as a combination of a tornado and a downburst (DB) that had wiped out the weakening tornado.

Since a tornado and downburst cannot be separated without performing an extensive aerial mapping, the entire damage areas in the right figure are identified as a wide-end (WE) tornado with an understanding that it includes both tornado and downburst.

FRANKFORT, KY TORNADO of April 3, 1974 was a typical example of a WE tornado. Joseph Golden of ERL, Boulder, and John McCarthy of the University of Oklahoma, Norman, flying in a northeasterly direction from Frankfort, followed the F4 tornado path. It widened to approximately 6 miles in width to the east of Stamping Ground, Ky. on US-227. The wide path continued across I-75 about 10 miles further northeast.

A few hours later, Fujita also flew across the wide path near Stamping Ground, Kentucky, witnessing the amazing extent of the wide-spread damage.

As a result of our post-flight analyses of the damage patterns, the three of us more or less concluded that the Frankfort tornado swirled out into a giant-sized tornado during its dissipating stage.

Three years later, in 1977, the wide-path area was re-analyzed, in light of an increased knowledge of downburst damage. Shown in Figure 7.3 is the revised patterns of the Frankfort tornado, consisting of a tornado and a downburst, 17 miles long and 6 miles wide. There were at least 16 swaths of F1 damage inside the downburst area.

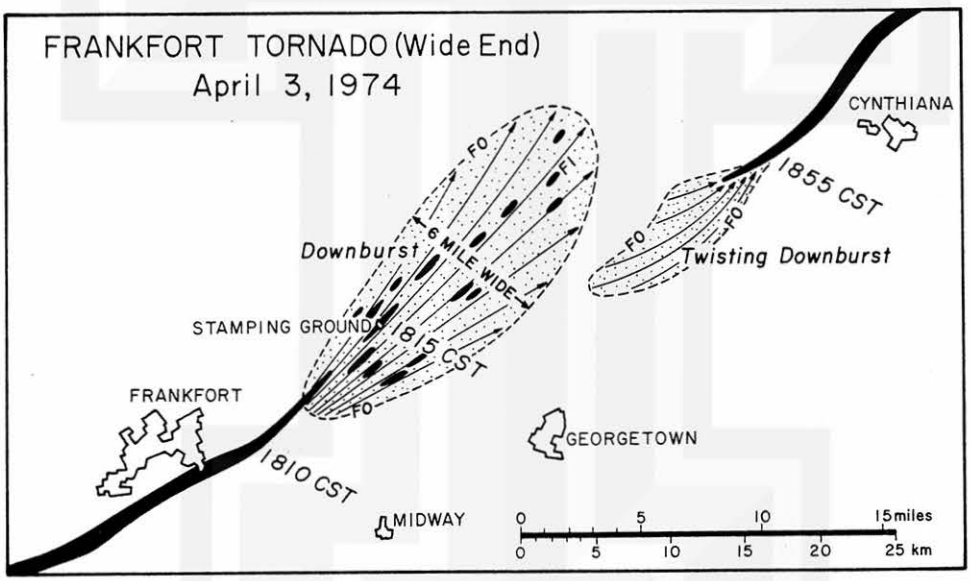

Figure 7.3 A six-mile wide downburst at the end of the Frankfort tornado of April 3, 1974. A 36-mile long path mapped by Fujita (1975) has now been re-mapped as a 21-mile long tornado and a 15-mile long downburst.

Apparently a strong downburst behind a weakening tornado undercut the tornado circulation; thus, in effect, wiping out the swirling motion.

A re-analysis of the 148 tornadoes which occurred on April 3-4, 1974 revealed the existence of nine tornadoes that were wiped out, leaving behind wide patterns of diverging winds (see Table 7.2).

Table 7.2 Path lengths of wide-end (WE) tornadoes on April 3-4, 1974 computed from old and new mapping methods. ID numbers and names are those used in Superoutbreak Tornado Map by Fujita (1975).

ID numbers	Names	Max widths	Old lengths	New lengths	Differences
15	Angola Tor. IN	3 mi	36 mi	27 mi	-9 mi
16	Hillsdale Tor. MI	3	21	15	-6
17	Charleston Tor. IL	1	16	15	-1
20	Hudson Tor. MI	1	10	7	-3
25	Melrose Tor. OH	1	8	7	-1
36	Hamburg Tor. IN	2	37	35	-2
49	New Castle Tor. KY	3	21	6	-15
54	Frankfort Tor. KY	6	36	21	-15
88	Corbin Tor. KY	1	21	18	-3
Total of 9 tornadoes			206	151	-55

DISSIPATION MECHANISM OF WATERSPOUTS was investigated extensively by Golden (1974a) and (1974b), who concluded that the onset of the decaying stage usually occurs abruptly as an advancing shower begins to overtake waterspout.

Golden classified the life cycle of the Florida Keys' waterspouts into five stages described as

STAGE 1. Dark spot forms on the sea surface. The spot can be seen from the air but not from the ground.

STAGE 2. Spiral pattern up to 1000 m in diameter forms on the sea surface around the dark spot.

STAGE 3. Spray ring forms around the eye region. The ring and the visible funnel are connected by an invisible vortex circulation.

STAGE 4. Mature waterspout in this stage is characterized by a condensation funnel with its maximum diameter and length.

STAGE 5. Decaying stage associated with a weakening dark spot on the sea surface and a nearby rainshower.

Figure 7.4 shows the late mature stage (Stage 4) followed by the decaying stage (Stage 5) of a typical waterspout. It is seen that the spiral ring is first blown apart by the outflow from the region of shower. When the outflow intensifies, as evidenced by white caps, the funnel cloud becomes separated from the spray ring which gradually weakens and disintegrates.

The decay process of waterspouts by Golden is very similar to that of the wide-end (WE) tornado wiped out by a downburst.

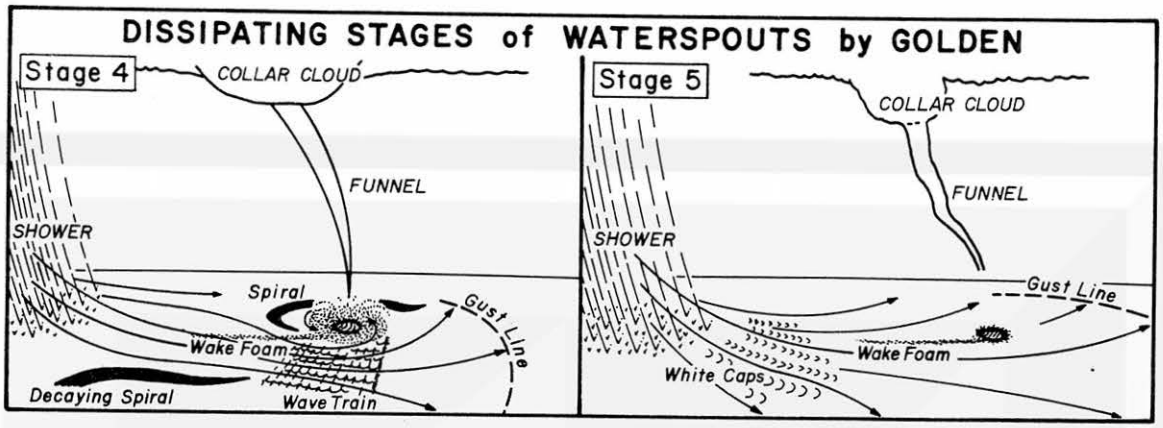

Figure 7.4 Late mature stage (left) and decaying stage (right) of waterspouts. Based on Figures 8 and 10 of Golden's (1974a) paper on "Life Cycle of Florida Keys' Waterspouts".

PATH OF A WIDE-START (WS) TORNADO in the previous map was depicted as a giant golf club. A detailed aerial survey of the start area almost always confirmed that the radius of curvature of the trajectories was too large to be regarded as being of tornadic origin (see Figure 7.5).

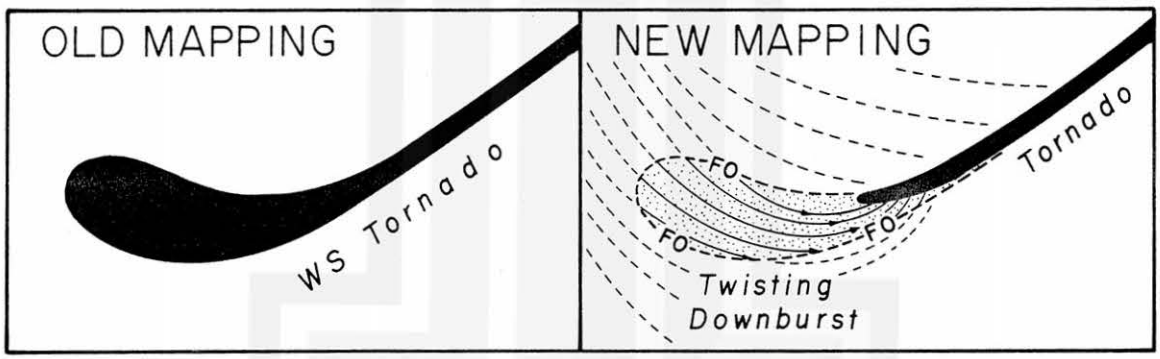

Figure 7.5 A wide-start (WS) tornado in old map is now regarded as a straight or meandering (SM) tornado preceded by a twisting downburst. The parent cloud of this type of tornado is a rotating thunderstorm characterized often by a so-called "hook echo".

There were eight wide-start (WS) tornadoes during the Superoutbreak. Of these, the start areas of three tornadoes in the Superoutbreak map by Fujita (1975) were not regarded as tornadoes or downbursts. Their damage areas were simply ignored (see Table 7.3).

Figure 7.6 shows two breaks in the Monticello tornado path. The break near Plato, Indiana had been confirmed earlier; however, the other break, near Chalmers, was found only recently.

Table 7.3 Path lengths of wide-start (WS) tornadoes on April 3-4, 1974 computed from old and new mapping methods. ID numbers and names are those used in Superoutbreak Tornado Map by Fujita (1975). The length in ( ) in "Old lengths" column denotes the path length of twisting downburst which had been ignored.

ID numbers	Names	Max widths	Old lengths	New lengths	Difference
14	Plato Tor. IN	2 mi	8 +(7) mi	8 mi	0 mi
34	Orleans Tor. IN	1	13	11	-2
38	London Tor. OH	1	15 +(4)	15	0
51	Peebles Tor. OH	2	16	12	-4
55	Cynthiana Tor. KY	3	25	20	-5
70	Parnell Tor. KY	3	24	14	-10
82	Moodybille T. KY-IN	1	19	16	-3
95	Phil Campbell T. AL	1	12 +(1)	12	0
Total of 8 tornadoes			132 + (12)	109	-24

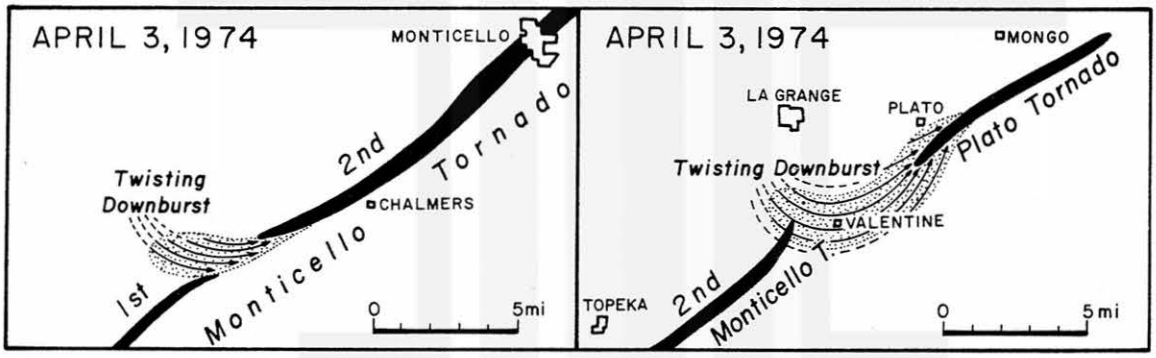

Figure 7.6 A re-analysis of the path of Monticello tornado, Indiana on April 3-4, 1974 revealed that the tornado consisted of three segments, the last two of which were preceded by twisting downbursts.

The F0 winds in these breaks were caused by twisting downbursts, characterized by trajectories with a 4- to 6-mile radius of curvature. Because the curvature is so small, the town of Valentine, located within the break, was damaged by straight-line winds. No signs of turning winds were evidenced inside the town.

This is why it is extremely difficult to determine exactly where a twisting downburst ends, being overtaken by a newly developing tornado (see Figure 7.6).

COLD AIR IN TWISTING DOWNBURST appears to be capable of developing into or merging with a tornadic circulation. Apparently the negative buoyancy of cold air does not prohibit the vertical stretching of the boundary layer air characterized by large vorticity and convergence.

Confirmed repeatedly by aerial surveys are trajectories of twisting downbursts that converge into the initial regions of wide-start tornadoes. How can cold, downburst air be accelerated upward?

The mean acceleration of an updraft with its vertical velocity, w, at height, h can be computed by

$$\bar{a} = \frac{w^2}{2h} \tag{7.1}$$

where $\bar{a}$ denotes the mean acceleration. If this acceleration were induced by a buoyancy force, we may equate

$$g \frac{\Delta T}{T} = \frac{w^2}{2h} \tag{7.2}$$

to obtain

$$\Delta T = \frac{T w^2}{2gh} \tag{7.3}$$

where g is the gravitational acceleration; T, the environmental temperature; and ΔT, the excess temperature of a rising parcel.

If the acceleration in Eq. (7.1) were induced by the vertical gradient of non-hydrostatic pressure, we may equate

$$\Delta P = \frac{1}{2} \rho w^2 \tag{7.4}$$

where ΔP denotes the difference in the non-hydrostatic pressures at the surface and at height h.

Presented in Table 7.4 are mean accelerations from Eq. (7.1) and from Eq. (7.3) in °C unit, mean convergence, and the non-hydrostaic pressure from Eq. (7.4).

Values in this table indicate that the negative buoyancy of cold, downburst air, say ΔT = -10 °C or -18 °F, is overwhelmed by the non-hydrostatic pressure when vertical velocities at 100 m exceed approximately 10 m/sec.

Since horizontal velocities of downbursts are 18 to 32 m/sec (F0) and 33 to 50 m/sec (F1), it would be feasible to induce a non-hydrostatic pressure when downburst currents slow down inside a large swirl. The positive non-hydrostatic pressure, thus induced, may reach several millibars, which should be sufficient to induce a swirling updraft in opposition to the negative buoyancy forces.

Table 7.4 Mean acceleration of rising air parcels inside swirling updrafts computed as a function of vertical velocities at 100 m above the ground. Air temperature and density were assumed to be 27°C and 1.17kg/m^3 respectively.

	VERTICAL VELOCITIES AT 100 meters AGL					
	5 m/sec	10 m/sec	15 m/sec	20 m/sec	25 m/sec	30 m/sec
in m/sec^2	0.13	0.50	1.13	2.00	3.13	4.50
in "g" unit	0.01	0.05	0.11	0.20	0.32	0.46
ΔT from Eq.(7.3)	4°C	15°C	34°C	61°C	96°C	138°C
Mean convergence (sec^{-1})	0.05	0.10	0.15	0.20	0.25	0.30
Non-hydrostatic Pressure (mb)	0.2	0.6	1.3	2.3	3.7	5.3

SCOTTSBLUFF TORNADO of June 14, 1977 was witnessed and photographed by Patrolman Schneider of the Nebraska State Highway Patrol. Responding to reported hook-echoes near Minature, Nebraska, the patrolman drove east on US-26 through the town in order to locate possible tornadoes.

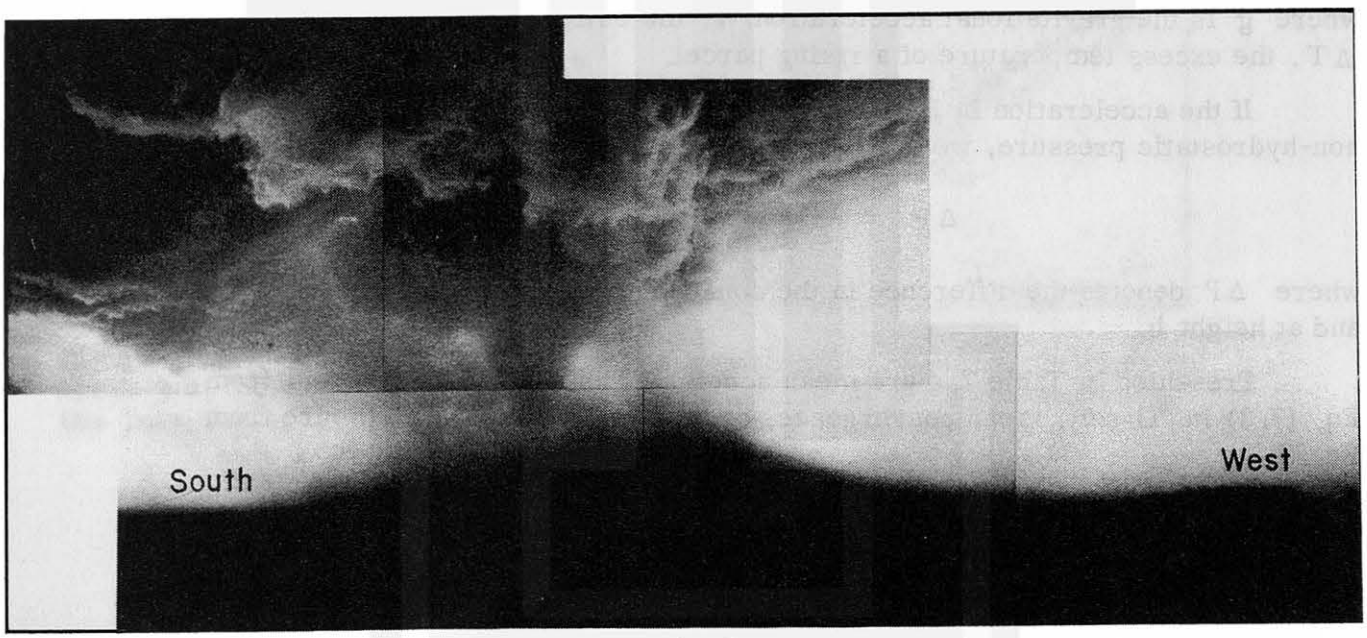

Figure 7.7 The formative stage of a wide-start (WS) tornado depicted by a mosaic of five pictures taken by Patrolman Schneider of Scottsbluff, Nebraska. Blidning dust clouds from a thunderstorm to the northwest was swirling into the tornado region, indicating the entrainment of downdraft (burst) air into tornado. This tornado was moving slowly from right to left over a grassland about 16 miles to the west-southwest of Scottsbluff.

Picture data: Time-- 1756 MST June 14, 1977; Distance to tornado-- 6,400 m; Direction-- SSE to WNW.

Gusty winds from a rain area to his left (north) were blowing dust across the highway. When the patrolman reached the east side of the blowing dust area he saw a tornado forming to his right (south) of the highway. The entire cloud system was so large that he had to take several pictures to cover the whole storm.

A mosaic of 5 pictures in Figure 7.7 shows an entrainment of dusty, downburst air from the right (northwest). A few minutes earlier he had driven by the forest which is seen to the west in the picture.

Aerial and ground mapping of the path was done by Fujita and Umenhofer in cooperation with Rafael L. Gallegos, MIC of the NWS office at Scottsbluff, Nebraska. Photogrammetric analyses revealed that the tornado was about to form 4.0 miles (6.4 km) south-southwest of the patrolman when he took the mosaic pictures. The diameter of the dust column surrounding the funnel cloud was 1.4 miles (2.2 km). It certainly was a swirling wind of a giant core diameter.

Patrolman Schneider followed the tornado, driving eastward on the north side of the tornado, taking a series of pictures showing its evolution from a core-funnel to a rope, extending into the dark cloud far to the left (east). Shortly before the rope disappeared, the top of the rope was moving to the left (east) while the vortex on the ground was moving westward.

Aerial mapping and photogrammetric analysis confirmed that this storm originated as a wide-start (WS) tornado and turned into a typical left-turn (LT) tornado (refer to Figure 7.21 in this chapter).

This Scottsbluff tornado is an extremely well documented case of a wide-start tornado which formed on the advancing end of a downburst inside a hook-echo circulation. The cold, dusty air first induced a huge column of swirling dust, inside of which a cone-shaped funnel cloud formed and descended all the way to the ground. The tornado traveled through a distance of 3.1 miles (5.0 km) while continuously changing its shape from cone to trunk and finally to a rope-shaped funnel. At its final stage, the tail end of the rope extended toward the west, outside of the parent cloud.

PRELIMINARY ANALYSIS OF TOKYO TORNADO of February 28, 1978 revealed that the storm was a wide-start (WS) tornado which formed over the mouth of the Arakawa (meaning rough river in Japanese).

The author's analyses, so far, are based on accounts by two of the largest Tokyo newspapers. A forerunner, tornadic storm started at 2120 JST, damaging 330 houses to the west of Haneda Airport near the train tracks of the New Tokaido Line (see Figure 7.8).

Scattered damage caused by high winds occurred over the landfill sections along the bay-front of Tokyo. Then, at 2134 JST, the last two cars of a 10-car train of the east-west subway line were overturned by high winds. The subway train was westbound over the Arakawa railroad bridge about 300-m long (see Figure 7.9). 21 persons in the two cars were injured.

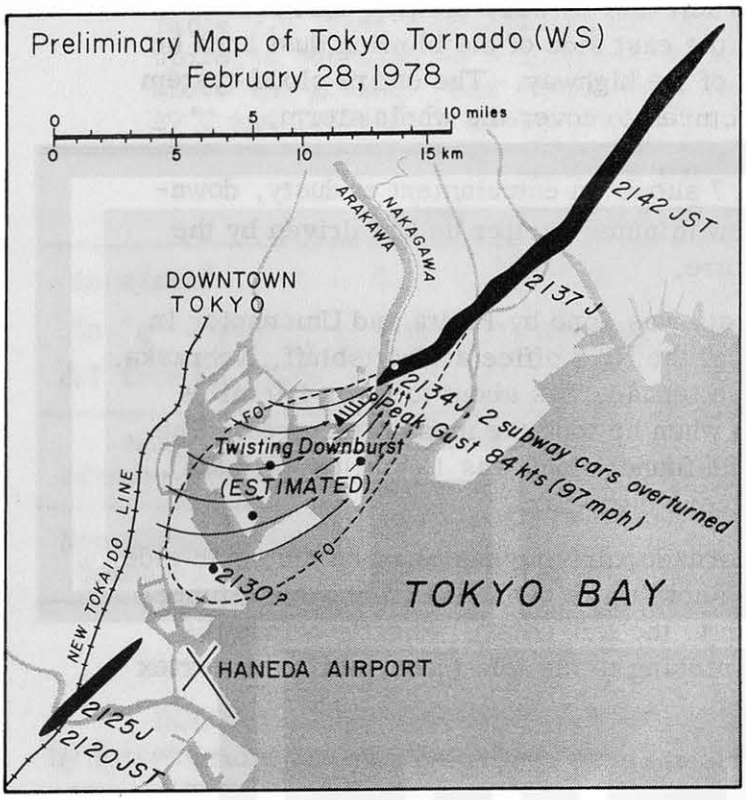

Figure 7.8 Schematic map of Tokyo tornado preceded by an estimated twisting downburst, 2 to 4 miles wide.

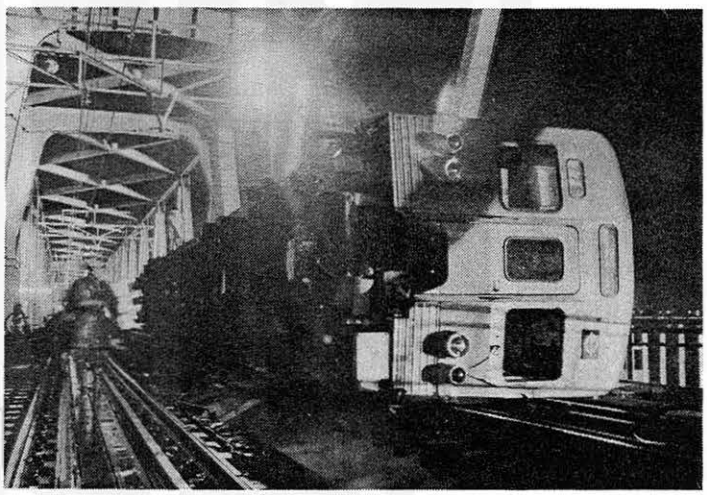

Figure 7.9 Last 2 cars of 10-car subway train overturned by a tornado. Courtesy of the Yomiuri Newspaper, Tokyo.

Gust recorder traces from a wind tower located 1.1 miles (1.7 km) southwest of the accident site showed a peak gust of 84 kts (97 mph) from the southwest. A damage path continued from near the accident site northeastward. The storm traveled through a distance of 25 miles (40 km) at the rate of about 54 mph (86 km/hr). The translational speed of the tornado is reasonable in view of the fact that the 500-mb wind over Tokyo at 2100 JST was estimated to be 70 kts (130 km/hr).

It is likely that this tornado in Tokyo was induced by a twisting downburst which descended over the bay-front region of the capitol city. The tail end of the downburst swirled into a large-core tornado which traveled northeastward, crossing the Arakawa railroad bridge while a subway train was traveling on the same bridge. Although the newspaper accounts are not suitable for an accurate F-scale assessment, the peak F scale was probably about F1.

NARROW-START (NS) TORNADOES were found to form and develop on the left side of weak downbursts where cyclonic vorticity inside the boundary layer is apparently the largest.

Shown in Figure 7.9 are trajectories of weak downburst winds from the southwest. Almost always we observed from the air traces of weak winds from the northwest (see dashed trajectories).

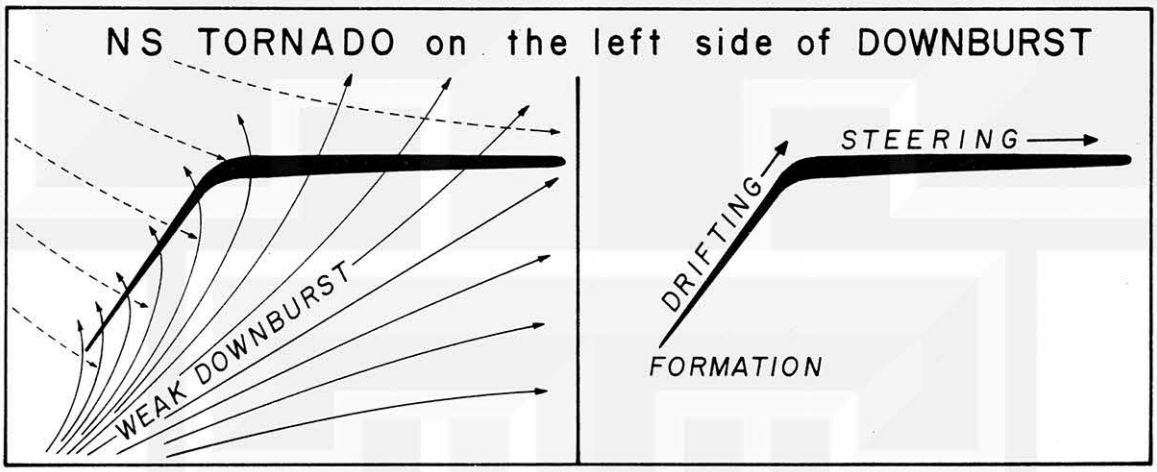

Figure 7.10 Formation and movement of a narrow-start (NS) tornado on the left side of a downburst.

Although it is not feasible to reconstruct the time-sequence of the event in Figure 7.10 precisely, the logical steps as determined by the order of the fall of corn stalks in several cases of NS tornado formations are as follows:

1. Weak, non-damaging winds from the northwest (dashed lines) occur first.

2. A weak downburst from the southwest (full lines) interrupted the northwest winds.

3. One or more swirl winds form on the left side of the weak downburst.

4. The swirl wind drifts from southwest to northeast while increasing its vortex height.

5. When the swirl develops into a full-grown tornado it is steered by the westerly winds above the boundary layer.

Thus, the path of a narrow-start tornado consists of a drifting path, a sharp right turn, and a steering path.

Examples of narrow-start tornadoes are seen in Color Map No. 5. The Leland tornado drifted about one mile northeastward. After a sharp right turn, it traveled three miles toward the east-southeast.

Sandwich tornado, consisting of three narrow-start tornadoes, was confirmed by aerial photography and mapping. A wind system which damaged two mobile homes to the southwest of the first Sandwich tornado could have been another narrow-start tornado.

Both the Plano and Bristol tornadoes in Color Map No. 5 were apparently narrow-start tornadoes, although the Bristol tornado failed to grow into its steering altitude.

SPRINGFIELD TORNADOES in Color Map No. 8 consisted of a number of narrow-start tornadoes. Tornado No. 2 consisted of three narrow-start tornadoes, each with less than a 0.5 mile long path. Tornado No. 3 drifted until making a sharp right turn. Tornado No. 5 and 7 were rather complicated, narrow-start tornadoes.

AERIAL PHOTOGRAPHS OF LELAND TORNADO are shown in Figure 7.11. The left picture reveals the pattern of corn stalks leaning from upper left (southwest) to lower right. The path of the drifting vortex extends from near the upper left corner to the farm to the right.

The track of a weak vortex such as this can be identified by taking oblique aerial pictures looking toward the direction of the sun. The forward scattering of sunlight from leaning corn stalks produces a sharp contrast in brightness on both sides of the vortex track. In the past, we missed a number of vortex tracks because we were not aware of this photographic technique.

The right picture (Figure 7.11) shows the vortex track of the Leland tornado in its drifting stage, which extended toward the east-southeast.

Figure 7.11 Path of the Leland tornado (Color Map No. 5) along the left edge of downburst 5. The path extends from upper left corner to the south edge of a farm (left picture). The tornado changed its course abruptly toward the east (right picture).

At one point the tornado passed over a small building on a farm, peeling a number of tiles from the roof. Two doors on the south side of a barn were blown out toward the vortex center. Evidently the tornado was characterized by slow rotational and fast traveling velocities. Note that the speed of the parent bow echo was 55 to 60 kts (refer to Figures 5.5 and 5.13).

Six corn stalks were pulled up from the ground. The flattened corn stalks showed the converging patterns of the trajectories without leaving any evidence of a complete swirl (see Figure 7.12).

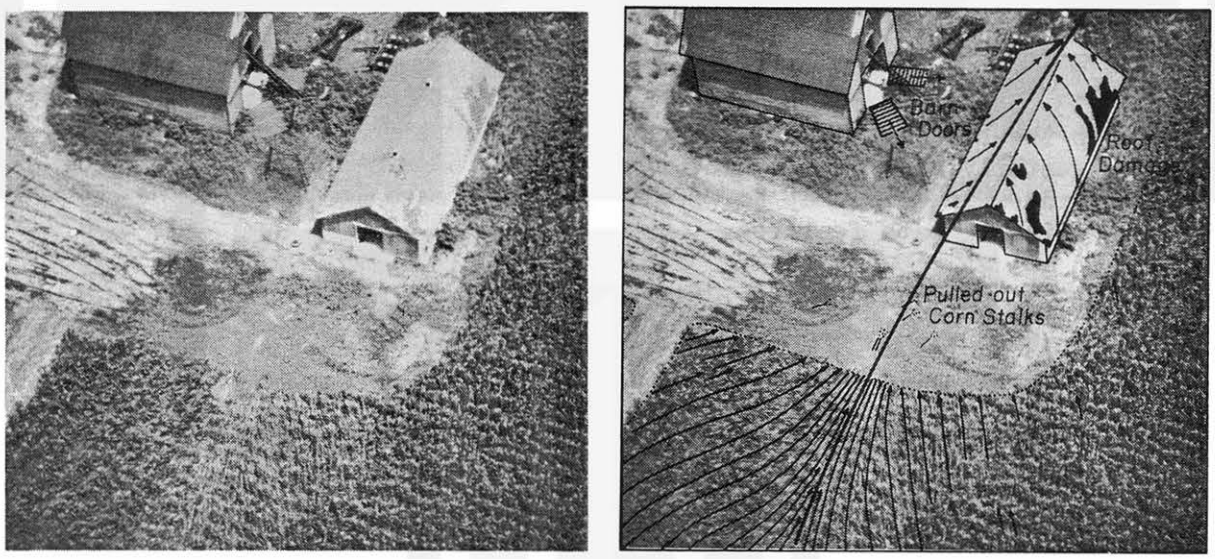

Figure 7.12 The Leland tornado was characterized by slow rotation and fast translational motion. Directions of damaged cornstalks were predominantly convergent.

Schematic diagrams showing the formation, drifting, sharp turn, and steering of a narrow-start tornado are presented in Figure 7.13. In these diagrams, the tornado is assumed to have developed inside the boundary layer where a large cyclonic vorticity (shear and curvature) coupled with convergence is known to exist.

If this is the case, the Leland tornado,along with other short-start tornadoes, first formed near the ground, then extended upward. A condensation funnel appears in the upper portion of the vortex when the central pressure drops below a critical value. Then, the funnel cloud extends downward.

Residents within an area of one to two miles of the Leland tornado were interviewed in an attempt to obtain eyewitness accounts. Practically everybody stated that it was raining so hard that they were not aware of the tornado until the damages were discovered immediately after the rain. Because no one saw the tornado;pictures were not taken. Yet, there was definite evidence of a tornado, which we confirmed in an aerial survey performed the following afternoon.

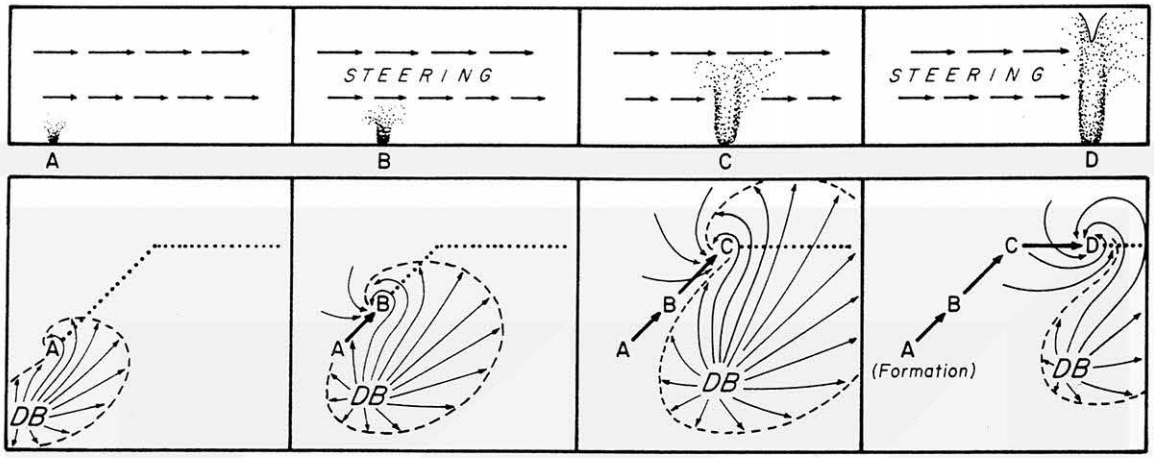

Figure 7.13 Schematic diagrams showing the formation of a narrow-start tornado in the boundary layer. As the swirling motions extend upward into the westerly steering levels, the tornado makes a sudden right turn. Three tornadoes in Color Map No. 5 and several others in Color Map No. 8 displayed similar path features.

STRAIGHT or MEANDERING TORNADOES have been found in various parts of the country. An amazing feature of the paths of these tornadoes is the superposition of relatively small amplitude meandering motion upon a relatively straight path.

A remarkable picture of such a path is visible in an ERTS picture taken on June 3, 1974. It was two months after the Guin tornado (F5) of April 3, 1974 smashed through northwestern Alabama, killing 30 persons and injuring 280 others. The distance between two arrows in the ERTS picture is 45 miles (see Figure 7.14).

Figure 7.15 shows an aerial view of the path extending northwest through the center of the city of Guin. Houses and trees in the path were badly damaged. Some trees were stripped entirely of their leaves and never regained their strength. This is why the tornado path was still visible in an ERTS picture taken on October 7, some six months after the tornado.

Figure 7.14 Path of the Guin tornado of April 3, 1974 in an ERTS picture taken on June 3, 1974. The path was still visible in the ERTS picture taken on October 7, 1974. The path was more or less straight, characterized by small-amplitude oscillations. Distances between Guin (left arrow) and William B. Bankhead National Forest (right arrow) is 45 miles or 72 km.

Figure 7.15 An aerial photo of the Guin tornado path. Taken on April 5, 1974 from above the City of Guin looking northeast.

MOUNTAIN-CLIMBING AND CANYON-CROSSING TORNADOES were found at numerous locations in Kentucky, Tennessee, Georgia, North Carolina, Virginia, and West Virginia after the April 3-4, 1974 Superoutbreak.

An example of a mountain-climbing tornado is seen in Figure 7.16. The Murphy tornado, North Carolina, moved from right (west) to left, passing directly over the highest point of the mountain. No deviation from its course nor intensity change was noticed along its mountain-climbing and descending path.

Some rather interesting questions regarding the nature of tornadoes on mountainous or hilly terrains are:

1. How does a tornado maintain its intensity against a large loss of energy during its traverse across ragged terrains?

2. Why is it that the course of a tornado does not deviate appreciably while traveling across canyons and mountains?

3. Why does a tornado make unexpected turns while moving over a relatively flat terrain?

In effect, the path of this type of tornado appears to be more or less independent of the topography on which it swirls.

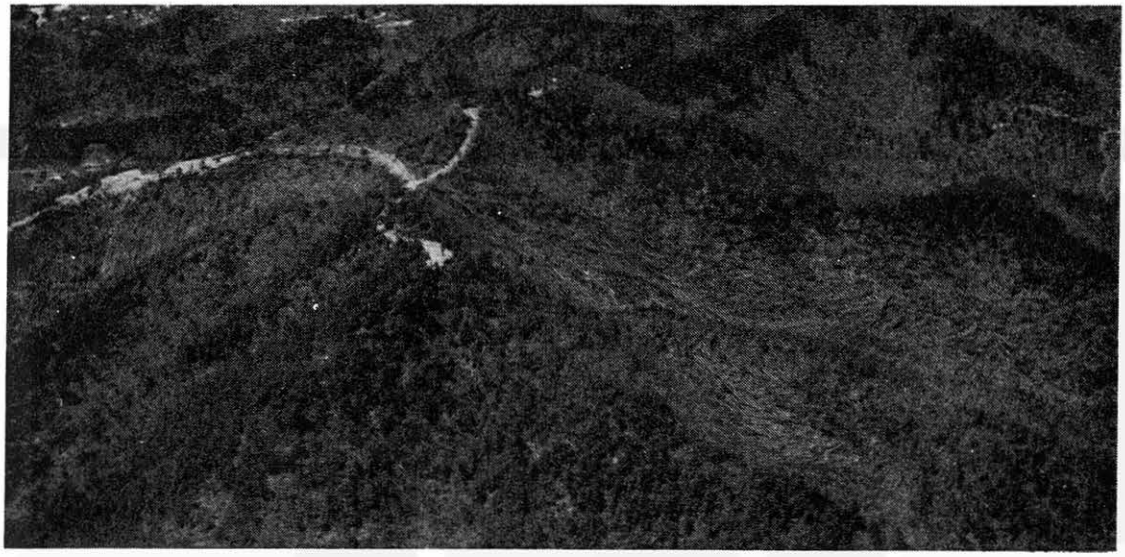

Figure 7.16 A mountain-climbing tornado of April 3, 1974 which left behind a damage path across the mountaintop southeast of Murphy, North Carolina. The tree damages in both upslope and downslope paths were equally severe, rated as F 3.

RIGHT-TURN MECHANISM of tornadoes was investigated through aerial photography and subsequent mappings. The results revealed the existence of downbursts when tornadoes undergo definite turns.

Rainville tornado, Indiana, on April 3, 1974 crossed US-41 toward the northeast, being characterized by cycloidal marks left in a plowed field. Shortly after the highway crossing, the marks were interrupted and the course deviated to the right (see Figure 7.17).

Figure 7.17 Rainsville tornado of April 3, 1974 affected by the downburst winds from the rear left. The tornado weakened abruptly while deviating to the right.

Mapping of tree damages around the right-turn area confirmed the existence of strong winds from the northwest. Since the tree damage on the left (northwest) side of the path started near US-41, the flow was caused probably by a downburst which descended to the northwest of the tornado.

Right turns similar to this case appear in Color Map No. 2. The two final right turns of the Mattoon tornado were caused by Downburst 8 and Microburst m 11. The 1st and the 2nd Canton tornadoes in Color Map No. 7 had right-turn paths caused, respectively, by Microburst m 2 and Microburst m 6. Tornado No. 14 in Color Map No. 8 made its final right turn because of Microburst m 14.

It is likely that a turning of a tornado can be caused by downburst winds within a relatively shallow layer above the ground. Meanwhile a violent tornado can be steered across ragged terrain along a straight or a meandering path, without being affected appreciably by the topography.

RIGHT TURN OF LOUISVILLE TORNADO of April 3, 1974 was documented by a series of still pictures taken by Mr. Cundiff of Crestwood, Kentucky (see Figure 7.18).

Cundiff was watching the Louisville tornado and its dark, parent cloud traveling from left (southwest) to right across the western sky. As shown in the left picture in Figure 7.19, the upper portion of the cone-shaped funnel extended up into the dark cloud while the lower tip near the ground was bent toward the left.

Within a few minutes the whole funnel emerged from the dark cloud, turning into a tall, grayish white funnel cloud. Thereafter, the funnel moved from left (west) to right in front of the parent cloud (see right picture in Figure 7.19).

In view of scattered tree damages to the southwest of La Grange, where a new tornado had started, we may speculate on the existence of a downburst on the left (northwest) side of the tornado (see Figure 7.18).

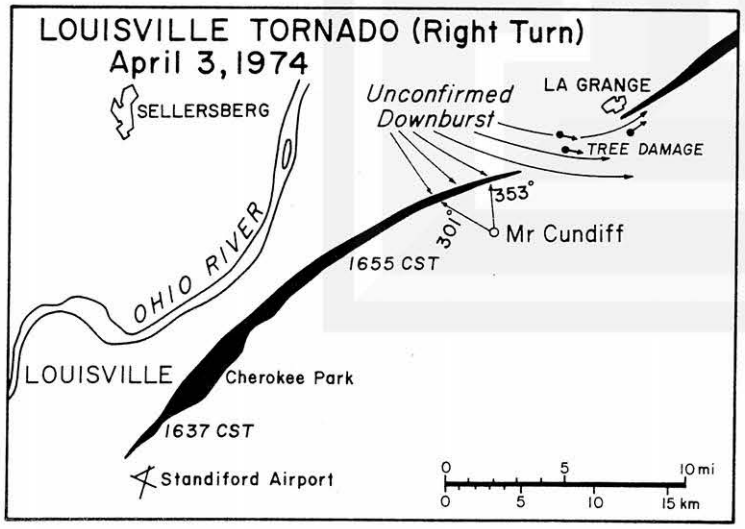

Figure 7.18 Louisville tornado which made a right turn during its dissipating stage. A sequence of pictures taken by Mr. Cundiff revealed that the tornado emerged from the parent cloud toward the south, apparently in response to a downburst from the north.

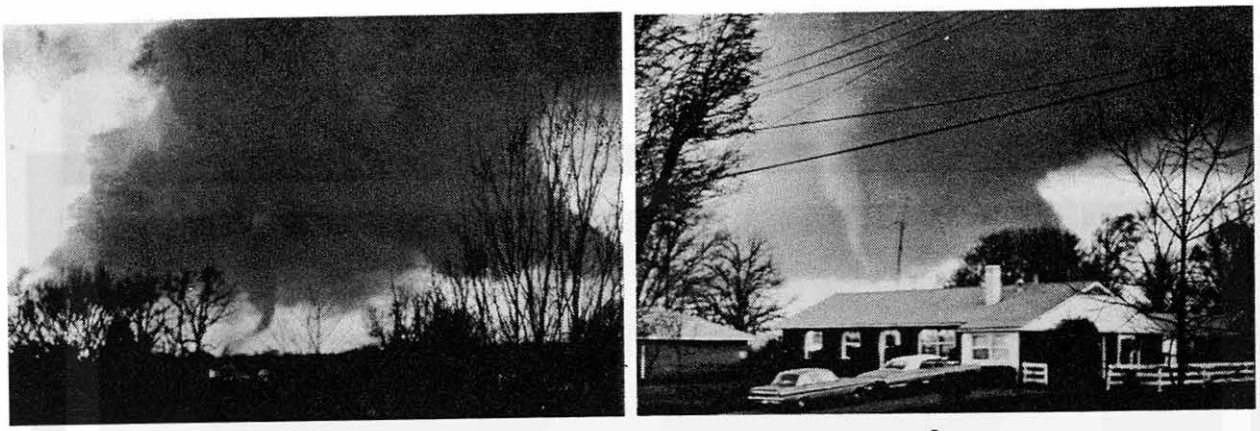

Figure 7.19 The left-side picture, looking toward 301°, shows a sharp bending of the tornado axis. The tornado gradually moved out of the dark parent cloud toward the photographer looking toward 353°. Courtesy of Mr. Cundiff.

The motion of cloud elements presented in Figure 7.20 indicates the height of the funnel bending to be only up to 200 m when the left picture of Figure 7.18 was taken. This may mean that the downburst wind had began undercutting the tornado circulation.

The funnel near the surface was continuously pushed out of the parent cloud by the downburst wind, while traveling eastward faster than the parent cloud.

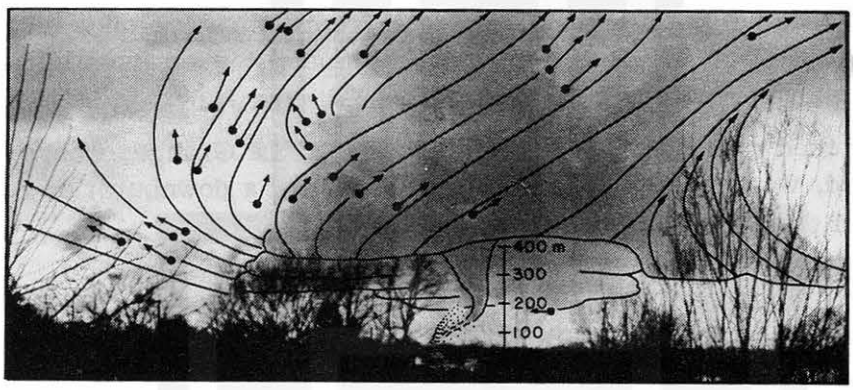

Figure 7.20 Displacements of small cloud elements between two successive pictures taken by Cundiff. It is not feasible to compute speeds, mainly because picture intervals are not recorded. It should be noted that the bending of the tornado axis took place inside the 200-m layer above the ground.

LEFT-TURN TORNADOES of April 3, 1974 have been mapped and discussed by Fujita (1974), (1975) and Forbes (1977), (1978) in detail. The left-turn paths of tornadoes in a family are very unique and unmistakable when determined through an aerial survey.

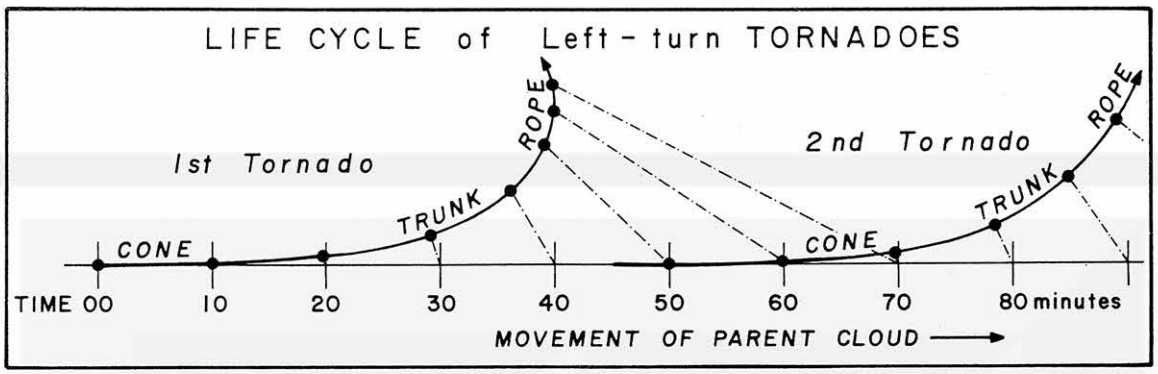

Figure 7.21 Typical paths of successive left-turn (LT) tornadoes spawned by a single parent cloud. Note that there are chances of observing a rope-shaped funnel and a cone-shaped funnel simultaneously.

The first tornado is characterized by a cone-shaped funnel when it appears. Then, the funnel is steered by the parent cloud for 10 to 20 minutes, until the tornado vortex at the ground deviates to the left while reducing its translational speed. As a result, the vortex on the ground is left behind to the left of its original location relative to the parent cloud. Meanwhile, the funnel shape changes from a cone to a trunk, and finally into a rope (see Figure 7.21).

One of the earliest documentations of left-turn tornadoes was Fujita's (1960) Fargo tornado paper. The early stage of the tornado (F4) was a mighty cone-shaped funnel. Later it turned into a 10-mile long rope funnel after making a significant left turn.

As in the case of the Scottsbluff tornado, the end of the rope funnel on the ground of the Fargo tornado was moving westward while the upper portion of the rope was traveling eastward, being attached to the parent cloud at a high level.

Fujita (1960) assumed that the left-turns of the Fargo tornadoes of June 20, 1957 were caused by the circular motion of tornadoes around the center of their parent rotating cloud. Agee et al (1976) considered that the paths of successive left-turn tornadoes as being portions of a cycloid generated by a combination of both rotational and translational motions.

Detailed analyses of left-turn paths relative to hook echoes in recent years have failed to support above hypothesis. In practically all cases tornadoes simply moved away from the central region of the parent clouds while turning into long, rope-shaped funnel clouds.

RARE SIMULTANEOUS PICTURES of a disintegrating rope and a newly-forming cone were taken by Messrs. Jay and Mark Carter. The cone funnel (right), at the formative stage of the Mason tornado, Ohio, was located near the center of the parent cloud over the northeast suburb of Cincinnati, Ohio. The rope funnel of the Sayler Park tornado on the ground was about 7 miles to the west of the cone funnel and was swirling practically under the blue sky (see Figure 7.22).

During its dissipating stage, the ground position of the rope funnel of a left-turn tornado is located outside the parent cloud. If the initial cone funnel forms inside the hook echo of a parent cloud, the vortex on the ground of a left-turn tornado will have to move out of the parent hook, somehow.

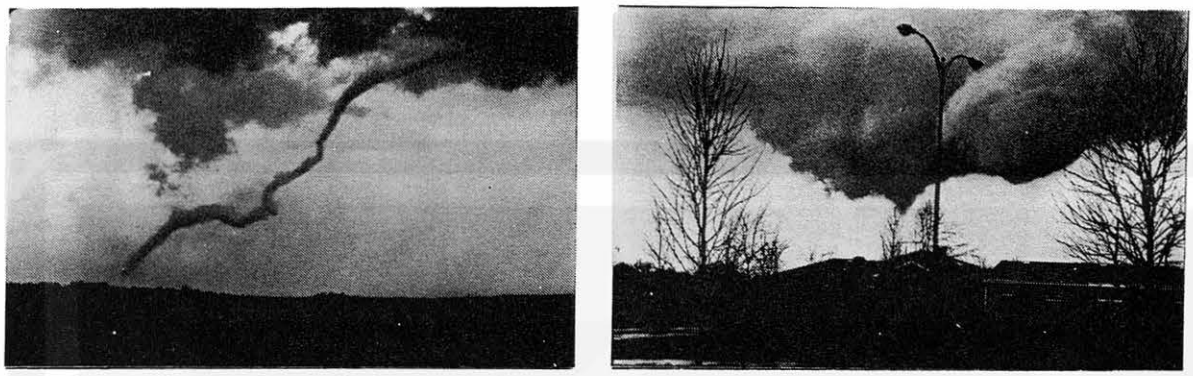

Figure 7.22 Two pictures taken almost simultaneously from two different locations in Cincinnati, Ohio. The rope-shaped funnel (left) was photographed by Mr. Jay Carter and the cone-shaped funnel (right) by Mr. Mark Carter who happened to be his nephew. Pictures were taken at 1640 CST, April 3, 1974.

TORNADOES WHICH GOT OUT OF THEIR PARENT HOOKS were found by Fujita (1975) who introduced four cases of tornado vs hook-echo relationships. They are:

1. Xenia tornado got out toward the northwest
2. Sayler Park tornado, toward the west
3. Brandenburg tornado, toward the west-southwest
4. Louisville tornado, toward the south.

The Fargo tornado of June 20, 1957, Scottsbluff tornado of June 14, 1977, and many others can be added to this list.

The evidence of tornado formations beneath rotating thunderstorms and of their dissipation leads to a suspicion that there must be a definite mechanism by which these tornadoes are pushed out of their parent clouds. The ground friction, by itself, is not enough to explain the relative motion between tornadoes and their parent clouds.

DOWNBURSTS BENEATH ROTATING THUNDERSTORMS could induce wind fields capable of changing the courses and speeds of tornadoes spawned by parent clouds.

The existence of downbursts on both sides of the tornado tracks has been shown in Color Maps Nos. 2, 3, 5, 7, and 8. It is also evident that the translational velocities of tornadoes are influenced by these downbursts (see Examples in Figures 7.17 through 7.18).

Presented in Figure 7.23 is a proposed mechanism of the life cycle a family of tornadoes spawned by a rotating thunderstorm. An explanation of the cycle in time sequence is as follows:

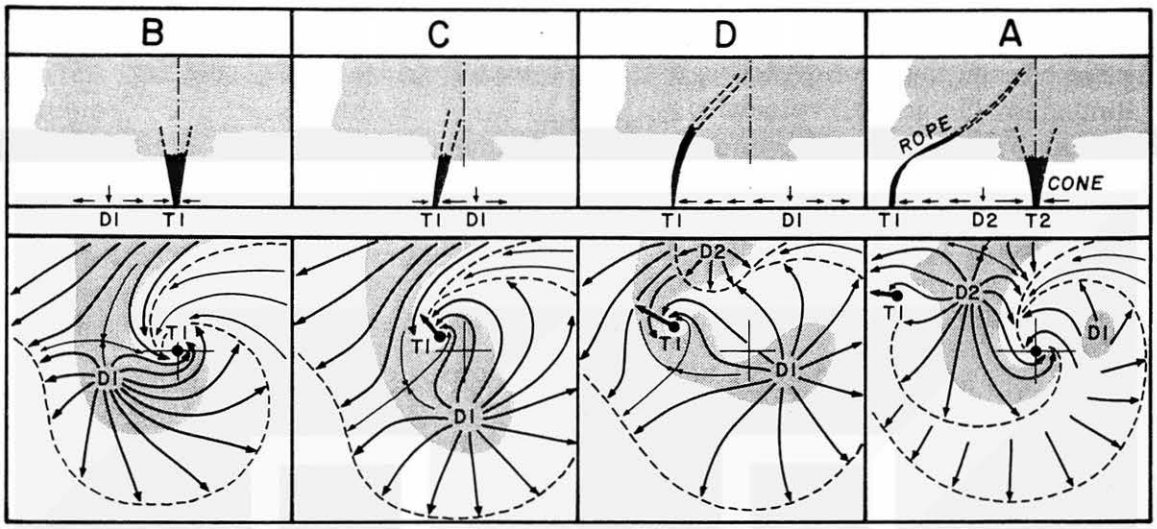

Figure 7.23 A schematic sequence showing a possible process of inducing a new tornado after the eviction of the old one which weakens while turning into a rope-type funnel.

At time B. Tornado, T1, is located inside the hook echo accompanied by a downburst, D1, beneath the hook. By virtue of its origin inside the rotating thunderstorm, twisting downburst, D1, acts as a vorticity feeder to tornado T1.

At time D. The tornado is pushed away further while the downburst center keeps rotating around the cloud center. Precipitation particles swirling around the tornado form an apparent hook around the tornado, thus distorting the hook, often beyond recognition.

At time A. A new downburst from the main precipitation area moves into the rear-left quadrant of the rotating thunderstorm. The old tornado, T1, changes into a long rope, still attached to the parent cloud. A new tornado, T2, forms inside the renewed hook.

The rope funnel of the old tornado, T1, will soon disintegrate into pieces, while the new tornado, T2, turns into a large cone funnel. Meanwhile, the new downburst, D2, moves into the rear quadrant of the parent cloud. The new life cycle of tornado T2 is repeated by following diagrams, A, B, C, D, A, B, ...

DOPPLER VELOCITIES of precipitation particles are very useful in understanding the flow field of the parent thunderstorm in relation to tornadoes. Several cases of dual-Doppler velocity fields of tornado-bearing storms were presented by various researchers.

Of interest are the two locations of downdrafts inside the June 6, 1974 storm which was studied by Brandes (1977a). These downdrafts were located on the western edge and in the northeastern quadrant of the storm traveling toward the northeast.

A tornadic storm of April 20, 1974 was investigated by Ray et al. (1975), demonstrating the effectiveness of depicting a storm's wind field by subtracting the mean vector field from the ground velocities.

The Harrah storm of June 8, 1974, studied by McCarthy et al. (1975), Brandes (1977b), and others, was accompanied by a right-turn tornado of F2 to F3 scale. Although the times of the tornado in relation to Doppler velocity fields are not known precisely, one of the two vorticity centers at 300-m AGL was located just to the north of the tornado track.

Brandes' analysis of the 1553 CST velocity field shows a center of divergence to the north of the Harrah tornado track near its right-turn location. He also showed a divergence center to the northwest of the Oklahoma City tornado, when it began turning to the right.

Because of ground clutter, Doppler velocities below 300 m AGL are highly unreliable. As far as we know, however, the divergence fields of downburst winds are probably most significant at the heights of 50 to 200 m AGL. Doppler measurements at these low heights will be possible only within a very short range from each radar, making it impractical to perform multi-Doppler measurements.

To overcome, at least in part, such difficulties it would be necessary to combine Doppler velocities with surface network, tower, acoustic-microwave Doppler, and other data. A detailed aerial and ground survey of storm-affected areas is also necessary in solving the tornado-downburst relationships.

INTERNAL STRUCTURE OF TORNADOES must be influenced by downbursts whenever their outflows enter the circulation field of tornadoes.

A tornado which is free from downbursts can be approximated as a combined flow of steering and axisymmetric wind fields. An example of such a simplified tornado is shown in Figure 7.24.

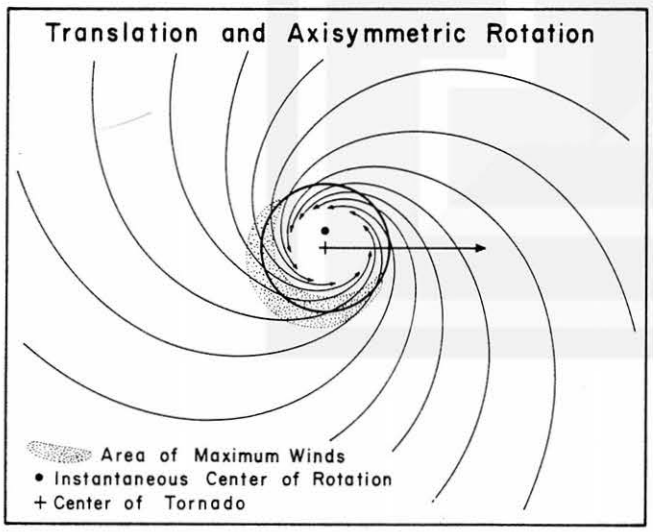

Figure 7.24 An idealized tornado characterized by an axisymmetric swirl and translational motions.

Maximum winds are seen on the right side of the traveling storm, behind the right-left line through the storm's center. The approximate area of maximum winds is stippled. The instantaneous center of rotation is where wind is calm momentarily. At the center of the tornado, however, the wind should be blowing toward the direction of the translational velocity.

EXISTENCE OF ASYMMETRIC CONVERGENCE around the tornado center is suspected because we often observe cycloidal ground marks left behind, especially by large-core tornadoes (see Figure 7.25).

Cycloidal ground marks in open fields consist of narrow bands of debris, suggesting that the debris was collected by small vortices (suction vortices) located inside the storm's core.

The rotational characteristic of a suction vortex is seen in Figure 7.25. It is a close-up view of blown down grass in Horicon Marsh, Wisconsin, in the direct path of a June 5, 1977 tornado.

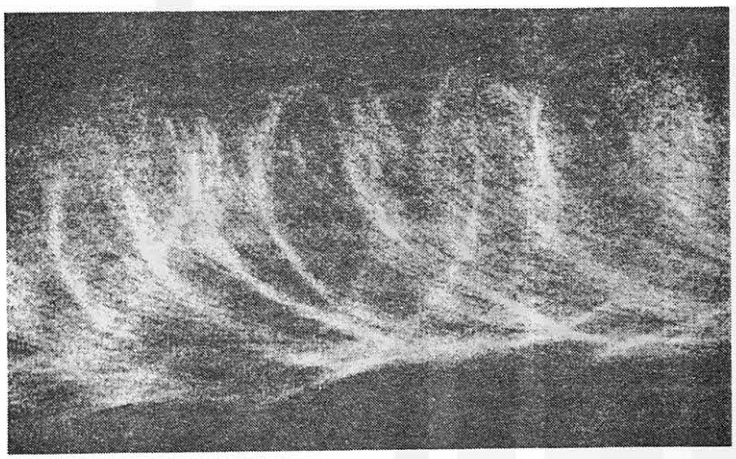

Figure 7.25 Cycloidal ground marks left behind by the Magnet tornado, Nebraska, of May 6, 1975. These marks usually consist of a deposition of debris collected by suction vortices.

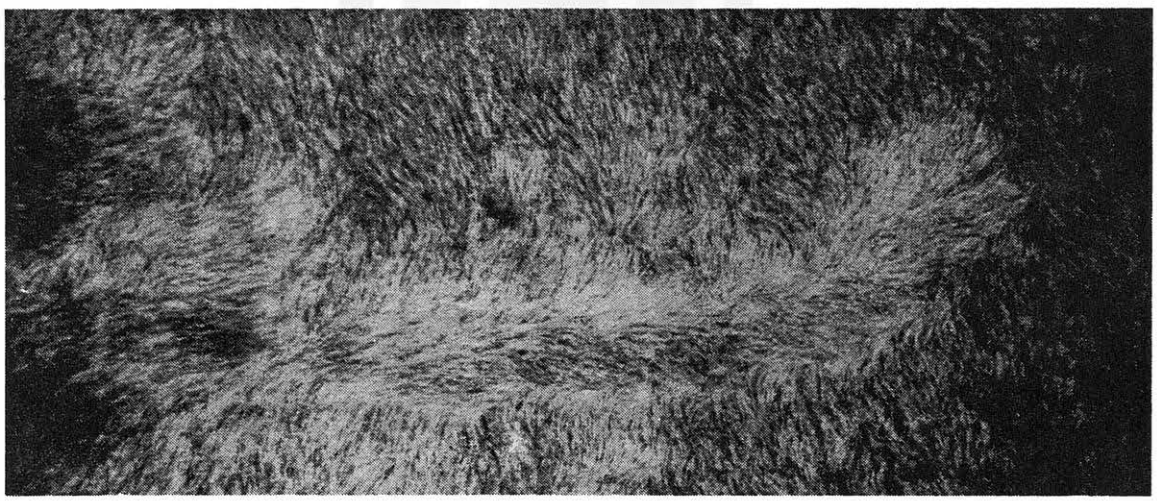

Figure 7.26 A close-up view of a suction-vortex mark left in a low-grass field. Photographed by Stiegler after the Horicon Marsh tornado, Wisconsin, of June 5, 1977.

DISTORTED TORNADO VORTICES due to downburst winds from the rear and from the rear-left are shown in Figure 7.27. These schematic diagrams show the existence of the localized convergence, "S", located where convergence lines are extended into the core (see Figure 7.27).

A suction vortex is likely to form at or near this spot "s" and travel around the tornado center. During the asymmetric stage of a tornado vortex, suction vortices will form successively, resulting in the multiple vortices revolving around inside the core.

Trajectories over the formation area of suction vortices are made visible by the streaks of corn stalks (see right-side pictures in Figure 7.28).

The paths of successive suction vortices are characterized by banded areas of trajectories with both cyclonic and anticyclonic curvatures. Close examination of damaged corn stalks often reveals the existence of complete circulations hidden below the corn stalks blown down by the final winds (see left-side pictures in Figure 7.28).

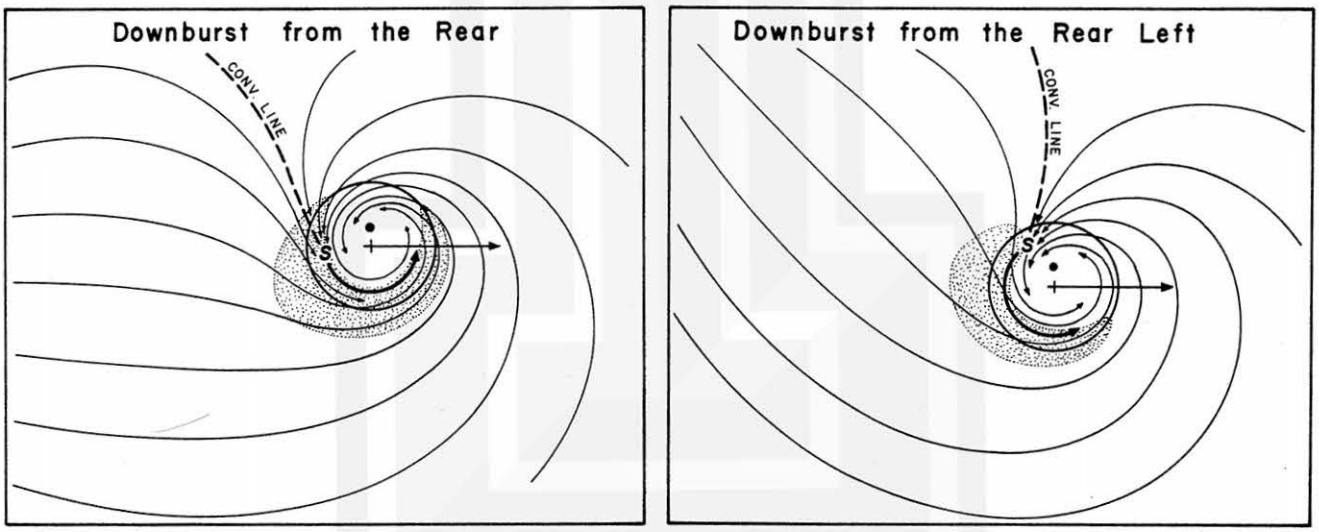

Figure 7.27 Disruption of axisymmetric convergence field around the tornado axis near the ground caused by downburst winds from the rear (left side) and from the rear left (right side). The largest convergence occurs at "s" where a suction vortex is likely to develop.

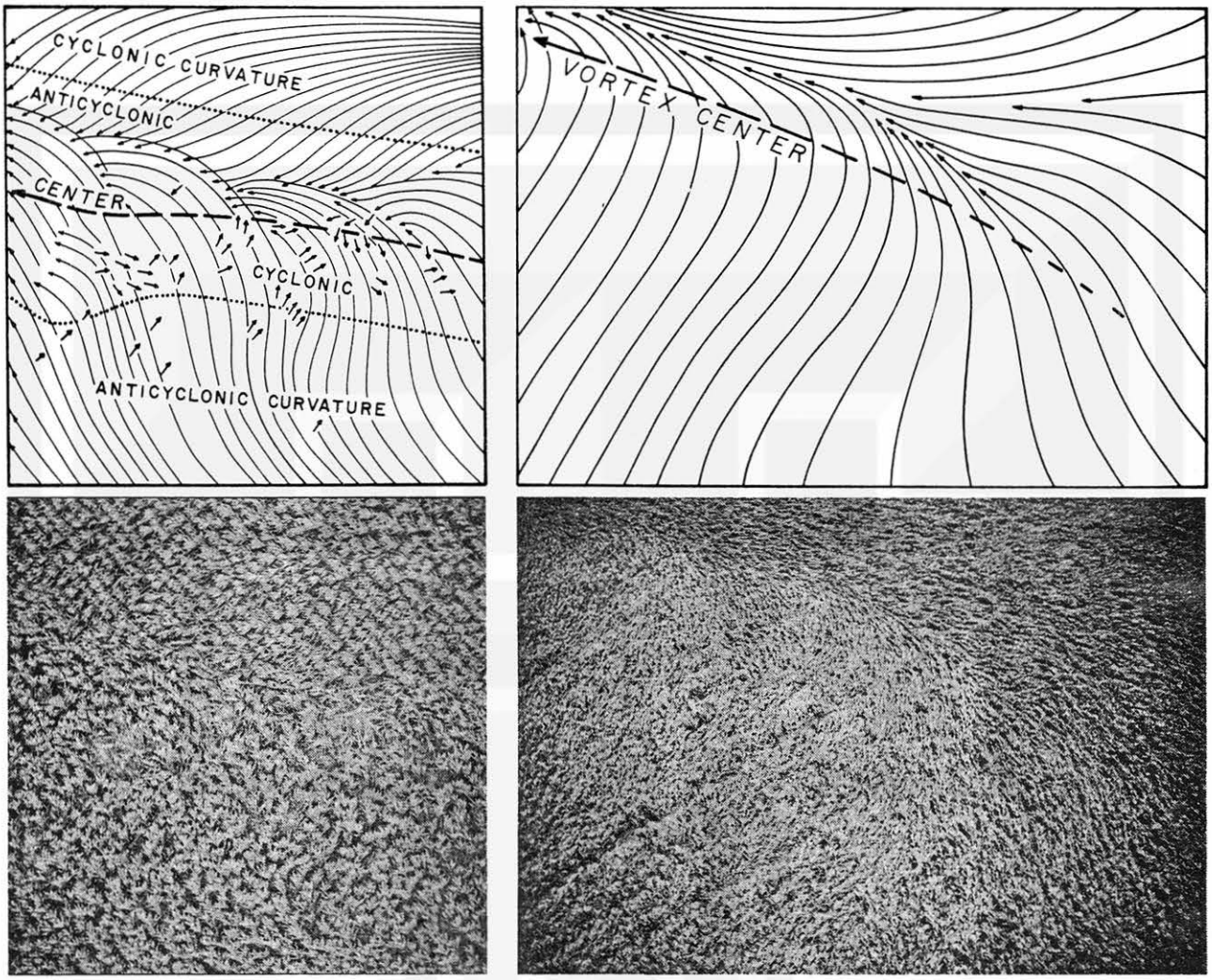

Figure 7.28 Trajectories of converging flows which swirl into a suction vortex. The horizontal scales of suction vortices are about one order of magnitude smaller than their parent tornado. The vortex center is located to the left of the trajectory convergence (right). A cyclonically-rotating suction vortex often leaves behind trajectories with cyclonic and anticyclonic curvatures (left).

MICROBURSTS NEAR TORNADOES will also affect the tornado structure as well as their courses. A microburst to the front of a tornado will induce suction vortices on the left side of the center. The position of the suction vortex rotates approximately 180° when a microburst is located the rear of a tornado (see Figure 7.29).

A microburst to the left will induce a peak convergence on the left side of the tornado. Semi-stationary suction vortices are found when a microburst is located to the right of a tornado. It is probably because the flow of the microburst air which blows into the tornado comes from a direction which is opposite to that of the tornado's translational velocity. A suction vortex forming under such conditions often ends up with a stationary vortex located near the instantaneous center of rotation shown by a dot.

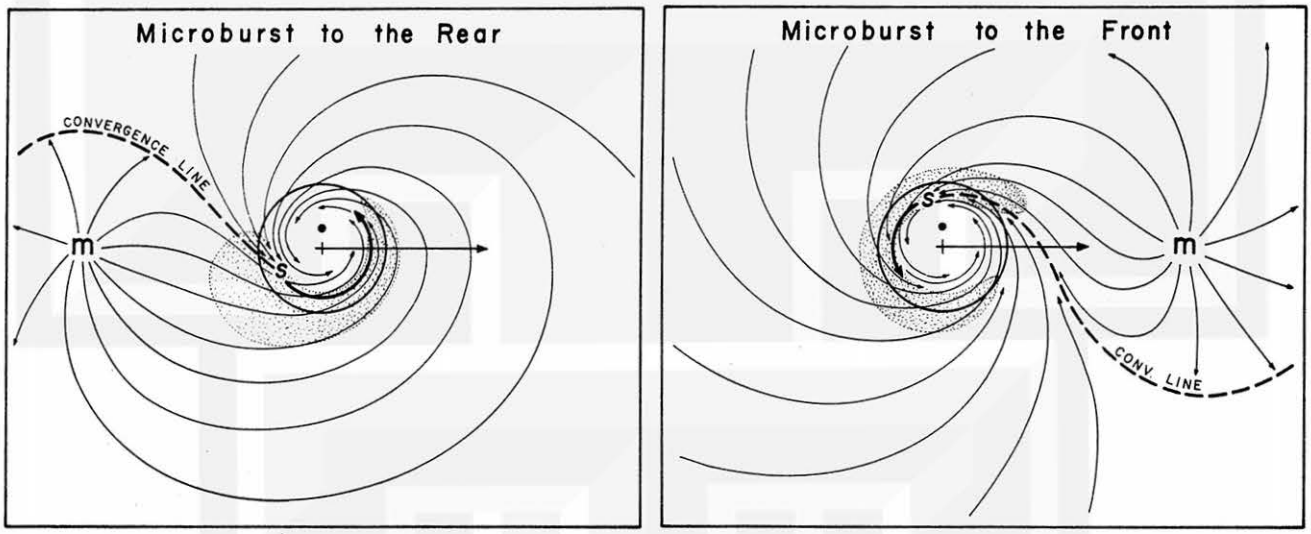

Figure 7.29 A microburst to the front of a moving tornado induces suction vortices in the rear left quadrant of the tornado (left). The preferable quadrant of suction vortices rotates by about 180° when the microburst location moves from the front to the rear of a tornado. A dot inside the tornado denotes the center of rotation where air is calm theoretically.

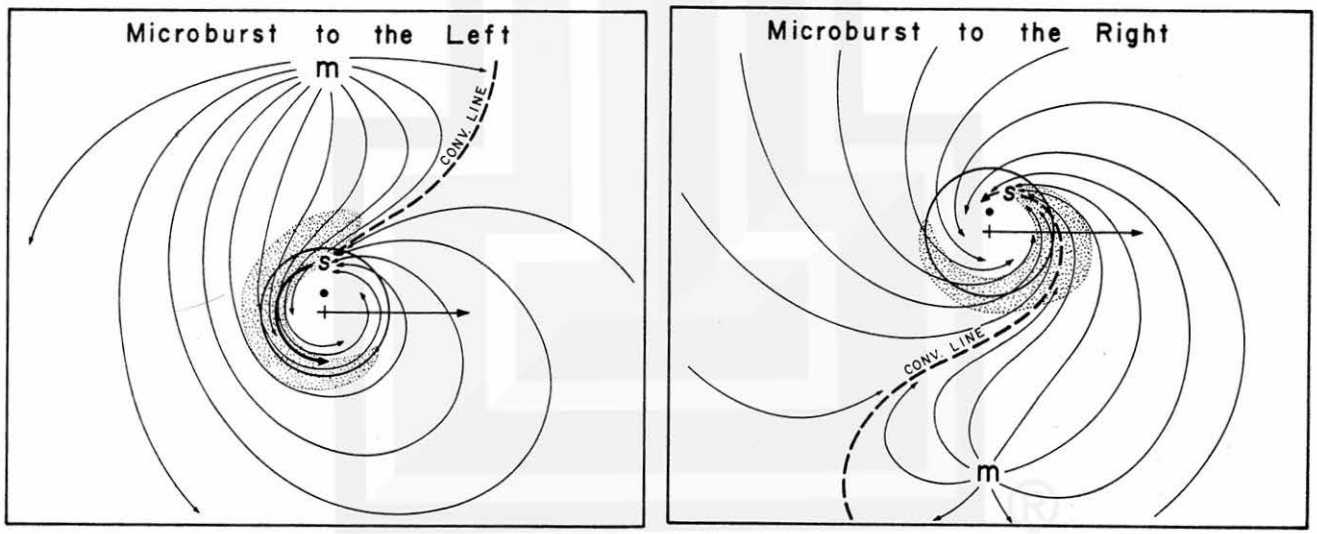

Figure 7.30 Existence of suction vortices in rear quadrants when a microburst is located to the left of the tornado center (left). A microburst to the right supplies a significant inflow from the front side of a tornado. A suction vortex often remains stationary, being affected by the opposing flows of tornado and microburst.

GOLDEN'S (1974a) and (1974b) WATERSPOUT EXPERIMENT in the Florida Keys revealed an important interaction between waterspouts and nearby showers.

On September 10, 1969 Golden dropped flares around an active waterspout in an attempt to determine the environmental flow field. Since a flare moves while releasing a smoke plume, the axis of the smoke represents the streak line attached to the flare. Taking the possible differences between streak lines and streamlines, he estimated the flow around the waterspout.

The flow patterns in Figure 7.31 were constructed by combining Golden's result with the author's model of microburst - tornado interactions. The outflow from a dark, shower region to the east of the waterspout was swirling into the waterspout circulation, and was characterized by 30-kt winds in the western sectors of the storm.

Flare smoke in the southwest sector, 500 to 1,000 m from the spray vortex, was drifting away from the waterspout, indicating the existence of a diverging flow in this sector. It should be noted that the waterspout was moving away from the shower region.

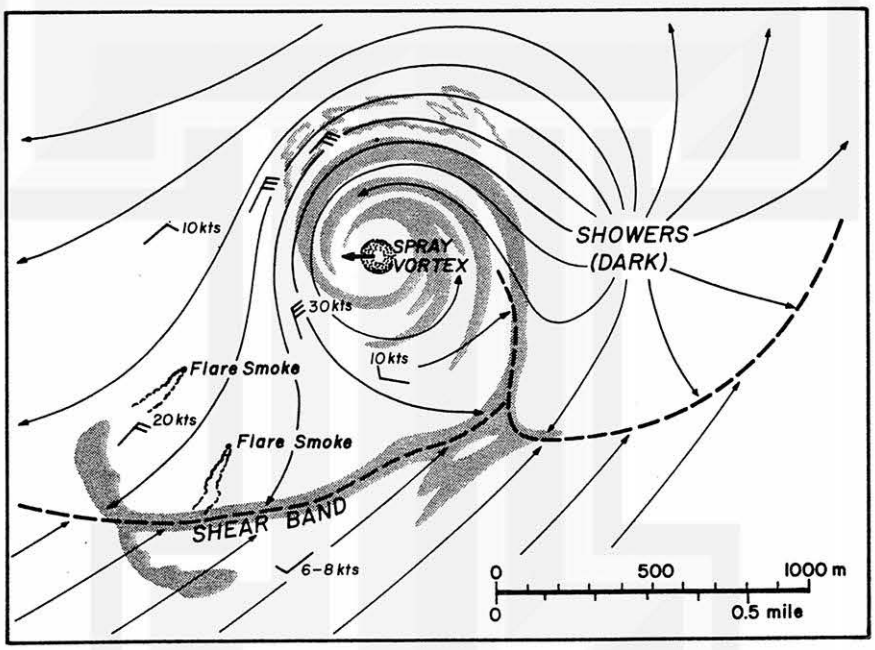

Figure 7.31 Interaction between a waterspout and a downdraft located to the rear. This figure was constructed by combining Figure 4 in Golden (1974b) with the left diagram of Figure 7.29 in this manual.

Golden's analysis of the waterspout of September 10, 1969 revealed that the spray vortex was moving away from the dark, shower region which is likely to be the source of an outflow. Wind barbs in the figure are those estimated by Golden.

An example of a complicated tornado, affected by a downburst and a microburst simultaneously, is shown in Figure 7.32. Two suction vortices, "B" and "C", were probably induced by a downburst flow from the rear-left. A single-turn vortex, "A", enlarged in the left and center pictures of Figure 7.33, was the result of a microburst to the right of the tornado path.

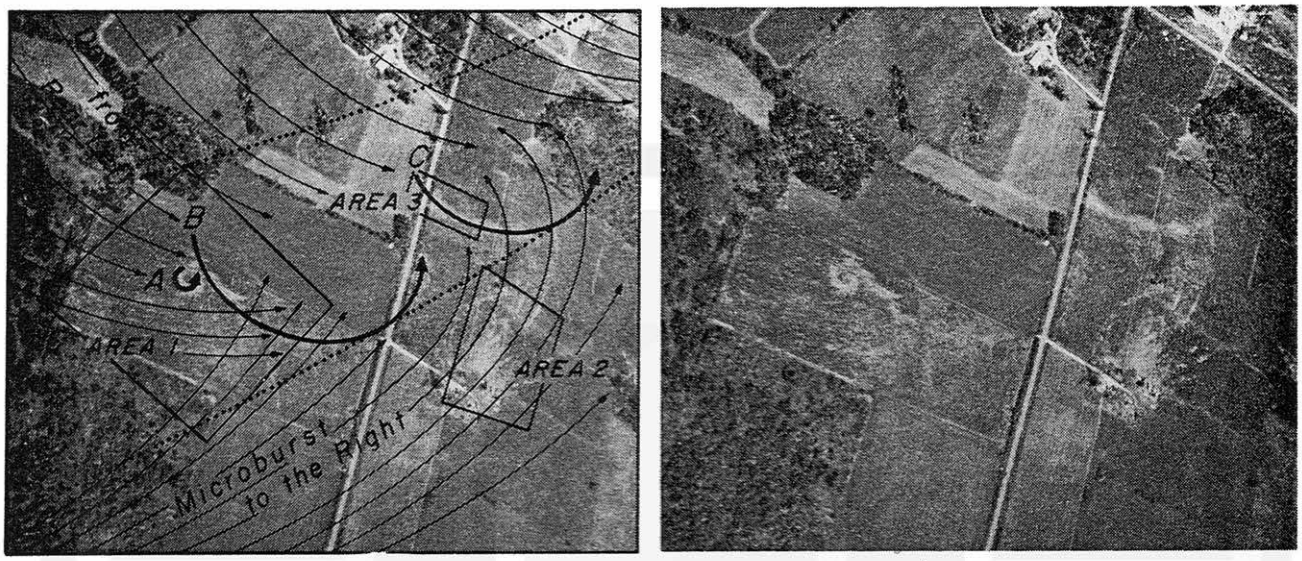

Figure 7.32 Rather complicated ground marks left by the Bloomer, Wisconsin tornado of July 30, 1977. A microburst to the right and a downburst from the rear left were affecting the tornado simultaneously.

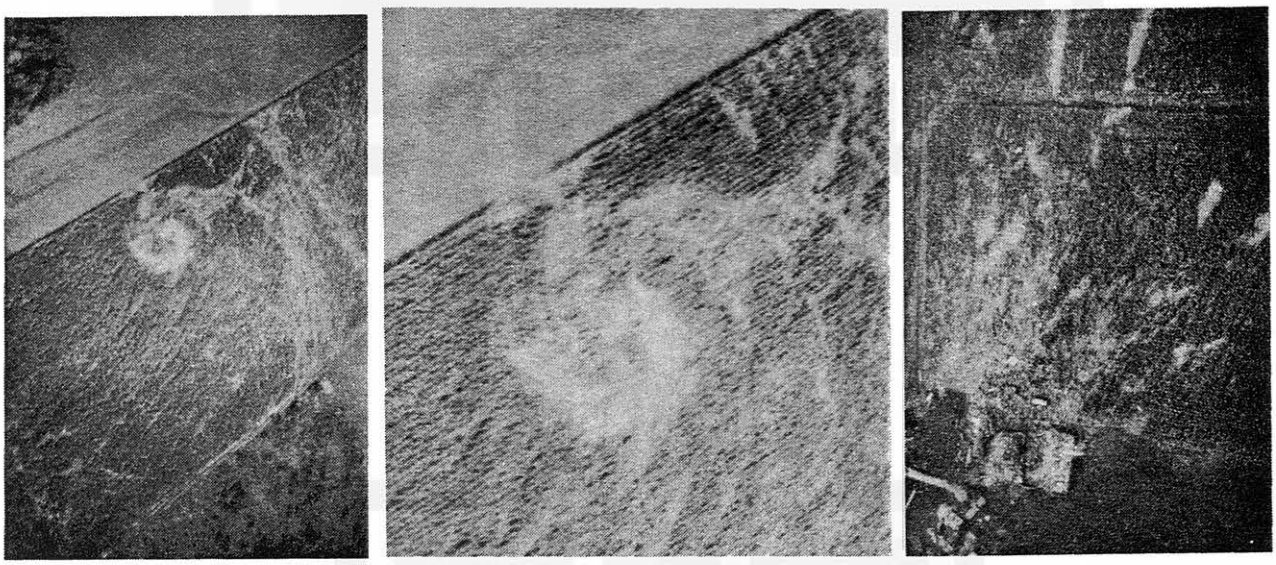

Figure 7.33 A stationary suction vortex in Area 1 induced by a microburst to the right (left picture) and its enlargement (center). A farm in Area 2 smashed by the microburst winds drawn violently into the tornado (right).

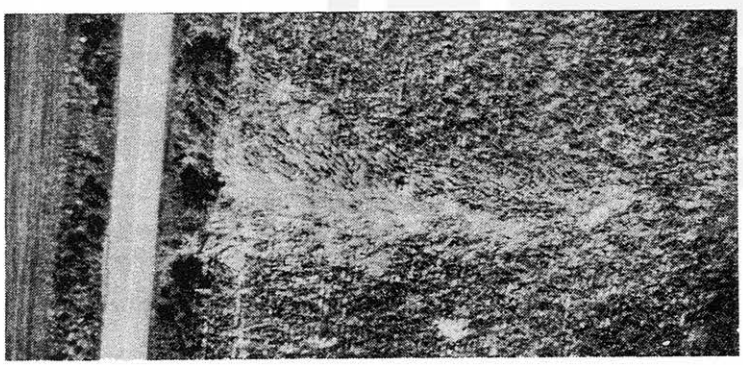

Figure 7.34 A close-up view (Area 3) of suction-vortex swath "C"; probably induced by the downburst from the rear left. Swath "B" preceded "C".

Farm buildings in Area 2 were smashed and blown some distance away by microburst winds which were accelerated while spiraling in toward the tornado (see right-side picture in Figure 7.34).

Suction vortex "C" developed in the field on the left side of a 2-lane highway in Figure 7.34. Then, it crossed the highway, leaving patterns of a cyclonic swirl. If there had been a car on the highway at the time of the vortex crossing, it could have been blown into the corn field. Since the width of the suction-vortex swath was very narrow, comparable to the width of the highway, only one or two cars could be seriously affected by the vortex. Others would simply drive away probably without even noticing such a small suction vortex.

EFFECTS OF DOWNBURSTS UPON TORNADO are rather complicated. A downburst may act as "poison" to a tornado, wiping it out (see Figure 7.2). On the other hand, a twisting downburst could act as "medicine" for a "wide-start" tornado (see Figure 7.5).

Despite the fact that a tornado travels straight across mountains and canyons, its course could be altered by a downburst (see Figures 7.18 and 7.19). It is likely that downbursts beneath a rotating thunderstorm push out the tornadoes, resulting in the periodic formations of left turn tornadoes (see Figures 7.21 and 7.23).

Asymmetric convergence inside the tornado core can be generated by one or more downbursts. Suction vortices forming in the area of the maximum convergence rotate around inside the core, resulting finally in significant variations of windspeeds inside a traveling tornado. Erratic damage patterns are what we observe after such tornadoes (see Figure 7.32).

Although the tornado-downburst relationships appear to be complicated, the more complicated behavior of tornadoes can be explained systematically by interacting tornadoes with downbursts.

It is highly desirable to combine all possible means of storm detection in an attempt to investigate various scales of motions ranging from suction vortices to mesocyclones by way of tornadoes and downbursts. This effort will continue during Project NIMROD, 1978 and 1979.

PROJECT NIMROD

1. OPERATIONS

Project NIMROD is a two-year (1978-79) research project which will be operated on the following two scales:

Northern Illinois Meteorological Research On Downburst

National Intensive Meteorological Research On Downburst

NORTHERN-ILLINOIS SCALE DATA COLLECTION is made in May and June, 1978 by operating a special network just to the west of Chicago, Illinois. The network consists of

- 3 Doppler radars, at O'Hare Airport, Yorkville, and near Monee
- 1 Non-Doppler radar near Joliet
- 27 PAM (Portable Automated Mesonet) Stations
- A Rawinsonde Station at Yorkville for serial ascents
  200 Recording Raingages
- 2 Wide-angle Cameras
- 2 Whole-sky Cameras
- 2 Lear Jets, one instrumented and the other for cloud-top photography
- 1 to 4 Kites to measure boundary-layer winds up to 300 m AGL
- 1 Helicopter and Cessnas for damage surveys

In support of the network operation radar and satellite data are collected frequently.

- Radar pictures at 40-sec intervals
  Marseilles, Ill., Des Moines, Ia., St. Louis, Mo., and Neenah, Wis. National Weather Service Radar Stations
- GOES/SMS pictures will be taken for every 3 minutes by using the eastern satellite

NATIONAL-SCALE DATA COLLECTION will be made during the 1978 and 1979 downburst season which begins in April and ends in October.

National Weather Services offices will be calling one of the following telephone numbers to inform the Project of the occurrence of strong and extensive downburst winds.

(312) 753-8112 753-8113 753-8114 753-8136	NIMROD Office, open between 8 a.m. and 5 p.m. weekdays
(312) 288-3045	Fujita's residence, weekends and holidays

In response to telephone messages, the University of Chicago meteorologists who are trained for downburst identification will be flying over the damage areas as informed by the NWS offices. The nature of the wind system will be confirmed through an extensive aerial mapping and possible ground survey.

Survey results will be forwarded to the NWS offices and NWS Headquarters upon request. Meanwhile, survey reports by NWS offices are to be transmitted to the University of Chicago.

2. OBJECTIVES

Meteorological data to be collected by Project NIMROD can be used both in understanding and predicting thunderstorms accompanied by damaging winds. However, the use of data is not limited to these wind-inducing thunderstorms. The data also can be used toward the solution of mesoscale atmosphere involving precipitation. Brief explanations of specific objectives are:

NO. 1. DIFFERENCES BETWEEN DOWNBURST AND RAIN STORMS. Storm-induced winds beneath convective clouds cannot be described as a simple function of the rainfall rate. We often experience heavy rain without noticeable air motion. Investigation of the Big Thompson Flash Flood by Maddox, Caracena, Hoxit, and Chappell revealed that the cores of radar reflectivity in the rain storm were located at relatively low altitude. The mechanisms of these rain storms are to be studied further.

NO. 2. EFFECTS OF OVERSHOOTING AND COLLAPSING CLOUD TOPS. Rapid-scan satellite pictures show fast changes in cloud-top features. The maximum sinking rate of a Texas thunderstorm as confirmed by Fujita was 41 m/sec at 48,000 ft. The cloud-top temperature of the northern Wisconsin downburst gradually increased during the storm. Sinking motions at the cloud-top level must influence the downward motions below. Time-dependent motion fields within the entire depth of thunderstorms, boundary layer to overshooting tops, will be investigated.

NO. 3. MECHANISM OF TORNADO FORMATION.
Do tornadoes descend from cloud to ground, or do they form first near the ground and extend upward into cloud? Evidence shows that some tornadoes form on the left side of downburst inside the boundary layer. Golden's waterspout studies indicated that dark spots, the first indicators of waterspouts, can be seen from the air only, not from the ground. It is necessary to investigate the boundary-layer flows in relation to Doppler-measured wind fields at the lowest height above the ground.

NO. 4. ESTIMATES OF SURFACE RAINFALL BASED ON IR AND RADAR SIGNATURES. Satellite-measured infrared temperatures and radar reflectivities have been used successfully in estimating rainfall rates of convective clouds in low latitudes. Situations seem to be more complicated in middle latitudes. It is, thus, necessary to combine radar echoes with satellite imagery along with velocity vectors of hydrometeors measured by Doppler radars.

NO. 5. INVESTIGATION OF AIRPORT WEATHER.
Landing and takeoff operations at O'Hare International Airport are often affected by thunderstorms. Three-dimensional airflows in and around O'Hare will be determined in an attempt to evaluate the representativeness of anemometers.

3. SUPPORT

Both operation and research phases of Project NIMROD are to be supported by four agencies of the U.S. Government.

National Aeronautics and Space Administration

National Oceanic and Atmospheric Administration

National Science Foundation

Nuclear Regulatory Commission

The National Center for Atmospheric Research at Boulder, Colorado will be playing a major role in operating the NIMROD network in May and June, 1978.

The National Environmental Satellite Service and the National Weather Service will be participating in data collections involving both the Northern Illinois and National scales.

A final report to be entitled "Downburst Thunderstorms" will be issued at the conclusion of Project NIMROD, 1978-79. Further information may be obtained from:

Office of T. Theodore Fujita
Department of the Geophysical Sciences
The University of Chicago
Chicago, Illinois 60637

REFERENCES

Abbey, R. F., Jr. (1976): Risk probabilities associated with tornado windspeeds. Proc., Symp. on Tornadoes, Texas Tech. Univ., 177-236.

Agee, E. M., J. T. Snow, and P. R. Clare (1976): Multiple vortex features in the tornado cyclone and the occurrence of tornado families. Mon. Wea. Rev., 104, 552-562.

Bedard, A. J., Jr., W. H. Hooke, and D. W. Beran (1977): The Dulles Airport pressure jump detector array for gust front detection. Bull. Amer. Met. Soc., 58, 920-926.

Bigler, S. G. (1958): Observations of a tornado using the AN/CPS-9 radar. Proc. 7th Wea. Radar Conf., K1-K5.

Bonner, W. D. and J. E. Kemper (1971): Broad-scale relation between radar and severe weather reports. 7th Conf. Severe Local Storms, 140-147.

Brandes, A. E. (1977a): Flow in severe thunderstorms observed by Dual-Doppler radar. Mon. Wea. Rev., 105, 113-120.

Brandes, A. E. (1977b): Gust front evolution and tornado genesis as viewed by Doppler radar. J. of Applied Met., 16, 333-338.

Brown, R. A., editor (1976): The Union City, Oklahoma tornado of 24 May 1973. NOAA Tech. Memo. ERL NSSL-80.

Burgess, M. A. (1977): Performance study report of Continental 63 accident at Tucson, Arizona. NTSB. 24 pp.

Byers, H. R. and R. R. Braham (1949): The Thunderstorm. Gov. Print. Office. 287 pp.

Caracena, F. (1978a): Mesoscale features involved in the crash of Allegheny Flight 121 at Philadelphia on June 23, 1976. Report to NTSB. 16 pp.

Caracena, F. (1978b): Analysis of meteorological conditions of June 3, 1977. Prepublication Personal Communication.

Caracena, F. and M. W. Maier (1978): Mesoscale analysis of a microburst in FACE network on July 1, 1975. Prepublication Personal Communication.

Corbell, R. P., C. J. Callahan, and W. J. Kotsch (1976): The GOES/SMS User's Guide. NESS/NASA, p 117.

Durand-Gréville, E. (1892): Les grains les Orages. Ann. Centr. Meteor. de France, 1, 249.

Faust, H. (1947): Untersuchungan von Forstschaden Hinsichtlich der Windstruktur bei einer Bö. Meteor. Rundschau., 1, 290-297.

Forbes, G. S. (1977): Thunderstorm-scale variations of echoes associated with left-turn tornado families. Preprint, 10th Conf. Severe Local Storms, 497-504.

Forbes, G. S. (1978): Three scales of motions associated with tornadoes. Ph.D. Dissertation, Univ. of Chicago, 359 pp.

Fujita, T. T. (1960): A detailed analysis of the Fargo tornadoes of June 20, 1957. U.S. Wea. Bureau Res. Paper 42, 67 pp.

Fujita, T. T. (1963): Analytical Mesometeorology: A Review. Meteor. Monographs, 5, 77-125.

Fujita, T. T. (1971): Proposed characterization of tornadoes and hurricanes by area and intensity. SMRP Res. Paper 91, Univ. of Chicago, 42 pp.

Fujita, T. T. (1972): Tornado occurrences related to overshooting cloud-top heights as determined from ATS pictures. SMRP Res. Paper 97, Univ. of Chicago, 32 pp.

Fujita, T. T. (1974): Jumbo tornado outbreak of 3 April 1974. Weatherwise, 27, 116-126.

Fujita, T. T. (1975): Superoutbreak tornadoes of April 3-4, 1974. Final Edition Color Map. Univ. of Chicago.

Fujita, T. T. (1976): Spearhead echo and downburst near the approach end of a John F. Kennedy Airport runway. SMRP Res. Paper 137, Univ. of Chicago, 51 pp.

Fujita, T. T. and H. R. Byers (1977): Spearhead echo and downburst in the crash of an airliner. Mon. Wea. Rev., 105, 129-146.

Fujita, T. T. and F. Caracena (1977): An alaysis of three weather-related aircraft accidents. Bull. of Amer. Met. Soc., 58, 1164-1181.

Fujita, T. T. and A. D. Pearson (1973): Results of FPP classification of 1971 and 1972 tornadoes. Preprints, 8th Conf. on Severe Local Storms, 142-145.

Fujita, T. T., J. J. Tecson, and R. F. Abbey, Jr. (1978): Intensity and path length of U.S. tornadoes, 1916-77. SMRP Res. Paper 164, Univ. of Chicago.

Fujiwara, S. (1943): Report of special observation of thunderstorms. Japan Meteorological Agency, 248 pp.

Glossary of Meteorology (1959): Amer. Met. Soc., 638 pp.

Golden, J. H. (1974a): Life cycle of Floriday Keys' waterspouts. I. J. Appl. Met., 13, 676-691.

Golden, J. H. (1974b): Scale-interaction implications for the waterspout life cycle. II. J. Appl. Met., 13, 693-709.

Hamilton, R. E. (1970): Use of detailed intensity radar data in meso-scale surface analysis of the July 4, 1969 storm in Ohio. Preprints, 14th Radar Met. Conf., 339-346.

Hardesty, R. M., P. A. Mandics, D. W. Beran, and R. G. Strauch (1977): The Dulles Airport acoustic-microwave radar wind and wind shear measuring system. Bull. of Amer. Meteor. Soc., 58, 910-918.

Hart, G. C. (1976): Estimation of structural damage due to tornadoes. Proc., Symposium on Tornadoes, Texas Tech. Univ., 645-665.

Her Majesty's Stationary Office (1957): Report on the accident near Kano Airport, Nigeria on 24 June, 1956. Ministry of Transport and Civil Aviation, 12 pp.

Ishizaki, H. (1978): Gust factors averaged in time and space. 3rd U.S. Nat. Conf. Wind Eng. Res. II-0-1 and 2.

Koschmieder, H. (1955): Ergebnisse der Deutschen Boenmessungen 1939/41. Friedr. Vieweg & Sohn. Braunschweig, 148 pp.

Lemon, L. R., R. J. Donaldson, Jr.,, D. W. Burgess, and R. A. Brown (1977): Doppler radar application to severe thunderstorm study and potential real-time warning. Bull. Amer. Met. Soc., 58, 1187-1193.

McCarthy, J. J. G. M. Heynsfield, L. G. Tidwell, and S. P. Nelson (1975): Evolution of a tornadic cyclone as seen by dual-Doppler instrumented airplane and chaff. Preprints, 9th Conf. Severe Local Storms, 389-395.

McDonald, J. R. (1976): Tornado-generated missiles and their effects. Proc., Symp. on Tornadoes, Texas Tech. Univ., 331-348.

Mehta, K. C. J. R. McDonald, J. E. Minor, and A. J. Sanger (1971): Response of structural systems to the Lubbock storm of May 11, 1970. Texas Tech. Univ., 428 pp.

Minor, J. E. (1976): Applications of tornado technology in professional practice. Proc., Symp. on Tornadoes, Texas Tech. Univ., 375-392.

Minor, J. E., J. R. McDonald, and K. C. Mehta (1977): Engineering-oriented examinations of the tornado phenomenon. 10th Conf., Severe Local Storms, 438-445.

Müldner, W. (1950): Die Windbruchschäden des 22.7.1948 im Reichswald bei Nürnberg, ein Beispiel für ein Wirbelfeld als Ieilerscheinung einer Böenfront. Berichte des Deutschen Wetterdienstes in der U.S. Zone, 19, 3-39.

Newton, C. W. (1950): Structure and mechanism of the pre-frontal squall line. J. Meteor., 7, 210-222.

Nolen, R. H. (1959): A radar pattern associated with tornadoes. Bull. Amer. Met. Soc., 40, 277-279.

Purdom, J. F. W. (1971): Satellite imagery and severe weather warning. 7th Conf. Severe Local Storms, 120-127.

Ray, P. S., R. J. Doviak, G. B. Walker, D. Sirmans, J. Carter, and B. Bumgarner (1975): Dual-Doppler observations of a tornadic storm. J. Appl. Met., 14, 1521-1530.

Stout, G. E. and F. A. Huff (1953): Radar records Illinois tornado genesis. Bull. Amer. Met. Soc., 34, 281-284.

Suckstorff, G. A. (1938): Kaltlufterzeugung dürch Niederschlag. Z. Meteor., 55, 287-292.

Wilson, L. F. and D. Kelly (1977): Tornado climatology by day of the week. Preprints, 10th Conf. on Severe Local Storms, 194-198.

SUBJECT INDEX